CRANFIELD UNIVERSITY

D BRUNDLE

APPLICATION OF NONLINEAR CONTROL THEORY IN WEAPON GUIDANCE AND CONTROL

COLLEGE OF AERONAUTICS

MPhil THESIS

CRANFIELD UNIVERSITY

COLLEGE OF AERONAUTICS

MPhil THESIS

Academic Year 2000-2001

D BRUNDLE

Application of nonlinear control theory in weapon guidance and control

Supervisor: P.G.Thomasson

March 2001

This thesis is submitted in partial fulfilment of the requirements
for the degree of Master of Philosophy

Abstract

This thesis considers the application of nonlinear control theory in two subjects pertinent to weapon applications. Initially, Section 2 considers the development of a simple nonlinear autopilot for a Laser Guided Bomb (LGB). Later a nonlinear autopilot design is developed using a Pulse-Width Modulated (PWM) controller derived from the method developed by Bernelli-Zazzera et al[4]. This is applied to an LGB utilising a "bang-bang" actuator, enabling the control surfaces to achieve a pseudo-proportional response. The PWM design stems from an equivalent Pulse-Amplitude Modulated controller, which required a design technique to be developed for a linear autopilot and, in addition, simulation of an electro-mechanical actuator. Simulation demonstrated that the PWM controller can achieve the desired response but the design must incorporate actuator dynamics.

Section 3 considers the use of nonlinear control theory to examine the nonlinear intercept equations using a Proportional Navigation (PN) guidance law. Using a simple heuristic example, PN is introduced and vector algebra used to develop a simple model of the intercept. The model is then used to illustrate the importance of the kinematic gain. Using the method pioneered by Ha et al[16], Lyapunov theory is used to demonstrate that PN is a robust guidance law. Although generally derived assuming the target maintains rectilinear flight, Lyapunov theory is used to demonstrate interception is always possible provided the pursuer has sufficient manoeuvre advantage over the target. Noting that many missiles incorporate a

directional warhead, Lyapunov theory is used to design a time-varying rate bias that controls the direction of approach to the target. Simulation demonstrates that the guidance requirements are indeed achieved by this law but additional effort is required by the control system.

In Section 3 it is demonstrated that the PN guidance law will always ensure an intercept, i.e. it does not by itself generate miss-distance. In the final part of Section 3, using adjoint software designed by Zarchan[42], it is demonstrated that miss-distance develops in practical systems as the result of sub-system dynamics.

Acknowledgements

I would like to acknowledge the following individuals for their help and encouragement whilst I undertook my studies:

Mr P.G.Thomasson, Senior Lecturer, Cranfield University

Mr D.A.Heley, Manager, Systems Integration, Hunting Engineering Ltd

Mr B.Shepherd, Deputy Head Defence Systems Division, Hunting Engineering Ltd

Mr I.Kerley, Former Senior Personnel Officer, Hunting Engineering Ltd

List of Contents

List of Figures

Notation

In general, notation is defined in the text throughout the thesis and listed here as a supplement to the main text. As the thesis is divided into two main sections, notation is similarly divided between the notation used in Sections 2 and 3.

Notation Used in Section 2

a Acceleration in body axes

$\underline{e}$ Error vector between Pulse-Width and Pulse-Amplitude control

h Sample period

l Position of inertial measuring unit in body axes

n Yawing moment

n_r Yawing moment derivative due to yaw rate, normalised by yaw inertia, this is defined as:

$$n_r = \frac{N_r}{I_{ZZ}}$$

n_v Yawing moment derivative due to sideslip, normalised by yaw inertia, this is defined as:

$$n_v = \frac{N_v}{I_{ZZ}}$$

n_ς Yawing moment derivative due to rudder deflection, normalised by yaw inertia, this is defined as:

$$n_\varsigma = \frac{N_\varsigma}{I_{ZZ}}$$

p Roll rate

q Pitch rate

r Yaw rate

$\underline{r}_{A/B}$ Position vector of inertial measuring unit in body axes

t Time

u Single control input

$\underline{u}$ Input vector

v Sideslip velocity

$\underline{v}$ Velocity vector body axes

w Heave velocity

$\underline{x}$ State vector

x, y, z Body fixed reference frame

y Sideforce

y_r Sideforce derivative due to yaw rate normalised by weapon mass, this is defined as:

$$y_r = \frac{Y_r}{M}$$

y_V Sideforce derivative due to sideslip normalised by weapon mass, this is defined as:

$$y_v = \frac{Y_v}{M}$$

y_ς Sideforce derivative due to rudder deflection normalised by weapon mass, this is defined as:

$$y_\varsigma = \frac{Y_\varsigma}{M}$$

$\underline{z}$ Measured state vector

A System matrix

B Input matrix

C Output matrix

D Feed forward matrix

E State measurement matrix (Also used to denote norm of $\underline{e}$ in Section 2.7.5)

F Input measurement matrix (Also used to define the discrete form of the state transition matrix in Section 2.7.7.3 and the observer system matrix in Section 2.7.7.4)

G Gain matrix (Also used to define the discrete form of the convolution integral in Sections 2.7.7.3)

H Reduced order observer input matrix

I Actuator motor current

I_{ZZ} Yaw inertia

J — Control surface rotational inertia

K — Input gain to autopilot

K_A — Accelerometer gain

K_G — Accelerometer gain

K_{GB} — Actuator gear ratio

K_P — Actuator gain

K_M — Actuator motor constant

L — Feedback matrix in reduced order observer

M — Weapon mass (Also used to denoted output matrix in a reduced order observer Section 2.7.7.4)

$\underline{M}$ — Direction cosine matrix, space to velocity axis

N — Reduced order observer output matrix

N_r — Yawing moment derivative due to yaw rate, this is defined as:

$$N_r = \frac{1}{4}\rho VSD^2 \frac{\partial C_n}{\partial\left(\frac{rD}{2V}\right)}$$

N_V — Yawing moment derivative due to sideslip, this is defined as:

$$N_v = \frac{1}{2}\rho VSD\frac{\partial C_n}{\partial \beta},\ \beta \approx \frac{v}{V}$$

N_ζ — Yawing moment derivative due to rudder deflection, this is defined as:

$$N_\varsigma = \frac{1}{2}\rho V^2 SD\frac{\partial C_n}{\partial \varsigma}$$

R Actuator motor resistance

U Weapon forward velocity

T Reduced order observer measurement matrix

$\underline{V}$ Velocity vector in space axes

$\underline{\hat{V}}$ Unit velocity vector in space axes

W Pulse weighting function

$\underline{X}$ Position vector

$\underline{\hat{X}}$ Unit position vector

X, Y, Z Space axes (X, Y, Z* define a right-hand axes frame)

$X_T, Y_T, Z_T,$ Velocity axes

Y_r Sideforce derivative due to yaw rate, this is defined as:

$$Y_r = \frac{1}{4}\rho VSD\frac{\partial C_Y}{\partial\left(\frac{rD}{2V}\right)}$$

Y_V Sideforce derivative due to sideslip, this is defined as:

$$Y_v = \frac{1}{2}\rho VS\frac{\partial C_Y}{\partial\beta},\ \beta \approx \frac{v}{V}$$

Y_ς Sideforce derivative due to rudder deflection, this is defined as:

$$Y_\varsigma = \frac{1}{2}\rho V^2 S\frac{\partial C_Y}{\partial\varsigma}$$

Z Unknown constant value

---

* In a right hand axes frame, Z is positive down, hence height values are negative since the origin is defined in the plane of the target.

Greek Symbols

β	Sideslip angle
δ	Pulse-width in Pulse-Width Modulation control
ε	Error vector due to pulse-translation in time
ε_P	Component of sightline vector in pitch plane
ε_Y	Component of sightline vector in yaw plane
ϕ	Euler angle in roll defining transformation from space to body axis frame
θ	State transition matrix in discrete form at $\frac{h}{2}$
θ_A	Current actuator position
θ_D	Demanded actuator position
θ_P	Euler angle defining transformation from space axes frame of reference to axis frame defined by the weapon velocity vector.
σ	Sightline angle in velocity axes.
τ	Pulse delay in Pulse-Width Modulation control
$\tilde{\tau}$	Pulse delay in Pulse-Width Modulation control relative to $\frac{h}{2}$
$\omega_{A/P}$	Actuator bandwidth
ω_n	Desired autopilot bandwidth
ξ	Sightline angle in velocity axes.
ξ'	Sightline angle in velocity axes, corrected for body roll.

ψ_P	Euler angle defining transformation from space axes frame of reference to axis frame defined by the weapon velocity vector.
ζ	Rudder deflection
$\varsigma_{A/P}$	Desired autopilot damping ratio
ς_n	Actuator damping ratio
$\Delta(h)$	Convolution integral in discrete form
$\Phi(h)$	State transition matrix in discrete form
$\Phi(t)$	State transition matrix in continuous form
$\underline{\Omega}$	Angular rate vector in body axes
Ξ	Denotes $\Psi(h)$
$\Psi(h)$	Modified convolution integral in discrete form (see text)

Subscripts

x, y, z	Denote components in body fixed reference frame
B	Component at weapon centre-of-gravity
E	Sightline error vector in velocity axes
M	Denotes amplitude of Pulse-Width Modulation control
P	Weapon vector in space axes
REL	Denotes movement of the inertial measuring unit relative to the weapon centre of gravity
S	Sightline vector in space axes
T	Target position vector in space axes

Sub-subscripts

d	Demanded response
a	Actual response

Notation Used in Section 3

r	Range to target
$\vec{r}$	Position vector
t	Time
$\vec{v}$	Velocity vector
y	Relative deviation of missile and target from a collision course
A	Acceleration
I	Performance index (see text)
K	Kinematic gain
T	Total time of flight
V	Velocity
$V(t)$	Lyapunov function
Y	Deviation from a collision course

Greek Symbols

α	Upper limit of target manoeuvre capability
β	Arbitrary positive constant defined by geometric constraint on initial conditions $\beta \in (0,1-\rho)$
ε	Small finite error in the impact conditions

γ	Flightpath angle
η	Proportional constant
θ	Angle of velocity vector relative to the sightline
ρ	Missile velocity advantage, $\rho = V_t / V_m$
σ	Sightline angle
ω_s	Sightline rate, $\dot{\sigma}$
$\vec{\omega}_s$	Sightline rate in vector format
$\vec{\omega}_0$	Initial sightline rate in vector format
ψ	Euler angle in yaw

Subscripts

b	Denotes sightline angle bias term
c	Denotes closing velocity
f	Denotes final condition
m	Denotes missile
r	Denotes error in range
t	Denotes target
D	Denotes desired conditions at impact
γ	Denotes error in flight path angle

Sub-Subscripts

0	Denotes initial conditions

1. Thesis Overview

The work presented in this thesis was sponsored by Hunting Engineering Ltd and considers the use of nonlinear control theory in guided weapon applications. In particular, two subjects of particular relevance to weapon applications are considered.

The first of these, is the application of nonlinear control theory to the design of the missile autopilot. An autopilot can be considered as a closed loop within the main guidance loop, which is designed to implement the control demands of the guidance system. In many weapon systems this is implemented in the form of aerodynamic control; the control devices are lifting surfaces controlled by the autopilot to achieve the lateral acceleration demands of the guidance system. Typically this requires an inertial measuring unit (IMU) consisting of rate gyroscopes and accelerometers to provide rate feedback within the autopilot loop. An autopilot loop can of course be designed using conventional linear approaches to control theory; however, many weapon systems feature a nonlinear autopilot where control is achieved using nonlinear devices.

Section 2 considers the development of an autopilot intended for an application using "bang-bang" actuators. A literature survey was performed and found that the literature available was fairly limited. The majority of references considered space vehicle control using on-off thrusters. One of the main features of nonlinear control theory is that, despite extensive research, there are few underlying principles with

which to replace linear control theory. As a result many of these examples were application specific and not readily adaptable to this particular problem. Bernelli-Zazzera et al[4] have developed a generic technique that converts a Pulse-Amplitude Modulated (PAM) control system into an equivalent Pulse-Width Modulated (PWM) control system. This is a flexible technique that is only limited by the requirement that the control design is based upon an equivalent linear design.

Neglecting actuator dynamics, simulation was used to demonstrate that the technique of Bernelli-Zazzera et al[4] could be used to control the airframe. After consideration of the actuator dynamics it was concluded that they must be considered during the design of the controller. However, there is no linear equivalent of a "bang-bang" actuator upon which to base the design of the control system. A linear equivalent was designed using a reduced order observer to estimate the actuator states and, hence, provide position feedback. Simulation was then used to demonstrate that this design could successfully control a "bang-bang" actuator to achieve a pseudo-proportional response.

The second subject to be examined was the use of Proportional Navigation (PN) in weapon guidance systems. A literature survey revealed that whilst there was a wealth of literature devoted to the study of PN, there remained a gap in the literature. Many weapon systems incorporate a warhead that is directional in nature and clearly there are performance benefits if the guidance system can be designed to tailor the conditions in the end-game. However, there was very little information available in

the open literature concerning variants of PN that enabled the impact conditions to be controlled.

Section 3 considers the use of nonlinear control theory to investigate the behaviour of the nonlinear intercept equations. PN is initially studied using a simple linearised model of the intercept to establish the importance of the kinematic gain. Using Lyapunov's direct method it is demonstrated that PN is exponentially stable, even in the presence of target manoeuvres, provided the pursuer has a significant manoeuvre advantage over the target.

The use of Lyapunov's direct method is then extended to the problem of achieving directional control over the line of approach to the target. A time-varying rate bias is derived to alter the direction of approach, whilst maintaining stability in the sense of Lyapunov. It is further demonstrated that although the guidance law that results is no longer exponentially stable it remains asymptotically stable.

The terms in the time varying rate bias rely upon information derived from an on-board Inertial Navigation System (INS) and an active missile seeker. A further development of this guidance law is proposed that is exclusively reliant upon seeker based information eliminating the requirement for the INS and an active seeker. Although the guidance law as derived is considered to have undesirable features it has been shown to perform well using six degree-of-freedom simulation.

Simulation has shown that the guidance law can meet the demand of controlling the approach direction but that a performance penalty results. Depending upon the desired angle of approach this penalty is generally small. However, a performance index based upon the integral of the square of the lateral acceleration shows, in comparison with a conventional PN guidance law, a large increase in control effort.

Finally, having demonstrated using nonlinear control theory that the basic PN algorithm is robust, the effect of the simplifying assumptions used to derive the theory is addressed. Using adjoint simulation developed by Zarchan[42] it is demonstrated that in practical systems a miss results due to the effect of sub-system dynamics and noise.

2. Nonlinear Autopilot Design

2.1 Introduction

An autopilot may be defined as a closed loop system that is itself part of the guidance loop. However, not all missile designs require an autopilot, for instance many anti-tank weapons function quite satisfactorily without one. A missile control system that uses inertial instrument feedback to modify the airframe response to a control demand is generally referred to as an autopilot. These may be broadly categorised into autopilots that control the pitch and yaw planes, referred to as lateral autopilots, or autopilots that control the roll orientation of the weapon, i.e. roll autopilots.

Many of the current generation of guided weapon systems feature a nonlinear autopilot. Typical examples include the UK Mk13/18 Paveway II Laser Guided Bomb (LGB), the Swedish Strix guided mortar round and the French Arçole LGB. Future Precision Guided Munitions (PGM) are likely to continue this trend, since nonlinear systems offer the weapon designer packaging advantages, reduced cost and reduced complexity.

A nonlinear autopilot design poses a number of challenges for the control engineer. Although all systems exhibit some degree of nonlinearity, the nonlinear element of the autopilot means that linear approaches to control system design break down. Traditional methods such as Laplace transforms, frequency response plots, root locus analysis or even state-space analysis are thus no longer valid. Even though

considerable research has been conducted in recent years the fact remains that there is no single control analysis approach with which to replace these techniques in nonlinear control design.

In this chapter the design of a nonlinear autopilot for an air launched PGM is considered. The system considered is an LGB, enhanced with an INS/GPS* guidance system. Rather than utilising a proportional actuator, the weapon is controlled by a simple "bang-bang" actuator.

This chapter describes an initial literature survey of related nonlinear control systems. In order to demonstrate that a nonlinear guidance system can be derived using INS/GPS guidance an "intuitive" design solution is presented based upon an existing seeker based guidance loop. Following on from this a sliding mode control design was considered but rejected as inappropriate due to its limitation to a single second order system. Using the data from the literature survey a number of potential design techniques for a nonlinear control system are considered and a design developed using the method of Bernelli-Zazzera et al[4] is presented.

The method of Bernelli-Zazzera et al[4] is a general-purpose technique in which a linear control system may be designed using the classical approach to control design; the system is then converted to work in a nonlinear manner. Initially this technique is applied to an autopilot design derived using state feedback but neglecting actuator dynamics. Further work demonstrates that the design must consider actuator

* An inertial navigation system coupled with a global position system receiver.

dynamics and considers several solutions to enable actuator dynamics to be incorporated into the control loop. Finally, an Observer based Pulse-Width Modulated controller design is developed.

2.2 Literature Survey

Although many weapon systems feature a nonlinear autopilot, this is not reflected in the available literature. It is presumed that many of the techniques that have been developed remain either classified or proprietary and little data is available in open literature. Some studies carried out at Hunting Engineering Ltd (HEL) were available for reference but the majority of the open literature available relates to spacecraft using on-off thruster systems.

Slotine et al[31] have produced a general reference work considering the application of nonlinear control theory. Although several techniques have been suggested for nonlinear systems, no universal techniques have yet been developed that can be used in the analysis of all nonlinear systems. The main techniques developed include phase-plane analysis, Lyapunov theory and the describing function.

Phase plane analysis is a graphical method of studying nonlinear system behaviour, however, the technique makes a number of assumptions and has certain limitations. The linear part of the plant is generally restricted to second order systems, higher order systems can be considered but interpretation of the result is difficult. It is further assumed that the parameters of the plant are stationary. General input signals cannot be handled; however, initial conditions are implicit within the method so it is

possible to consider the effects of step, ramp or impulse inputs. The technique essentially involves solving the nonlinear second order equation graphically, rather than analytically, and the result is a family of state space trajectories in a two-dimensional plane, the phase plane.

Basic Lyapunov theory comprises the two methods introduced by Lyapunov, namely the direct and the indirect method. The indirect or linearisation method states that the stability properties of a nonlinear system in the close proximity of an equilibrium point are essentially the same as those of its linearised approximation. The direct method generalises the concept of a stable mechanical system; i.e. a mechanical system is stable if its total mechanical energy decreases all the time. In using the direct method the concept is to create a scalar energy-like function (the Lyapunov function) for the system and to demonstrate that it reduces with time. It is a powerful technique; the main limitation of the method is the difficulty in finding a suitable Lyapunov function for a given system.

Although the direct method was originally devised as a method of stability analysis it has found an important application in the design of nonlinear controllers. The technique involves constructing a Lyapunov function of the system states and designing a control law to force this function to decrease, thereby guaranteeing the stability of the system.

The final technique considered is the describing function. This approximates nonlinear systems using linear equivalents and then uses frequency domain

techniques to analyse the results. The describing function technique is mainly used in the analysis of limit cycles but is also used in the analysis of subharmonic generation and system response to sinusoidal inputs. It is a technique that offers many advantages; the system order is not limited, it is similar to linear systems and, therefore, more intuitive for engineers to understand. It can accommodate many of the nonlinearities found in control systems. The main disadvantage of the technique is that it is an approximation and it can produce inaccurate predictions.

In an internal HEL study Rogers[29] considered the use of pulsed thrusters mounted at the centre-of-gravity of a surface-to-air missile. Initially using a scheme suggested by Zarchan[42], Rogers[29] implemented a thruster augmented autopilot where the thruster pulse was used to augment the acceleration demand from the guidance system eliminating any deficit in the achieved lateral acceleration. Somewhat surprisingly this scheme showed no benefit in terms of reduced miss-distance. Later Rogers used phase plane analysis by considering a single and double integration of the guidance error as the phase plane variables. Rogers postulates a switching line for the thrusters, which is intended to drive the error integral to zero. Using this scheme Rogers was able to demonstrate that a greatly reduced miss-distance results. The study illustrates that whilst nonlinear controls can be of benefit to the control designer, their implementation is often non-intuitive and that the design of the controller is critical in determining the success (or otherwise) of their implementation.

A number of papers published by Thurman et al[34,35] consider the use of pulsed thrusters for the control of spacecraft and illustrates the implementation of a nonlinear autopilot with examples of a course change correction and a planetary lander. A brief review of previous literature is also considered.

A great deal of the preceding literature assumes the use of continuously throttle-able or fixed thrust propulsion systems and attempts to find an optimal trajectory using linear approximations to the spacecraft dynamics. Another approach adopted is the use of phase plane analysis, coupled with detailed computer simulation to develop a phase-plane switching controller.

The approach adopted by Thurman et al[34,35] is to modify the robust control approach originally developed by Corless[8] and Leitman[24]. In this approach, the demanded thrust vector is considered to consist of three components, a feedback linearisation component, a feedback law and a compensation term. The compensation term is designed to accommodate errors introduced by the thruster mechanism using discrete thrusters and, also, nonlinear spacecraft dynamics. Lyapunov's direct method is used to design a controller to implement the compensation term. The algorithm is developed from the analytical characterisation of the transient errors and includes the effects of limit cycles and dead band nonlinearities without the use of linearisation.

The first application considered was a Martian soft-lander. This included the implementation of a nonlinear autopilot to control re-entry and the final descent

under a thruster system, with the system subject to navigation errors and drift following a parachute descent following re-entry.

Another example is the use of a nonlinear autopilot to control the attitude change of a rigid body using the Euler rotation theory. This approach is complicated by the dynamical coupling inherent in such an approach and previous applications have attempted to overcome this using low rotation rates, open loop implementation of a pre-computed angular acceleration profile or feedback linearisation. Control laws involving feedback linearisation are continuously time varying functions and with pulsed thrusters there is the added complication of developing a firing logic that implements the desired control input with acceptable accuracy. Thurman et al[34,35] demonstrate that this can be implemented using a nonlinear controller designed using the above technique and that by including the nonlinearities in the controller design a simple digital autopilot can be developed that does not require feedback linearisation or gain scheduling. Also demonstrated is that the effect of sampling rate on performance can be assessed to evaluate the robustness and performance of the digital implementation of the autopilot. Simulations are used to demonstrate that the required manoeuvres can be accomplished with precision and that the residual errors result from the navigation system not the control implementation.

The techniques developed by Thurman et al[34,35] are useful in that the nonlinear element of the system is incorporated into the design of the controller thereby ensuring an acceptable performance. The principle disadvantage of the technique is that, like many nonlinear design methods, it is rather application specific and

difficult to apply to other problems. Like most Lyapunov based methods it may also be difficult to find a suitable Lyapunov function for more general systems.

The describing function technique is used by Anthony et al[1], for the nonlinear control analysis of a flexible spacecraft equipped with thrusters; in particular using the technique to analyse the effects of a pulse-modulated thruster in terms of its gain and phase for structural mode limit analysis. This is applied to a variety of pulse width control systems, including the Scmitt trigger, the Pulse-Width Pulse-Frequency Modulator, the Derived Rate modulator and a Pulse-Width Modulation technique. Noting that the describing function is a technique involving approximation the uncertainties are included as an uncertainty factor in the nonlinear control robustness analysis. Finally, the method is applied to a pulse-modulated control system of a satellite.

In the example presented the describing function method is used to successfully predict the onset of a limit cycle due to a coupling of the control system with a structural response. The technique is then used to design a compensator to eliminate this limit cycle and to avoid the instability that may result. However, like the techniques described previously developed by Thurman et al[34,35] this is rather application specific and difficult to apply to other problems.

Bernelli-Zazzera et al[4] present a method to design a Pulse-Width Modulated (PWM) controller that is equivalent to an existing Pulse-Amplitude Modulated (PAM) controller. The technique is of some merit as it enables the PAM equivalent to be

designed using a conventional linear approach and the design is later converted into a PWM system. The technique developed involves generating a PWM control input that is approximately equivalent to a PAM input by integrating the control response over a sample period. An optimum pulse delay is found which minimises the error in the dynamic response between the PAM and PWM equivalents. It is also demonstrated that if the optimum delay is achieved then the PWM system retains the stability characteristics of the PAM system. The use of the method is illustrated by two examples. The first example is a simple second order spring-mass damper and the second an antenna array mounted on a spacecraft controlled by thrusters and piezo-electric actuators.

Although this technique was developed for a thruster based application it is a general-purpose technique that may be applied to any system for which a PAM equivalent may be designed. The method is extremely simple to implement, as the pulse delay is a simple function of the state space system matrices and the sample rate.

The technique is further developed by Zimpfer et al[43] who adapt the technique to consider large inputs using a pulse weighting function to modify the pulse delay. This results in an improvement in the dynamic response of the PWM system. The modified technique is then applied to a space based application. Ieko et al[20,21] also build upon this technique and refine it further with the implementation of a digital redesign of the PWM system.

More recently Bernelli-Zazzera et al[5] have considered a further refinement of the basic technique. Rather than considering a single PWM equivalent pulse within sample period, multiple PWM pulses are now proposed. Equivalence between the PAM and multiple PWM pulses is maintained by matching the systems state response at the end of the sample period. It is demonstrated that provided a sufficient number of sampling pulses is used the degree of approximation between the two systems can be as close as desired, even at low sample rates. The principal disadvantage of the new technique is that the implementation is not as straight forward as the previous technique, since the pulse delays are no longer a simple function of the system matrices. The pulse delays must be found using an iterative procedure, although in the examples presented the solution converged within a few iterations.

2.3 Intuitive Guidance Design

In this section an "intuitive" design solution for a nonlinear autopilot/guidance system is derived by developing a guidance law that essentially imitates an existing seeker based guidance design. The design selected was the UK Mk 13/18 LGB shown in Figure 1.

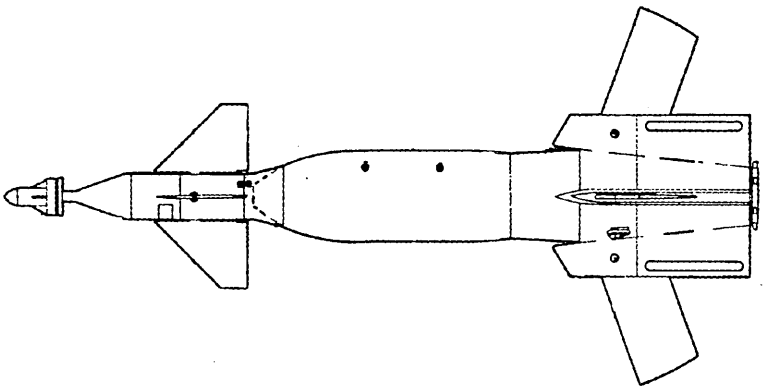

Figure 1 UK Mk 13/18 Laser Guided Bomb (Paveway II)

At the front of the weapon is the canard nose section incorporating an aero-stabilised seeker head and four cruciform canard control surfaces. Two "bang-bang" pneumatic actuators driven by either a hot or cold gas source control the canard control surfaces. The centre section is the UK 1000 lb. bomb and at the rear is an assembly incorporating four penknife-folding fins.

The guidance system is based around a four-quadrant laser seeker as shown in Figure 2, together with the canard pairs controlled by the guidance computer using seeker information. The seeker is gimballed in pitch and yaw and thus decoupled from the body dynamics and free to align itself with the local velocity vector. If the laser spot is detected in the upper quadrant the elevator canard pair are deflected in a positive sense as shown in Figure 2. Similarly if the laser spot is detected in the left-hand quadrant the rudder pair are deflected as shown in Figure 2. At the centre of the seeker is a dead band in which there is no demand from the control system. As the velocity vector diverges from the target sightline vector, the response of the control system is to deflect the canards such that the velocity vector returns to the sightline. The flight path to the target is thus approximately rectilinear with the

weapon tending to lag below the sightline. There is a tendency for this guidance loop to cause the weapon to impact short of the desired target, which is corrected for by an empirical correction in the weapon aiming solution.

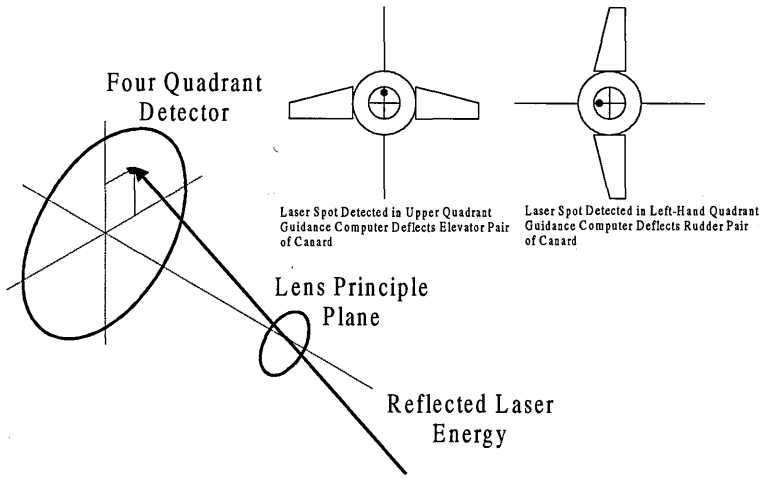

Figure 2 LGB Guidance Using Four Quadrant Detector

In order to derive the "intuitive" guidance design, the output from the INS/GPS is used to derive an artificial sightline vector. This is then transformed into a frame of reference defined by the current velocity vector and the unit error vector calculated. Noting that although the seeker is gimbaled, it is still coupled to the body in roll, the error vector is then rotated through the Euler angle in roll to define the vector in terms of its components in the pitch and yaw planes. The demanded control deflections are then derived based upon these components. This is now discussed in more detail in the following paragraphs.

There are three frames of reference used in the guidance design. The weapon position is defined in a right hand axes frame, with the origin fixed at the release point. Co-ordinates within this frame of reference are denoted by (X, Y, Z). A

velocity axes is defined by the instantaneous velocity vector; this is a right hand axis frame denoted by (X_T, Y_T, Z_T). A transformation from space to velocity axis is defined by the Euler angles (ψ_P, θ_P) as shown in Figure 4. Finally, a body fixed axis system is considered, a standard right hand axes frame with the transformation from space axes to body axes defined by the Euler angles (ψ, θ, ϕ). The Euler angle ψ represents a positive rotation about the Z-axis, this is followed by a rotation θ about the transformed Y-axis and finally a positive rotation ϕ about the transformed X axis completes the transform from space to body axes. A positive rotation is a clockwise rotation when viewed from the perspective of the negative axis looking to the positive axis.

2.3.1 Guidance Design

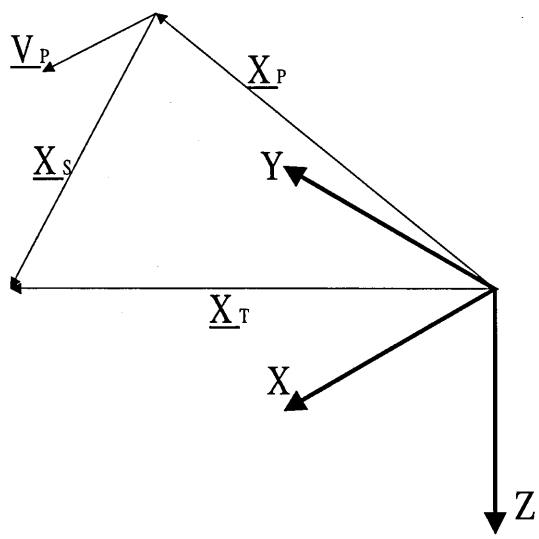

Figure 3 Weapon and Target Geometry in Space Axes

Firstly, considering the weapon and target geometry in space axes as shown in Figure 3. A right hand axes frame, centred at the release point defines the current weapon position in space. The current weapon velocity vector in space axes is

denoted by the vector, $\underline{V}_P$. The current position in space axes is denoted by the vector, $\underline{X}_P$, and the target position in space axes by the vector, $\underline{X}_T$, closing the vector loop the sightline vector in space axes is given by:

$$\underline{X}_S = \underline{X}_T - \underline{X}_P \tag{1}$$

Defining the unit vectors in space axes, $\hat{\underline{X}}_S$, and $\hat{\underline{V}}_P$, by:

$$\hat{\underline{X}}_S = \frac{\underline{X}_S}{|\underline{X}_S|} \text{ and } \hat{\underline{V}}_P = \frac{\underline{V}_P}{|\underline{V}_P|} \tag{2}$$

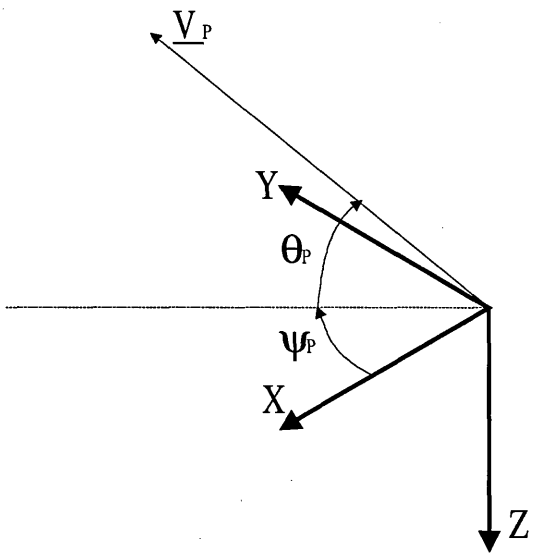

Figure 4 Transformation into Axis Defined by Velocity Vector

For now ignoring the roll axis, the velocity-based frame of reference is fixed with the x-axis aligned with the unit velocity vector. Denoting the unit velocity vector in space axes as:

$$\hat{\underline{V}}_P = \begin{bmatrix} \hat{\underline{V}}_P(1) \\ \hat{\underline{V}}_P(2) \\ \hat{\underline{V}}_P(3) \end{bmatrix} \tag{3}$$

As shown in Figure 4 the transformation from the space reference frame to the velocity reference frame is described by the Euler angles, ψ_P, and, θ_P, defined by:

$$\theta_P = \sin^{-1}(-\hat{\underline{V}}_P(3)) \tag{4}$$

$$\psi_P = \tan^{-1}\left(\frac{\hat{\underline{V}}_P(2)}{\hat{\underline{V}}_P(1)}\right) \tag{5}$$

Hence, these two angles define a transformation matrix, $\underline{M}$, from space to velocity axes given by:

$$\underline{M} = \begin{bmatrix} \cos(\psi_P).\cos(\theta_P) & \sin(\psi_P).\cos(\theta_P) & -\sin(\theta_P) \\ -\sin(\psi_P) & \cos(\psi_P) & 0 \\ \cos(\psi_P).\sin(\theta_P) & \sin(\psi_P).\sin(\theta_P) & \cos(\theta_P) \end{bmatrix} \tag{6}$$

Using the transformation the sightline vector in the velocity frame of reference may be now be derived:

$$\hat{\underline{X}}_E = \underline{M}.\hat{\underline{X}}_S \tag{7}$$

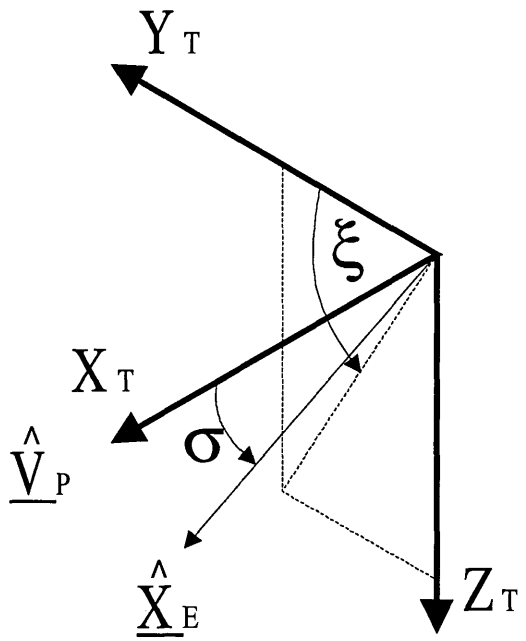

Figure 5 Sightline Angles Relative to Velocity Vector

Denoting the unit sightline vector in velocity axes as:

$$\underline{\hat{X}}_E = \begin{bmatrix} \underline{\hat{X}}_E(1) \\ \underline{\hat{X}}_E(2) \\ \underline{\hat{X}}_E(3) \end{bmatrix} \tag{8}$$

The sightline vector, shown in Figure 5, can be described by sightline angles defined as:

$$\sigma = \tan^{-1}\left(\frac{\sqrt{\underline{\hat{X}}_E^2(2) + \underline{\hat{X}}_E^2(3)}}{\underline{\hat{X}}_E(1)} \right) \tag{9}$$

$$\xi = \tan^{-1}\left(\frac{\underline{\hat{X}}_E(3)}{\underline{\hat{X}}_E(2)} \right) \tag{10}$$

Although an aero-stabilised seeker is decoupled from the body and aligned with the local velocity vector, it remains coupled to the body in roll. The sightline angle, ξ, is modified by the Euler angle in roll, ϕ, to determine the sightline vector relative to the canard planes:

$$\xi' = \xi - \phi \tag{11}$$

Finally, it is more convenient to express the error vector in terms of the components in the individual canard planes. Denoting the error in yaw by ε_Y and the error in pitch by ε_P defined by:

$$\varepsilon_Y = \tan^{-1}\{\tan(\sigma).\cos(\xi')\} \tag{12}$$

$$\varepsilon_P = \tan^{-1}\{\tan(\sigma).\sin(\xi')\} \tag{13}$$

A sightline error vector has now been derived from the navigation system equivalent to that which would be derived from the seeker. This may now be used as input to the weapon guidance computer. Hence, this signal can be used to modulate the input to the canards in order to successfully guide the weapon to the target. Denoting the threshold at which the canards are deflected by ι, the canards are modulated as:

$$\begin{cases} |\varepsilon_Y| < \iota, \varsigma = 0.0 \\ |\varepsilon_Y| \geq \iota, \varsigma = \varsigma_{MAX} \dfrac{\varepsilon_Y}{|\varepsilon_Y|} \end{cases} \tag{14}$$

$$\begin{cases} |\varepsilon_P| < \iota, \eta = 0.0 \\ |\varepsilon_P| \geq \iota, \eta = \eta_{MAX} \dfrac{\varepsilon_P}{|\varepsilon_P|} \end{cases} \quad \textbf{(15)}$$

Where: ς Demanded canard deflection in yaw.

η Demanded canard deflection in pitch.

As with the seeker based guidance algorithm upon which this design is based, the guidance is essentially open loop. The canards are deflected so as to maintain the weapon along a rectilinear flight path to the target. As the velocity vector diverts from the sightline to the target, the canards are deflected to correct the flight path.

In order to demonstrate this as a viable guidance algorithm it has been incorporated into a six degree of freedom trajectory simulation code. A typical trajectory is presented in Figure 6 for a straight and level weapon release from 20,000 ft at Mach 0.85.

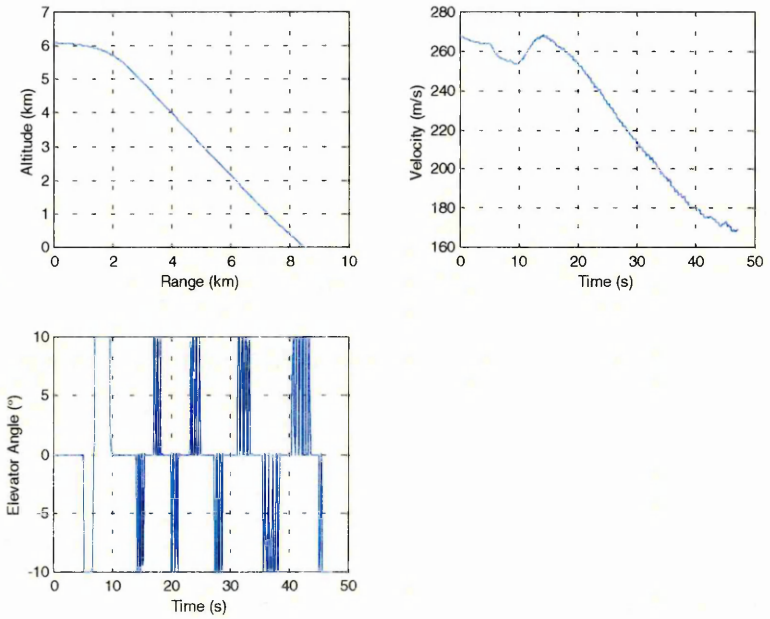

Figure 6 Typical Trajectory Using "Bang-Bang" Control System

Referring to Figure 6 the following points should be noted. First of all the flight path is very nearly rectilinear and is not energy efficient, therefore the impact velocity is compromised and ultimately range reduced. Secondly, the impact angle is relatively shallow, increasing the chance of ricochet or failure to penetrate a hard target. It would be advantageous for the weapon design to take advantage of the additional information from the navigation system in order to control both impact velocity and impact angle, together with a more energy efficient trajectory to maximise range. This could of course be accomplished by replacing the existing actuation system with a proportional actuator, thereby simplifying the autopilot design but this has significant cost implications. It would be of advantage to the weapon designer to be able to use an autopilot loop that incorporated the existing 'bang-bang' actuator.

One final point is worth noting, the system is almost exclusively reliant on position information. Position information would be available in a system that incorporated GPS, with the additional of a roll reference would be sufficient for this design to function. There is the potential therefore for a simplified guidance system to be proposed using GPS, with the inertial pack reduced to a single rate or position gyro. However, such a system would be vulnerable to GPS jamming/spoofing.

2.4 Linear Autopilot Design

2.4.1 Airframe Response

This section describes the design of a simple autopilot loop, around which the PWM control design is based. It is essentially a standard accelerometer/rate sensor based autopilot loop. A state space technique is applied that is used to select the accelerometer and rate gyro gains to achieve the required second order response in the control loop.

It is assumed that the weapon is axi-symmetric and there is no cross-coupling between the pitch and yaw planes. This is a reasonable assumption for small incidences (pitch incidences below 10°) and is characteristic of typical air-to-ground weapons. It is also assumed that a skid-to-turn autopilot is to be used and that based upon these assumptions the pitch and yaw planes may be considered separately.

It is further assumed that given the weapon is axi-symmetric the same autopilot design may be used in both planes. Using the assumption of small incidence angles

the lateral response of the airframe be described by a pair of first order simultaneous differential equations:

$$M.a_y = Y_v.v + Y_r.r + Y_\zeta.\zeta \tag{16}$$

$$I_{ZZ}.\dot{r} = N_v.v + N_r.r + N_\zeta.\zeta \tag{17}$$

Noting Euler's equation for a rotating body and dividing equation **(16)** by the weapon mass, M, and equation **(17)** by the weapon inertia, I_{ZZ}, the airframe response to a control input may be expressed in state space form as:

$$\begin{bmatrix}\dot{v}\\ \dot{r}\end{bmatrix} = \begin{bmatrix}y_v & (y_r - U)\\ n_v & n_r\end{bmatrix}\begin{bmatrix}v\\ r\end{bmatrix} + \begin{bmatrix}y_\zeta\\ n_\zeta\end{bmatrix}\zeta \tag{18}$$

The output required is the achieved acceleration and hence the system measurement equation is:

$$a_y = \begin{bmatrix}y_v & y_r\end{bmatrix}\begin{bmatrix}v\\ r\end{bmatrix} + \begin{bmatrix}y_\zeta\end{bmatrix}\zeta \tag{19}$$

For convenience equation **(18)** is written as:

$$\dot{\underline{x}} = A\underline{x} + Bu \tag{20}$$

And equation **(19)** as:

$$y = C\underline{x} + Du \tag{21}$$

2.4.2 Instrument Equation

An inertial measuring unit (IMU) comprising of three accelerometers and three rate gyroscopes is placed at a known location in the weapon. The position vector of the IMU in the body axis is denoted by $\underline{r}_{A/B}$ as illustrated in Figure 7.

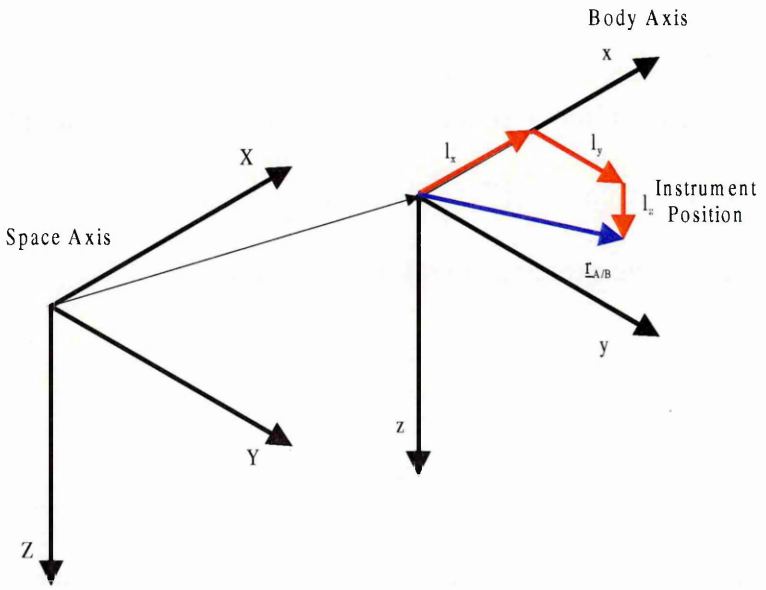

Figure 7 Missile Instrument Position Relative to Weapon c.g. Position

Denoting the angular rate vector in body axes by:

$$\underline{\Omega} = \begin{bmatrix} p \\ q \\ r \end{bmatrix} \tag{22}$$

The weapon velocity in body axes by:

$$\underline{v} = \begin{bmatrix} U \\ v \\ w \end{bmatrix} \tag{23}$$

The acceleration vector at the IMU is:

$$\underline{a} = \underline{a}_B + \dot{\underline{\Omega}} \times \underline{r}_{A/B} + \underline{\Omega} \times \left(\underline{\Omega} \times \underline{r}_{A/B} \right) + 2\underline{\Omega} \times \underline{v}_{REL} + \underline{a}_{REL} \tag{24}$$

Where the subscript REL denotes the relative movement of the IMU with respect to the weapon c.g. Assuming a rigid structure, equation **(24)** reduces to:

$$\underline{a} = \underline{a}_B + \dot{\underline{\Omega}} \times \underline{r}_{A/B} + \underline{\Omega} \times \left(\underline{\Omega} \times \underline{r}_{A/B} \right) \tag{25}$$

Expanding equation **(25)**:

$$\underline{a} = \begin{bmatrix} a_x + \left(\dot{q}.l_z - \dot{r}.l_y \right) + q.\left(p.l_y - q.l_x \right) + r.\left(p.l_z - r.l_x \right) \\ a_y + \left(\dot{r}.l_x - \dot{p}.l_z \right) - p.\left(p.l_y - q.l_x \right) + r.\left(q.l_z - r.l_y \right) \\ a_z + \left(\dot{p}.l_y - \dot{q}.l_x \right) - p.\left(p.l_z - r.l_x \right) - q.\left(q.l_z - r.l_y \right) \end{bmatrix} \tag{26}$$

Generally the IMU is placed close to the weapon axis, hence $l_y \approx 0$, $l_z \approx 0$, hence:

$$\underline{a} = \begin{bmatrix} a_x - q^2.l_x - r^2.l_x \\ a_y + \dot{r}.l_x + p.q.l_x \\ a_z - \dot{q}.l_x + p.r.l_x \end{bmatrix} \tag{27}$$

Finally considering only the lateral plane, i.e. $p = q = 0$, the acceleration measured by the accelerometer is:

$$\bar{a}_y = a_y + \dot{r}.l_x \tag{28}$$

Hence, the instrument measurement equation may be expressed as:

$$\begin{bmatrix} \bar{a}_y \\ \dot{\bar{r}} \end{bmatrix} = \begin{bmatrix} (y_v + l_x.n_v) & (y_r + l_x.n_r) \\ 0 & 1 \end{bmatrix} \begin{bmatrix} v \\ r \end{bmatrix} + \begin{bmatrix} (y_\zeta + l_x.n_\zeta) \\ 0 \end{bmatrix} \zeta \tag{29}$$

For convenience let this be denoted by:

$$\underline{z} = E.\underline{x} + F.u \tag{30}$$

2.4.3 Gain Selection

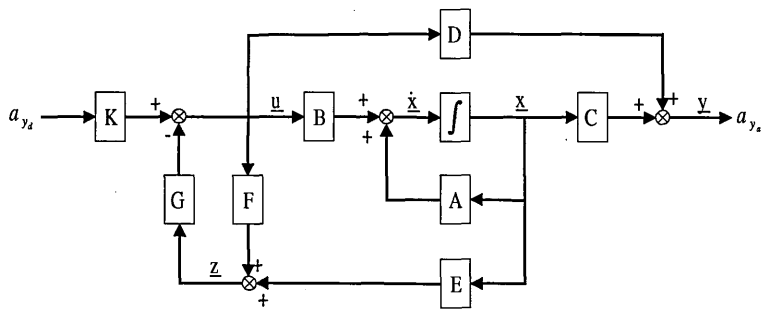

Figure 8 Autopilot Block Diagram

The autopilot design using state feedback is shown in Figure 8, noting that for the moment actuator dynamics have been ignored. The input is the demanded acceleration; the desired autopilot characteristics are determined by suitable selection of the gain matrix G. Overall unity gain for the autopilot is maintained by the gain K. The gain matrix G is defined as:

$$G = [K_A \quad K_G] \tag{31}$$

Referring to Figure 8 the input to the airframe is given by:

$$u = K.a_{y_d} - G.\underline{z} \tag{32}$$

Substituting for z from equation **(30)** and re-arranging gives:

$$u = (1+G.F)^{-1}.\left(K.a_{y_d} - G.E.\underline{x}\right) \tag{33}$$

Substituting equation **(33)** into equation **(20)** gives:

$$\dot{\underline{x}} = \left(A - B(1+G.F)^{-1}.G.E\right)\underline{x} + B.(1+G.F)^{-1}.K.a_{y_d} \tag{34}$$

Similarly for the output equation:

$$\underline{y} = \left(C - D.(1+G.F)^{-1}.GE\right)\underline{x} + D.(1+G.F)^{-1}.K.a_{y_d} \tag{35}$$

Considering some of the matrix terms separately:

$$\begin{aligned}(1+G.F)^{-1} &= \left\{1+\begin{bmatrix}K_A & K_G\end{bmatrix}\begin{bmatrix}\left(y_\varsigma + l_x.n_\varsigma\right)\\ 0\end{bmatrix}\right\}^{-1} \\ &= \left(1+K_A\cdot\left(y_\varsigma + l_x.n_\varsigma\right)\right)\end{aligned} \tag{36}$$

And:

$$\begin{aligned}G.E &= \begin{bmatrix}K_A & K_G\end{bmatrix}\begin{bmatrix}\left(y_v + l_x.n_v\right) & \left(y_r + l_x.n_r\right)\\ 0 & 1\end{bmatrix} \\ &= \begin{bmatrix}K_A\cdot\left(y_v + l_x.n_v\right) & K_A\cdot\left(y_r + l_x.n_r\right) + K_G\end{bmatrix}\end{aligned} \tag{37}$$

And for convenience let $G.E = \begin{bmatrix}K_1 & K_2\end{bmatrix}$:

Noting that equation **(36)** is a scalar

$$B.(1+G.F)^{-1}.G.E = \frac{1}{1+K_A.\left(y_\zeta + l_x.n_\zeta\right)}\begin{bmatrix} K_1.y_\zeta & K_2.y_\zeta \\ K_1.n_\zeta & K_2.n_\zeta \end{bmatrix} \tag{38}$$

Which for convenience is re-written as:

$$B.(1+G.F)^{-1}.G.E = \begin{bmatrix} K_1'.y_\zeta & K_2'.y_\zeta \\ K_1'.n_\zeta & K_2'.n_\zeta \end{bmatrix} \tag{39}$$

And hence the closed loop system matrix is:

$$A - B.(1+G.F)^{-1}.G.E = \begin{bmatrix} y_v - K_1'.y_\zeta & y_r - U - K_2'.y_\zeta \\ n_v - K_1'.n_\zeta & n_r - K_2'.n_\zeta \end{bmatrix} \tag{40}$$

The characteristic equation is given by:

$$\left|s.I - \left(A - B.(1+G.F)^{-1}.G.E\right)\right| = 0 \tag{41}$$

Expanding equation **(41)** results in a Laplace equation. Substituting the term α for $\left[n_\zeta.y_v - n_v.y_\zeta\right]$ (this term is commonly used in autopilot design), results in:

$$\begin{aligned} &s^2 + \left(K_1'.y_\zeta - y_v + K_2'.n_\zeta - n_r\right)s + \\ &\left(U.n_v - y_r.n_v + y_v.n_r + K_1'.\left(y_r.n_\zeta - U.n_\zeta - y_\zeta.n_r\right) - K_2'.\alpha\right) = 0 \end{aligned} \tag{42}$$

The autopilot design parameters are expressed in terms of the required second order response, i.e. to meet a desired characteristic equation in terms of the required bandwidth, $\omega_{A/P}$, and damping ratio, $\varsigma_{A/P}$. The desired characteristic equation is:

$$s^2 + 2\zeta_{A/P}\omega_{A/P}s + \omega_{A/P}^2 \tag{43}$$

Comparing equations **(42)** and **(43)** two simultaneous equations are obtained for K_1' and K_2' which are solved using an iterative procedure. Assuming some typical values for a missile taken from Garnell and East[10], which are given in Table 1.

Table 1 Missile Characteristics

Derivative	Value
y_v	-3
y_r	0
y_ζ	180
n_v	1
n_r	-3
n_ζ	-500
U	500
l_x	0.5

Substituting into equation **(42)** the following is obtained:

$$s^2 + \left(6 + 180K_1' + 500K_2'\right).s + \left(509 + 25{,}540K_1' + 500K_2'\right)$$

Noting that the term in S_0 is dominated by K_1' an approximate value is obtained from:

$$K_1' \approx \frac{-y_r.n_v + U.n_v + y_v.n_r - \omega_{A/P}^2}{y_\zeta.n_r + U.n_\zeta - y_r.n_\zeta} \tag{44}$$

And from the term in S_1 an initial estimate of K_2' is:

$$K_2' = \frac{2\zeta_{A/P}\omega_{A/P} + y_v + n_r - K_1'.y_\zeta}{n_\zeta} \tag{45}$$

A solution is then found by iterating using:

$$K_1' = \frac{-y_r.n_v + U.n_v + y_v.n_r - \omega_{A/P}^2 - K_2'.\alpha}{y_\zeta.n_r + U.n_\zeta - y_r.n_\zeta} \tag{46}$$

Hence, noting:

$$\begin{aligned} K_1' &= \frac{K_1}{1 + K_A \cdot \left(y_\varsigma + l_x.n_\varsigma\right)} = \frac{K_A \cdot \left(y_v + l_x.n_v\right)}{1 + K_A \cdot \left(y_\varsigma + l_x.n_\varsigma\right)} \\ \Rightarrow K_A &= \frac{K_1'}{\left(y_v + l_x.n_v\right) - K_1' \cdot \left(y_\varsigma + l_x.n_\varsigma\right)} \end{aligned} \tag{47}$$

And:

$$\begin{aligned} K_2' &= \frac{K_2}{1 + K_A.\left(y_\zeta + l_x.n_\zeta\right)} = \frac{K_A.\left(y_r + l_x.n_r\right) + K_G}{1 + K_A.\left(y_\zeta + l_x.n_\zeta\right)} \\ \Rightarrow K_G &= K_2'.\left(1 + K_A.\left(y_\zeta + l_x.n_\zeta\right)\right) - K_A.\left(y_r + l_x.n_r\right) \end{aligned} \tag{48}$$

The steady state autopilot gain should be unity hence:

$$\begin{aligned} 0 &= \left(A - B.(1 + G.F)^{-1}.G.E\right)\underline{x} + B.(1 + G.F)^{-1}.K.a_{y_d} \\ \Rightarrow \underline{x} &= -\left(A - B.(1 + G.F)^{-1}.G.E\right)^{-1}.B.(1 + G.F)^{-1}.K.a_{y_d} \end{aligned} \tag{49}$$

From the output equation:

$$a_{y_a} = \left(C - D\cdot(1+G\cdot F)^{-1}G\cdot E\right)\underline{x} + D\cdot(1+G\cdot F)^{-1}K.a_{y_d}$$

$$\Rightarrow \left.\frac{a_{y_a}}{a_{y_d}}\right|_{ss} = 1 \qquad \textbf{(50)}$$

$$\Rightarrow K = \left\{\begin{matrix}-\left(C - D\cdot(1+G\cdot F)^{-1}G\cdot E\right)\cdot\left(A - B\cdot(1+G\cdot F)^{-1}G\cdot E\right)\cdot B\cdot(1+G\cdot F)^{-1} \\ +D\cdot(1+G\cdot F)^{-1}\end{matrix}\right\}^{-1}$$

This section has presented the derivation of the underlying theory behind a basic analytical technique to find the autopilot gains required to meet a given set of characteristics, expressed as the desired second order response. The use of this technique was confirmed using simulations in SIMULINK using the block diagram shown in Figure 9.

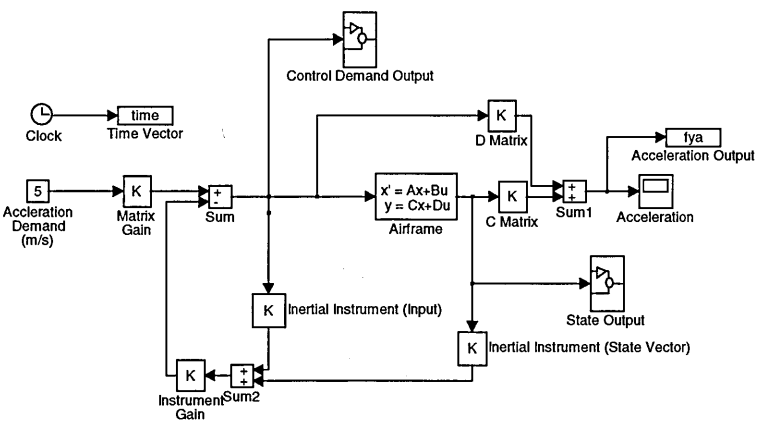

Figure 9 Linear Autopilot Design Using State Feedback

Using MATLAB/SIMULINK the effect of instrument position was examined over the range ±0.5 m from the c.g., the desired autopilot characteristics being a bandwidth of 5 Hz and damping ratio of 0.7. The results are shown in Figures 10 to 13.

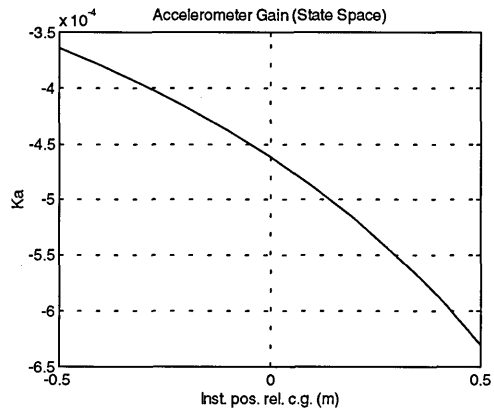

Figure 10 Accelerometer Gain as a Function of Instrument Position

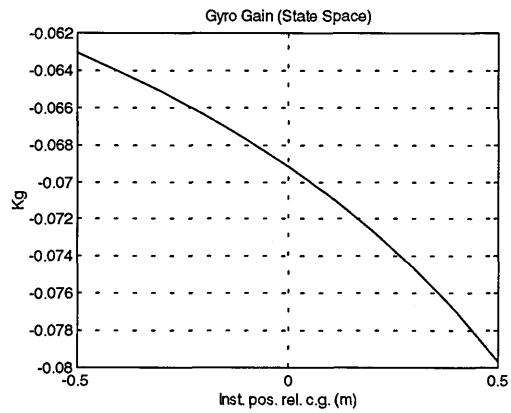

Figure 11 Gyro Gain as a Function of Instrument Position

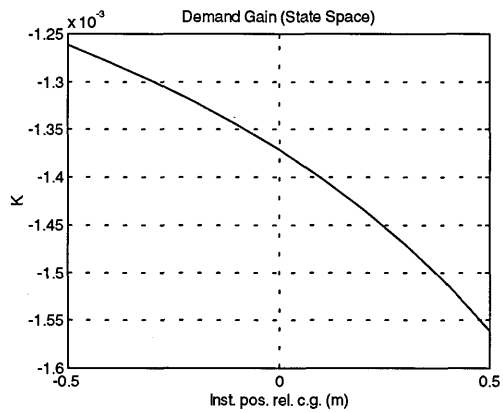

Figure 12 Demand Gain as a Function of Instrument Position

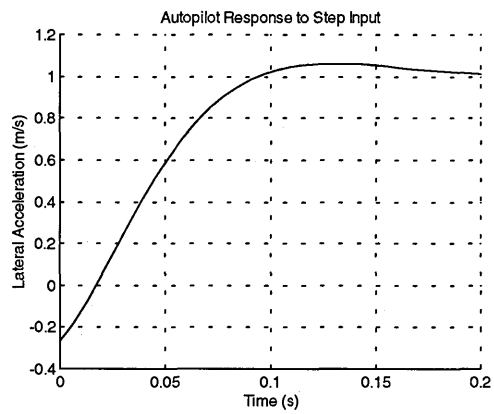

Figure 13 Autopilot Response as a Function of the Instrument Position

As might be expected the accelerometer gain is sensitive to instrument position, K_A nearly doubles as the instruments move over the range ±0.5 m. K_G and K are both less sensitive to instrument position. Referring now to Figure 13 it can be seen that the required second order response is obtained with an overshoot of 6.13% and the first peak occurs at 0.13 s, i.e. the system has achieved the required second order response. This was confirmed using MATLAB to find the eigenvalues of the characteristic equation.

2.5 Actuator Model

All of the simulations involving an actuator assume a brushless DC motor so that simulations may be compared directly. This section first of all describes the development of a linear model of a conventional proportional actuator and the modification of this model to represent a "bang-bang" actuator. The impact of air loads is not considered in either case.

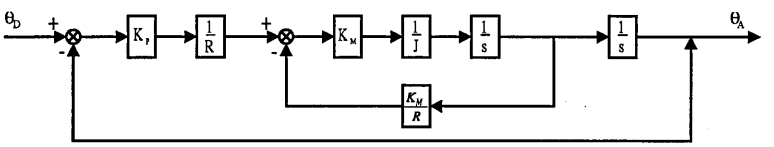

Figure 14 Block Diagram of Actuator Module

Figure 14 shows a block diagram for a conventional actuator based upon a brushless DC motor. The voltage applied at the motor is:

$$V = K_P.(\theta_D - \theta_A) \tag{51}$$

A counter e.m.f. is induced by the rotation of the motor and hence:

$$V = I.R + K_M.\omega \tag{52}$$

The torque developed by the motor is thus:

$$T = K_M.I = \frac{K_M}{R}.V - \frac{K_M^2}{R}.\omega \tag{53}$$

Hence, the rotational acceleration of the actuator is:

$$T = J.\frac{d\omega}{dt} = \frac{K_M}{R}.K_P.(\theta_D - \theta_A) - \frac{K_M^2}{R}.\omega \tag{54}$$

Which can be re-written as a second order differential equation:

$$J.\frac{d^2\theta_A}{dt^2} + \frac{K_M^2}{R}.\frac{d\theta_A}{dt} + \frac{K_M.K_P}{R}.\theta_A = \frac{K_M.K_P}{R}.\theta_D \tag{55}$$

Often a reduction gearbox may be added, this modifies the above equation by the gear ratio, K_{GB}:

$$J.\frac{d^2\theta_A}{dt^2} + \frac{K_M^2}{R}.\frac{d\theta_A}{dt} + \frac{K_M.K_P}{R.K_{GB}}.\theta_A = \frac{K_M.K_P}{R.K_{GB}}.\theta_D \tag{56}$$

Both of these equations can be used to define a second order transfer function which represents the actuator response i.e.:

$$\frac{\theta_A}{\theta_D} = \frac{\omega_n^2}{s^2 + 2\zeta_n\omega_n s + \omega_n^2} \tag{57}$$

Or in State Space form:

$$\begin{bmatrix} \dot{\theta}_A \\ \ddot{\theta}_A \end{bmatrix} = \begin{bmatrix} 0 & 1 \\ -\omega_n^2 & -2\zeta_n\omega_n \end{bmatrix} \begin{bmatrix} \theta_A \\ \dot{\theta}_A \end{bmatrix} + \begin{bmatrix} 0 \\ \omega_n^2 \end{bmatrix} \theta_D \tag{58}$$

A "bang-bang" actuator is different in that there is no resolution of the achieved deflection and therefore no position feedback. Rather than apply a voltage to the motor proportional to the error, the maximum voltage is applied as a step input in response to a demand. The motor is then driven to the end stops and held there by

the motor torque. Such a response is clearly nonlinear and nonlinear characteristics such as torque limiting, rate limiting and deflection limits must be included.

It should be noted that both models are essentially identical if the feedback loop is ignored, a simple actuator model was therefore developed that considered only the motor response. This could then be used in either case, with the feedback loop removed to model the "bang-bang" system.

Correctly modelling actuator nonlinearities is not a simple problem and as Thomasson[33] notes modern control tools enable such nonlinearities to be modelled incorrectly all too easily. The method presented involves the recognition of the piecewise continuous nature of the problem and that the correct governing equations for each regime. Figure 15 illustrates the transition diagram for a second order response which may be described by a single set of differential equations.

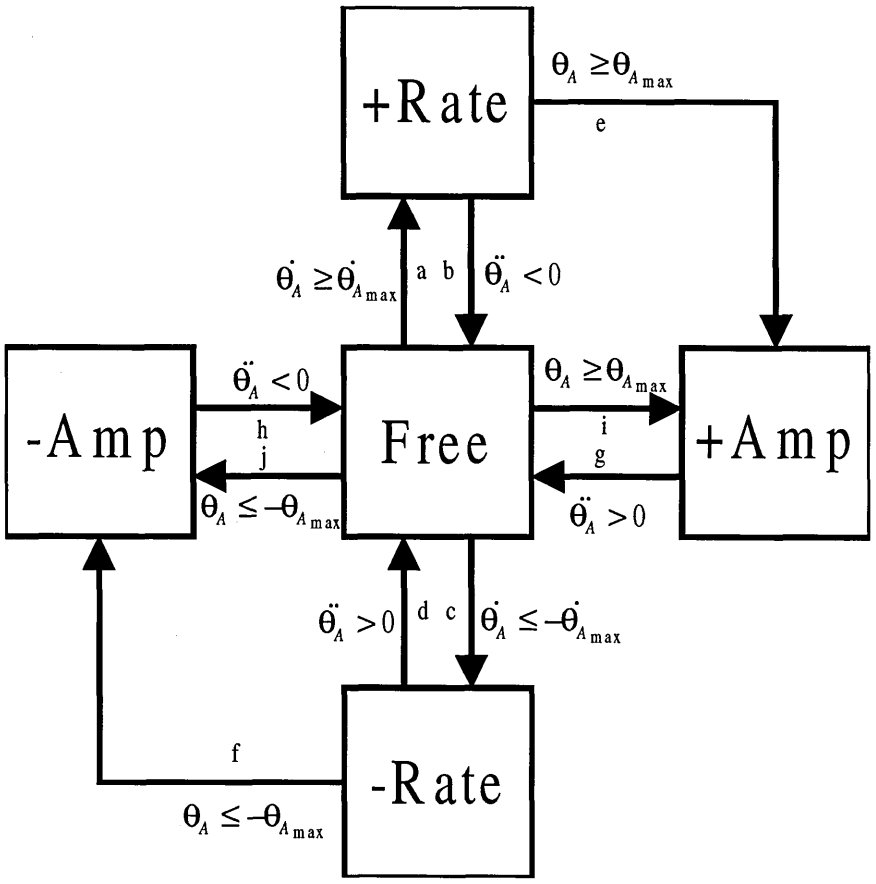

Figure 15 Transition Between Limits in Actuator Model

Thomasson[33] assumes a proportional actuator with position feedback and considers the second order response in equation **(58)**, hence the differential equations have therefore to be modified in order to model a "bang-bang" actuator. This is summarised in the Table 2.

Table 2 Transition Between Regimes for Nonlinear Actuator Systems

Path	Transition	Criterion	Action
a	Free to Positive Rate Limit	$\dot{\theta}_A \geq \dot{\theta}_{A_{max}}$	Set input to acceleration integrator to 0.0.
b	Positive Rate Limit to Free	$\ddot{\theta}_A < 0$	Set input to acceleration integrator to $\ddot{\theta}_A$
c	Free to Negative Rate Limit	$\dot{\theta}_A \leq -\dot{\theta}_{A_{max}}$	Set input to acceleration integrator to 0.0
d	Negative Rate Limit to Free	$\ddot{\theta}_A > 0$	Set input to acceleration integrator to $\ddot{\theta}_A$
e	Positive Rate to Positive Deflection Limit	$\theta_A \geq \theta_{A_{max}}$	Set input to acceleration integrator. Set input to rate integrator to 0.0. Reset rate integrator to 0.0.
f	Negative Rate to Negative Deflection Limit	$\theta_A \leq -\theta_{A_{max}}$	Set input to acceleration integrator. Set input to rate integrator to 0.0. Reset rate integrator to 0.0.
g	Positive Deflection Limit to Free	$\ddot{\theta}_A < 0$	Set input to acceleration integrator to $\ddot{\theta}_A$
h	Negative Deflection Limit to Free	$\ddot{\theta}_A > 0$	Set input to acceleration integrator to $\ddot{\theta}_A$
i	Free to Positive Deflection Limit	$\theta_A \geq \theta_{A_{max}}$	Set input to rate integrator to 0.0. Reset integrator to 0.0
j	Free to Negative Deflection Limit	$\theta_A \leq -\theta_{A_{max}}$	Set input to rate integrator to 0.0. Reset integrator to 0.0

Figure 17 shows the implementation of this logic in a SIMULINK simulation; Figure 16 shows the results of a simulation where the deflection demand is a sine wave of amplitude 15°. The simulation shows the effect of deflection and rate limiting are simulated in the correct manner.

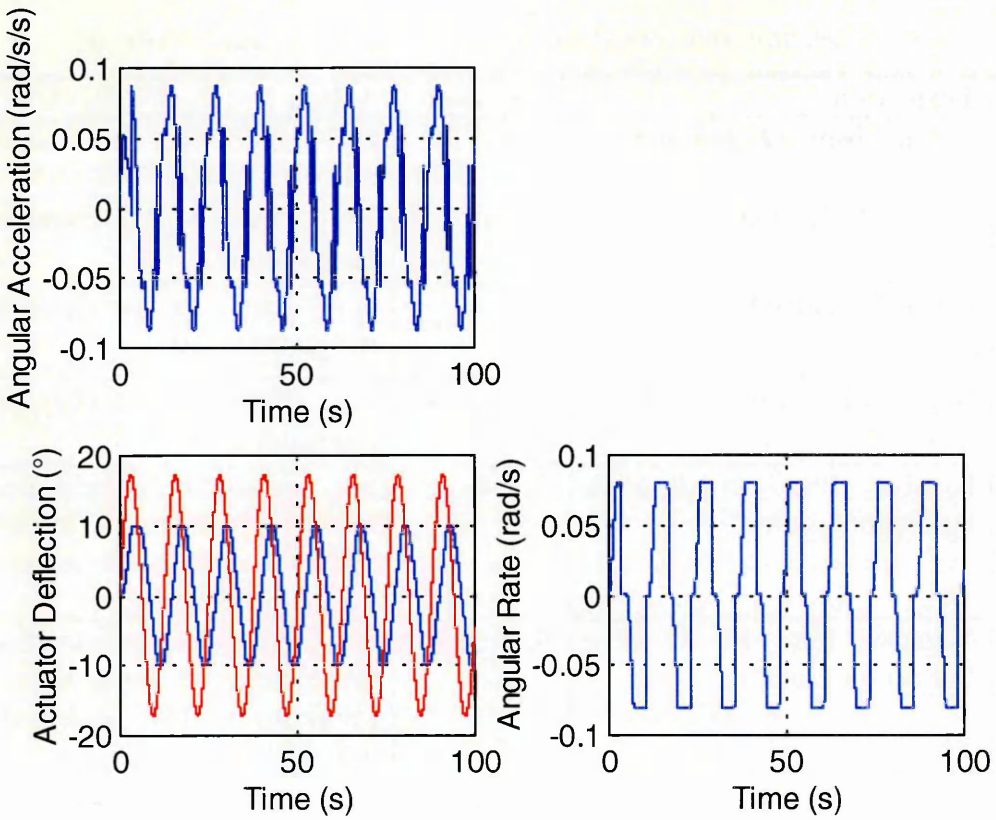

__ Demanded Deflection __ Achieved Deflection

Figure 16 Effect of Rate and Deflection Limits on Actuator Response

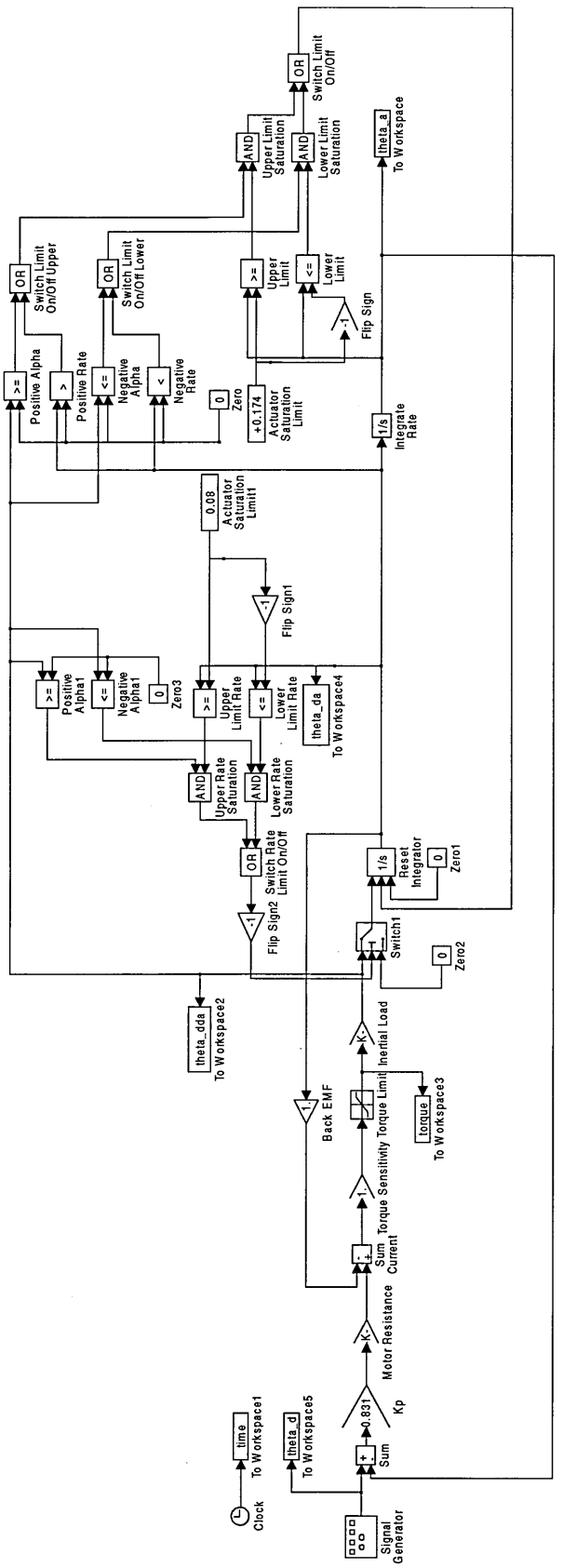

Figure 17 Nonlinear Actuator Model

Finally in developing a "bang-bang" actuator model it is recognised that this has three set positions, these being maximum positive deflection, zero and maximum negative deflection. Clearly the model above will simulate the upper and lower bounds but it will not model the zero deflection correctly. This was overcome by modelling the actuator as two separate motors with the upper limit of one being zero, with the other having the lower limit at zero. A fin controller was designed which flipped between the two models as this limit was encountered. The controller is shown in schematic form in Figure 18.

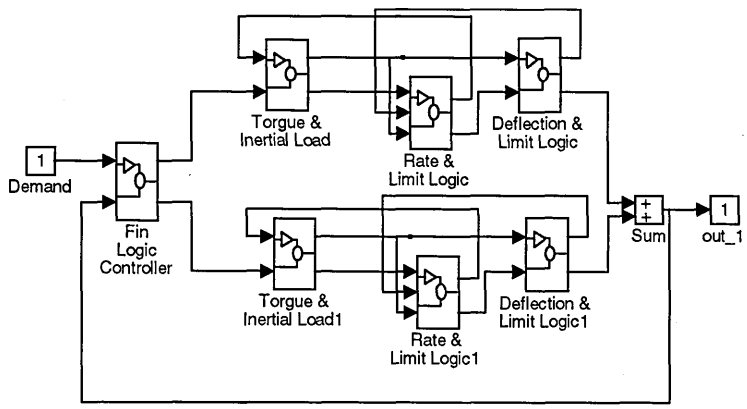

Figure 18 "Bang-Bang" Fin Controller

2.6 Sliding Control

The first technique considered was the use of Phase Plane analysis. This has been successfully used by Rogers et al[29] in an autopilot design for a conventional air intercept missile augmented by pulsed thrusters at the centre of gravity (c.g.). The system utilises proportional navigation as the guidance system, Rogers performs a double integration of the error between the demanded lateral acceleration and the achieved acceleration. A simple switching line divides the two integral variables and as the error propagates in the phase plane the thrusters are pulsed to drive the

error to zero. Rogers successfully demonstrates that this simple design is capable of drastically reducing miss distance in the end game.

Initially it was considered that this might be a technique that could possibly be used for a canard actuator system, using acceleration feedback from the IMU to define the switching line. Further investigation showed that this technique was impractical for this application. The simple design postulated by Rogers above simply considered the effect of thrusters mounted at the c.g. Application of the thruster thus directly affects the lateral acceleration with the disturbance in pitch rate compensated for by the rate feedback loop in the autopilot. In this application there is no autopilot and so the switching line concept used by Rogers is not applicable since it does not consider the yaw rate response of the airframe.

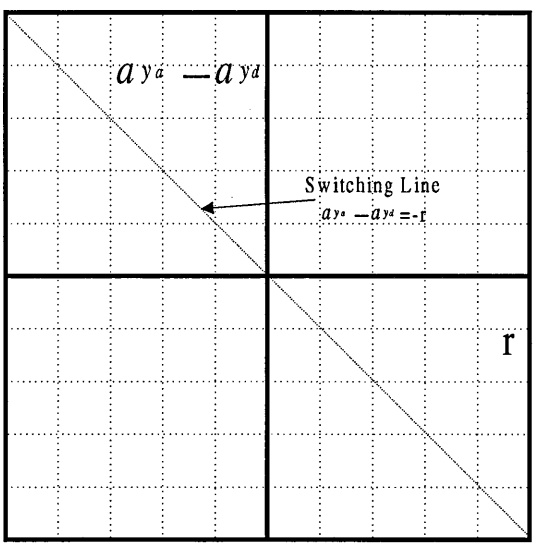

Figure 19 Switching Line Proposed for "Bang-Bang" Control

A similar concept was advanced where the phase plane variables were the yaw rate and the error in the lateral lateral acceleration. A switching line was postulated, shown in Figure 19, in order to drive the error to zero. However, simulation using

SIMULINK showed that this resulted in a large limit cycle with the weapon oscillating in pitch. Further refinements to the switching line could have reduced the limit cycle; however, the fact remains that the loop is dependent upon the open loop airframe response. The airframe bandwidth is low, the response lightly damped and the bandwidth is a function of Mach number, altitude and local temperature. In order to work satisfactorily this would require a great deal of *a priori* knowledge, additional instrumentation and produce a system whose performance would at best be marginal. It was therefore concluded that this technique is not readily applicable to this particular design problem.

2.7 Pulse-Width Modulation Control

As a numerical experiment the standard autopilot loop shown in Figure 8 was modified. Rather than the proportional input to the airframe demanded by the control system the airframe input was modulated to a fixed value (±10° Rudder); the sign of which was determined by the proportional input. Surprisingly for such a crude modification the autopilot loop worked well, a typical result is shown in Figure 20. Since it appeared that Pulse-Width Modulation (PWM) offered a simple means of controlling the nonlinear system this was considered further.

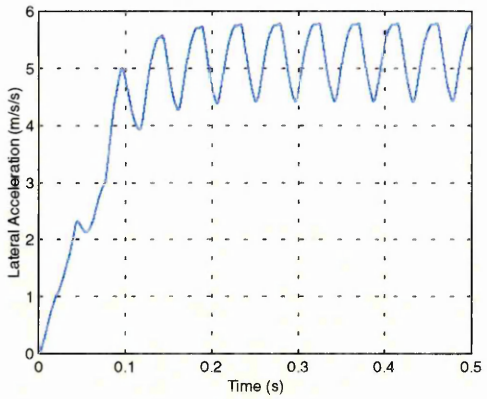

Figure 20 Autopilot Response to Simple PWM Input

The literature survey failed to find a single example where this has been used successfully in this particular application. Most of the available reference sources considered concentrated on spacecraft controlled by pulsed thrusters and many control designs were application specific. After considering a number of the literature sources the concept produced by Bernelli-Zazzera et al[4] was selected for further study. The concept used considers a control system designed to use a conventional Pulse-Amplitude Modulated (PAM) input. This may of course be designed using a conventional linear design method. Bernelli-Zazzera et al[4] develop the concept of an equivalent PWM input where both inputs are of equal area together with a pulse delay to minimise the error dynamics between the PWM and PAM inputs. This concept was further developed by Zimpfer et al[43] introducing a weighting factor to compensate for large PAM inputs. Both concepts were further refined by Ieko et al[20] who introduce the concept of a PWM design developed from a discrete time system.

The study concentrated on using the technique as originally developed by Bernelli-Zazzera et al[4] and later introduced the refinements proposed by Zimpfer et al[43].

2.7.1 Pulse-Width Modulation Controller Design

The technique used in the controller design is based upon that originally developed by Bernelli-Zazzera et al[4]. However, the detail included in the paper was limited and the derivation presented here includes additional detail beyond that of the original paper. The design of the controller also includes the improvements suggested by Zimpfer et al[43].

Assuming the state space equations in the standard format defined by Dutton et al[9], i.e.:

$$\dot{\underline{x}} = A\underline{x} + B\underline{u} \tag{59}$$

$$\underline{y} = C\underline{x} + D\underline{u} \tag{60}$$

The full solution of the state space variables as a function of time is:

$$\underline{x}(t) = \Phi(t)\underline{x}(0) + \int_0^t \Phi(t-\tau).B.\underline{u}(\tau).d\tau \tag{61}$$

And assuming a zero order hold the PAM response may be expressed by expressing the above equation in discrete form:

$$\underline{x}_{k+1} = \Phi(h)\underline{x}_k + \Delta(h)\underline{u}_k \tag{62}$$

Where:

$$\Phi(h) = e^{Ah} = I + Ah + \frac{A^2h^2}{2!} + \frac{A^3h^3}{3!} + ... \tag{63}$$

$$\Delta(h) = A^{-1}(\Phi(h) - I)B = \left[I + \frac{Ah}{2!} + \frac{A^2h^2}{3!} + ... \right] Bh \tag{64}$$

Introducing the notation $\Psi(h)$ where:

$$\Psi(h) = \sum_{i=0}^{\infty} \frac{A^i h^i}{(i+1)!} \tag{65}$$

The discrete response can be written as:

$$\underline{x}_{k+1} = \Phi(h)\underline{x}_k + \Psi(h)B\underline{u}_k h \tag{66}$$

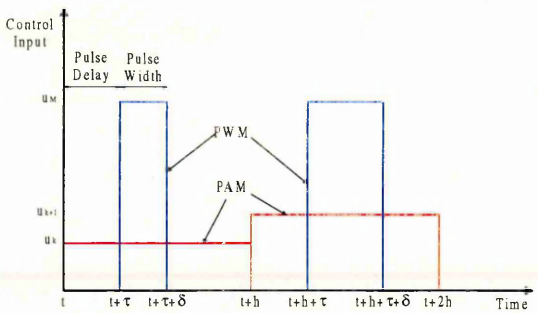

Figure 21 Pulse-Amplitude Modulated and Equivalent Pulse-Width Modulated Inputs

Referring now to Figure 21 and considering a single input to the system. In the PAM input the input, u, is held constant over the sample period, h. The design of the PWM controller seeks to find an equivalent PWM input that will minimise the error in the dynamic response by solving for the two unknowns i.e. the pulse width, δ, and the delay from the sampling instant, τ.

Assuming that the pulse width is small, the state transition matrix can be expressed in discrete form as:

$$e^{-A\delta} \approx I - A\delta \tag{67}$$

Using this assumption and returning to the solution of the state space equations in the time domain it can be shown that the response to PWM input is:

$$\underline{x}_{k+1} = \Phi(h)\underline{x}_k + e^{A(h-\tau)}Bu_M\delta \tag{68}$$

Comparison of the two responses shows that there are no differences in the state transition matrix, however, there are major differences in the input term.

Considering now the steady state response to the PAM input. In the steady state:

$$\underline{x}_{k+1} = \underline{x}_k = -A^{-1}Bu \tag{69}$$

There is no direct equivalent for the PWM input since the input cannot be constant over the sampling period, hence the state vector cannot be constant. It would desirable, however, if the average value of the state vector over the sampling period was to approach the steady state value of the equivalent PAM system. Over the sample period the average value of the state vector is:

$$\bar{\underline{x}} = \frac{1}{h}\int_{t}^{t+h} \underline{x}(\lambda)d\lambda \tag{70}$$

Evaluating the integral:

$$\underline{\bar{x}} = -\frac{1}{h}A^{-1}Bu_M\delta \tag{71}$$

Comparing the two responses it can be seen that the time averaged response of the PWM will be equivalent to the PAM system provided that the following condition is satisfied:

$$uh = u_M\delta \tag{72}$$

I.e. the time average response of the system to input, whether PWM or PAM, will be the same regardless of the pulse delay provided the area of each pulse is equivalent. Hence, the pulse duration can be simply derived by equating the area of the two pulses.

Now a pulse delay, τ, is derived that minimises the error vector between the two inputs. Noting the above result the error vector may be written as:

$$\underline{e} = \left[\Psi(h) - e^{A(h-\tau)}\right]Bu_M\delta \tag{73}$$

Which can be expressed as a series:

$$\underline{e} = -\sum_{i=1}^{\infty}\frac{A^i\left[(i+1).(h-\tau)^i - h^i\right]}{(i+1)!}Bu_M\delta \tag{74}$$

The error in the dynamic response is proportional to the integral of the error over the sampling period. To consider how the error is related to the pulse delay consider

three values, τ=0, τ=h-δ and finally τ=h/2. First of all considering a zero delay, the error vector reduces to:

$$\underline{e} = -\sum_{i=1}^{\infty} \frac{A^i h^i i}{(i+1)!} B u_M \delta \tag{75}$$

Now considering τ=h-δ:

$$\underline{e} = -\sum_{i=1}^{\infty} \frac{A^i \left[(i+1).\delta^i - h^i\right]}{(i+1)!} B u_M \delta \tag{76}$$

And further assuming that h>>δ this reduces to:

$$\underline{e} = +\sum_{i=1}^{\infty} \frac{A^i h^i}{(i+1)!} B u_M \delta \tag{77}$$

Now consider the pulse delayed to half the sampling period and further assume that h>>τ

$$\underline{e} = -\sum_{i=1}^{\infty} \frac{A^i \left[(i+1).(h/2)^i - h^i\right]}{(i+1)!} B u_M \delta \tag{78}$$

The results show that depending upon the pulse delay the error vector changes in sign from negative to positive and then becomes negative again. Therefore, there must exist a value for the delay that minimises the error vector. Bernelli-Zazzera et al[4] suggest minimising the norm of the error vector but the paper is unclear as to the exact technique used. Two different approaches to deriving the value of τ will now be presented and both reproduce the corresponding result found in the paper.

Before considering the derivation of the delay the following notation is introduced:

$$\tau = \frac{h}{2} + \tilde{\tau} \tag{79}$$

The magnitude of the error vector may be derived from:

$$E = \sqrt{\underline{e}'.\underline{e}} \tag{80}$$

To minimise the error requires E=0, introducing the notation from equation **(79)** above into equation **(73)** the following is obtained:

$$\underline{e} = \left(\Psi(h) - e^{A\frac{h}{2}}.e^{-A\tilde{\tau}} \right) B u_M \delta \tag{81}$$

Assuming $\tilde{\tau}$ is small and that:

$$e^{-A\tilde{\tau}} \approx I - A.\tilde{\tau} \tag{82}$$

For convenience, omitting the scalar term $u_M \delta$ equation **(81)** is reduced to the vector equation:

$$\underline{e} = \underline{e}_{\tau=h/2} + e^{Ah/2} AB\tilde{\tau} \tag{83}$$

Hence, for E=0 the following is required:

$$\underline{e}'.\underline{e} = [\underline{e}'.\underline{e}]_{\tau=h/2} + \left[\left(e^{Ah/2} AB \right)'.\underline{e}_{\tau=h/2} + \underline{e}'_{\tau=h/2}.e^{Ah/2} AB \right] \tilde{\tau} = 0 \tag{84}$$

And finally from equation **(84)** the value of τ to minimise the error vector is found.

$$\tilde{\tau} = -\frac{[\underline{e}'.\underline{e}]_{\tau=h/2}}{[(e^{Ah/2}AB).\underline{e}_{\tau=h/2} + \underline{e}'_{\tau=h/2}.e^{Ah/2}AB]} \tag{85}$$

Bernelli-Zazzera et al[4] introduce the notation:

$$\theta = e^{Ah/2} \text{ and } \Xi = \Psi(h) \tag{86}$$

And hence the error vector at half the sample period (neglecting the input term) becomes:

$$\underline{e}_{\tau=h/2} = (\Xi - \theta)B \tag{87}$$

Equation **(85)** can be re-written as:

$$\tilde{\tau} = -\frac{B'.(\Xi-\theta)'.(\Xi-\theta).B}{B'.(\theta'.A'.[\Xi-\theta]+[\Xi-\theta]'.A.\theta).B} \tag{88}$$

Now assuming that $\tilde{\tau}$ is small and at τ=h/2 the absolute value of the error varies approximately linearly with τ, denoting the derivative with respect to τ by /τ the change in the error can be approximated by:

$$(\underline{e}'.\underline{e})_{\tau=h/2} = \left([\underline{e}'.\underline{e}]_{/\tau}\right)_{\tau=h/2}.\frac{h}{2} + Z \tag{89}$$

$$0 = \left([\underline{e}'.\underline{e}]_{/\tau}\right)_{\tau=h/2}\left(\frac{h}{2} + \tilde{\tau}\right) + Z \tag{90}$$

Where Z is an unknown constant, eliminating the unknown constant Z the following is obtained:

$$(\underline{e}'.\underline{e})_{\tau=h/2} = -\left([\underline{e}'.\underline{e}]_{/\tau}\right)_{\tau=h/2}.\tilde{\tau} \qquad \textbf{(91)}$$

Which is the same result presented by Bernelli-Zazzera et al[4], noting that:

$$\left([\underline{e}'.\underline{e}]_{/\tau}\right)_{\tau=h/2} = B'.[\theta''.A'.(\Xi-\theta)+(\Xi-\theta)'.A.\theta].B \qquad \textbf{(92)}$$

Equation **(91)** can be seen to produce an identical result to equation **(88)**. Note that the delay produced by this technique is a constant that depends upon the system matrices A and B and on matrices Ξ and θ, which depend only on h.

It can be seen that embodied in these equations is a basic technique for converting a PAM control system into a PWM control system. This has the advantage that conventional approaches to control design may be used and the design implemented in PWM form without the stability and dynamics of the control system being unduly affected. However, the technique is limited to considering small pulses only and is basically limited to pulses for which $\delta < h - \tau$. Zimpfer et al[43] consider a refinement of the basic technique that improves the transient response and allows large amplitude control inputs.

2.7.2 Refinement of the Basic Technique

Zimpfer et al[43] found that application of the basic technique provided a close match in the steady state response, however, the transient response was poorly matched.

Equation **(71)** indicates that this results can be anticipated provided the PAM and PWM pulses are of equal area, the time average response of the two systems should be identical. The application of differing delays merely shifts the pulse in the system response in time.

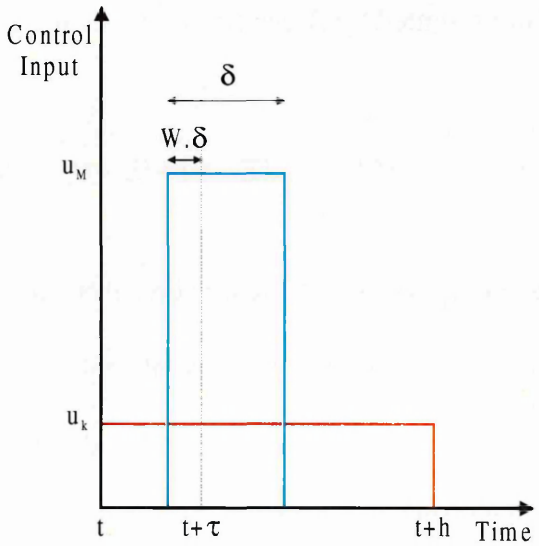

Figure 22 Modified PWM Input Using Weighting Function

During the transient response Zimpfer et al[43] found that large amplitude control inputs were required which dominated the system. Recognising that the basic technique provided a satisfactory response in the steady state condition Zimpfer et al[43] considered a modification to the basic response as shown in Figure 22. Rather than simply delaying the pulse by a constant delay Zimpfer et al[43] propose a weighting function to determine a new delay time. The weighting function, W, is a function of the pulse duration and modifies the delay to accommodate large control inputs. The new delay time can then be calculated using:

$$\hat{\tau} = \tau - W.\delta \qquad \textbf{(93)}$$

The basic strength of the technique proposed by Bernelli-Zazzera et al[4] is that the delay function is a simple function of the system matrices and the sample period. This means that the delay may be calculated *a priori* and it would be ideal if W were a simple function that could be calculated in a similar manner. This is achieved by satisfying the boundary condition as the pulse duration, δ, approaches the sample period, h, the pulse delay, $\hat{\tau}$, should approach zero.

$$\hat{\tau} = 0 = \tau - W.h \Rightarrow W = \frac{\tau}{h} \tag{94}$$

The other boundary condition that as the pulse duration, δ, approaches zero, the pulse delay, $\hat{\tau}$, should approach the nominal value, τ, is simply achieved by the fact that the duration itself is zero.

2.7.3 Closed Loop Stability

In the closed loop the input into the airframe is given by equation **(33)**, substituting into the discrete equation given in equation **(66)** the following is obtained:

$$\begin{aligned} \underline{x}_{k+1} = \left(\Phi(h) - \Psi(h)\cdot B\cdot(1+G\cdot F)^{-1}G\cdot E\cdot h\right)\underline{x}_k + \\ \Psi(h)\cdot B\cdot(1+G\cdot F)^{-1}K\cdot a_{y_d}\cdot h \end{aligned} \tag{95}$$

Now applying the principle of equivalent area as demonstrated in equation **(72)**, the PWM input to the airframe can be determined from equation **(33)** and substituted into equation **(68)** resulting in:

$$\underline{x}_{k+1} = \left(\Phi(h) - e^{A(h-\tau)} \cdot B \cdot (1 + G \cdot F)^{-1} G \cdot E \cdot h\right)\underline{x}_k + e^{A(h-\tau)} \cdot B \cdot (1 + G \cdot F)^{-1} K \cdot a_{y_d} \cdot h \quad \textbf{(96)}$$

Now if the optimum delay is applied and the error vector minimised over the sample period the two inputs are approximately equivalent and it can be inferred that:

$$\Psi(h).B.u.h = e^{A(h-\tau)}.B.u_m.\delta \quad \textbf{(97)}$$

And applying the principle of equivalent area equation **(97)** can be written as:

$$\Psi(h).B.h = e^{A(h-\tau)}.B.h \quad \textbf{(98)}$$

Comparing equations **(95)** and **(96)** and considering equation **(98)** the time-averaged response in the closed loop is the same for both PAM and PWM inputs and more importantly the system matrices are equivalent. The stability of the PAM system is maintained.

2.7.4 Example Calculation

Using the characteristics given in Table 3 the airframe system is described by:

$$\begin{bmatrix} \dot{v} \\ \dot{r} \end{bmatrix} = \begin{bmatrix} -0.5588 & -323.247 \\ 0.3158 & -1.2616 \end{bmatrix} \begin{bmatrix} v \\ r \end{bmatrix} + \begin{bmatrix} 4.8472 \\ 85.5041 \end{bmatrix} \zeta$$

$$a_{y_a} = \begin{bmatrix} -0.5588 & 0 \end{bmatrix} \begin{bmatrix} v \\ r \end{bmatrix} + [4.8472]\zeta$$

Assuming a sample rate of 10 Hz, Ψ(h) and $e^{Ah/2}$ are:

$$\Xi = \Psi(h) = \begin{bmatrix} 0.9955 & -1.6051 \\ 0.0016 & 0.9920 \end{bmatrix}, \theta = e^{Ah/2} = \begin{bmatrix} 0.9959 & -1.6082 \\ 0.0016 & 0.9924 \end{bmatrix}$$

Using equation **(88)** $\tilde{\tau}$ = -4.73×10^{-6} and hence $\tau \approx 0.005$ s. The weighting factor is therefore, W=0.5005.

2.7.5 Effect of Pulse Delay on the Error Vector

This section will consider the effect of the pulse delay, τ, on the error vector. The case chosen for study was a canard controlled glide bomb whose characteristics are:

Table 3 Characteristics of Canard Controlled Glide Bomb

Derivative	Value
y_v	-0.5588
y_r	0.0
y_ζ	4.8472
n_v	0.3158
n_r	-1.2616
n_ζ	85.5041
U	323.247

The standard system matrices were used for an airframe response, equation **(18)**.

Figures 23 to 29 show the effect of the sample rate upon the error vector; some conclusions are immediately apparent. As the sample period increases so does the norm of the error vector. Hence, for low sample rates it is vital to find an accurate value for the pulse delay. For very low sample rates, the assumptions implicit in the derivation of the error vector are breaking down. As these breakdown, there are multiple solutions for the pulse delay and in some cases would result in equation **(88)** choosing a pulse delay that results in a maximum error in the dynamic response.

For this example 10 Hz is approximately the lowest sample rate that may be tolerated.

Note also that since equation **(80)** involves a square root there are two solutions for the magnitude of the error vector, E, and that E can clearly be approximated as a straight line even for small sample rates. This observation suggests that a third technique may be possible for estimating the pulse delay by exploiting this linear behaviour. At high sample rates the linear behaviour of the magnitude of the error vector extends over a greater region of the pulse. Note that the norm of the error vector is a parabolic function of τ, hence the assumption of a linear relationship is only valid provided $\tilde{\tau}$ is indeed small. It is apparent that for high sample rates, $\tilde{\tau}$, is indeed small, however, for low sample rates this is clearly inappropriate. A linear relationship using the magnitude of the error vector may work better in these cases.

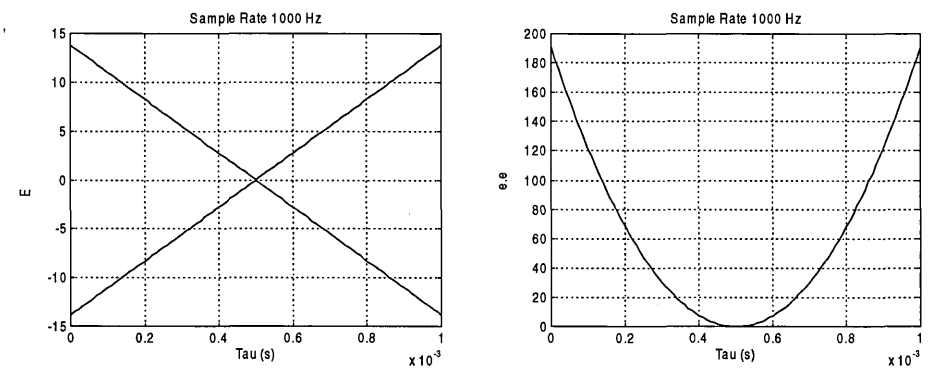

Figure 23 Error as a Function of Pulse Delay - 1000 Hz Sample Rate

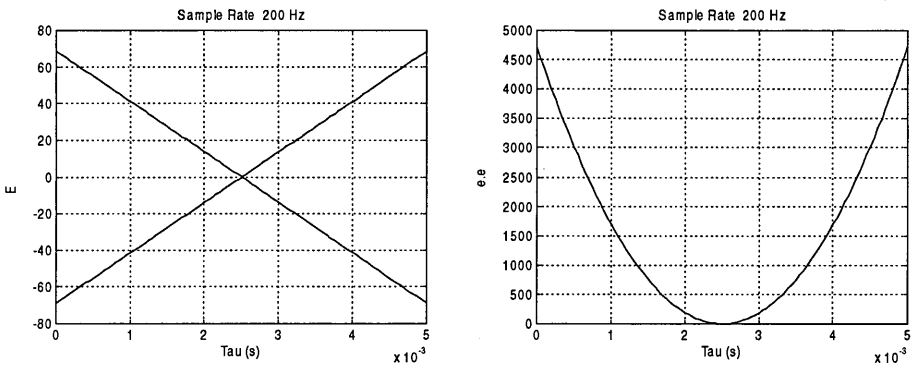

Figure 24 Error as a Function of Pulse Delay - 200 Hz Sample Rate

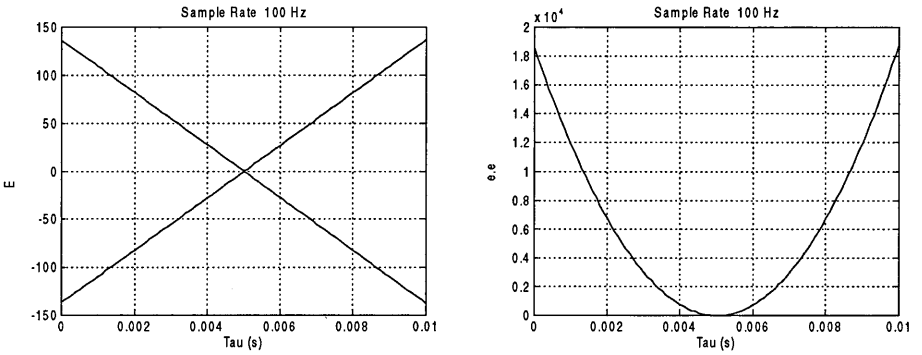

Figure 25 Error as a Function of Pulse Delay - 100 Hz Sample Rate

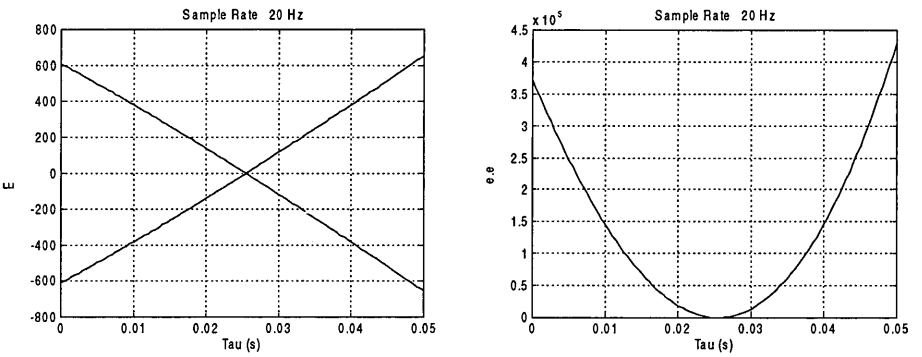

Figure 26 Error as a Function of Pulse Delay - 20 Hz Sample Rate

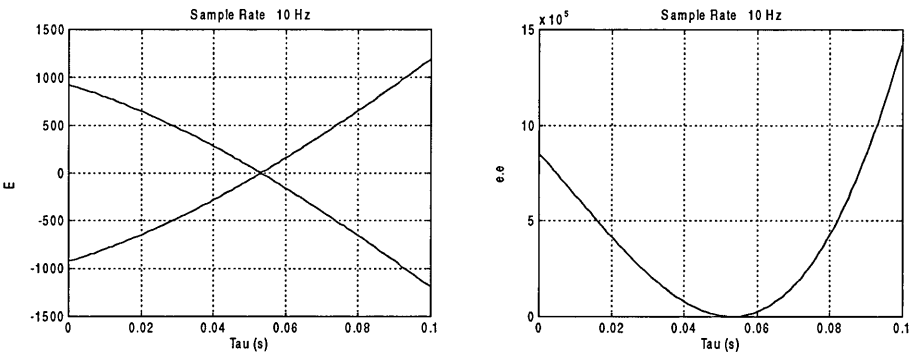

Figure 27 Error as a Function of Pulse Delay - 10 Hz Sample Rate

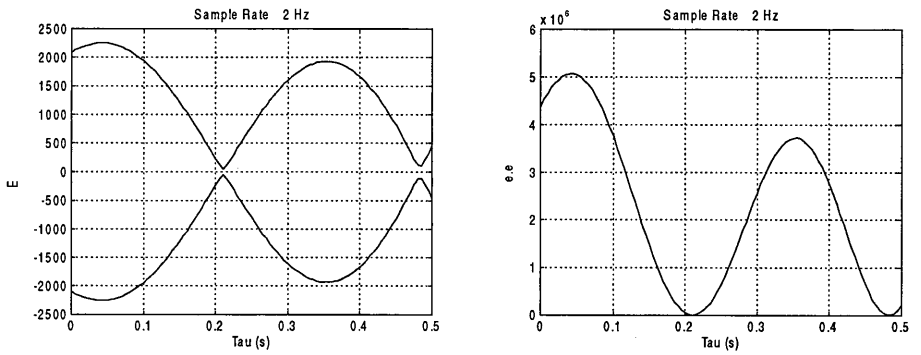

Figure 28 Error as a Function of Pulse Delay - 2 Hz Sample Rate

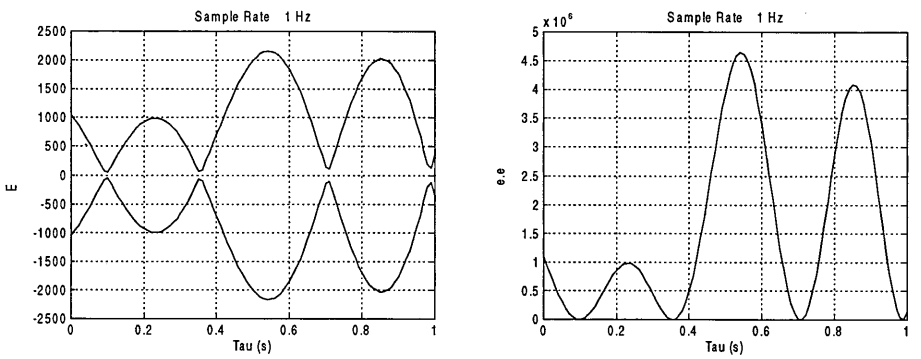

Figure 29 Error as a Function of Pulse Delay - 1 Hz Sample Rate

2.7.6 Autopilot Response Neglecting Actuator Dynamics

The linear autopilot design discussed in section 2.4 assumes that the actuator dynamics can be neglected. This section now examines the use of the PWM design technique in an autopilot loop but neglecting actuator dynamics. Also examined are the relative merits between the use of the original Bernelli-Zazzera et al[4] scheme and the improvements introduced by Zimpfer et al[43]. The weapon characteristics assumed are given in Table 3.

As shown in Figure 30 a PAM simulation was created in SIMULINK, where the input to the airframe, the rudder demand, was sampled using a zero order hold. Similarly Figure 31 shows the block diagram for a second simulation, that

considered the basic Bernelli-Zazzera et al[4] scheme and the final simulation[†] incorporated the improvements suggested by Zimpfer et al[43]. A MATLAB script file was created to calculate the pulse delay and weighting factor as a function of the airframe characteristics and sample rate. As none of the intrinsic functions in SIMULINK leant themselves readily to the PWM controller a MATLAB function was created for this purpose.

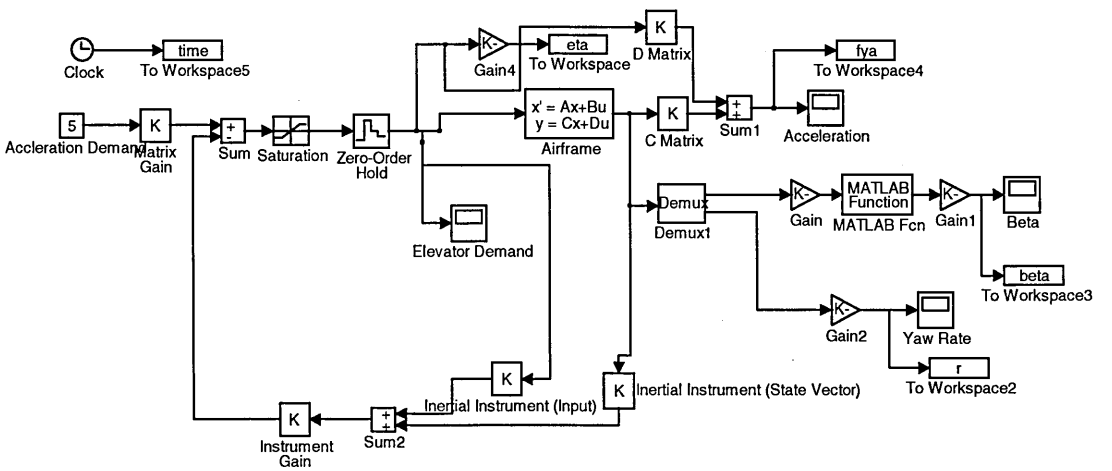

Figure 30 PAM Autopilot

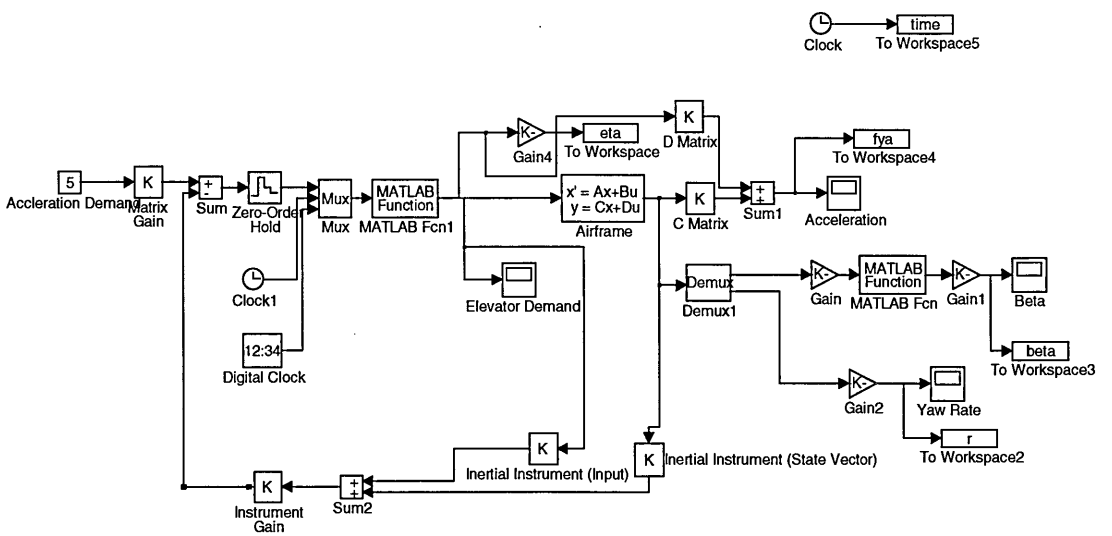

Figure 31 PWM Autopilot - Bernelli-Zazzera Scheme

[†] A block diagram is not presented since the diagram is essentially the same as Figure 31. The two simulations differ only in the MATLAB function used.

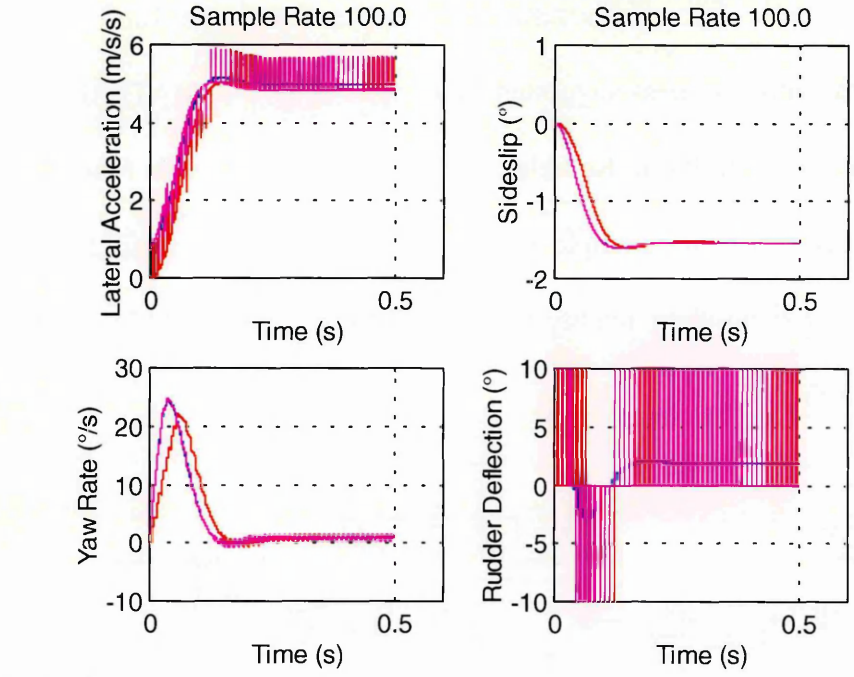

PAM, *PWM (Original Scheme),* *PWM (Zimpfer Scheme)*

Figure 32 Comparison of PAM and PWM Responses (Autopilot Bandwidth = 5Hz)

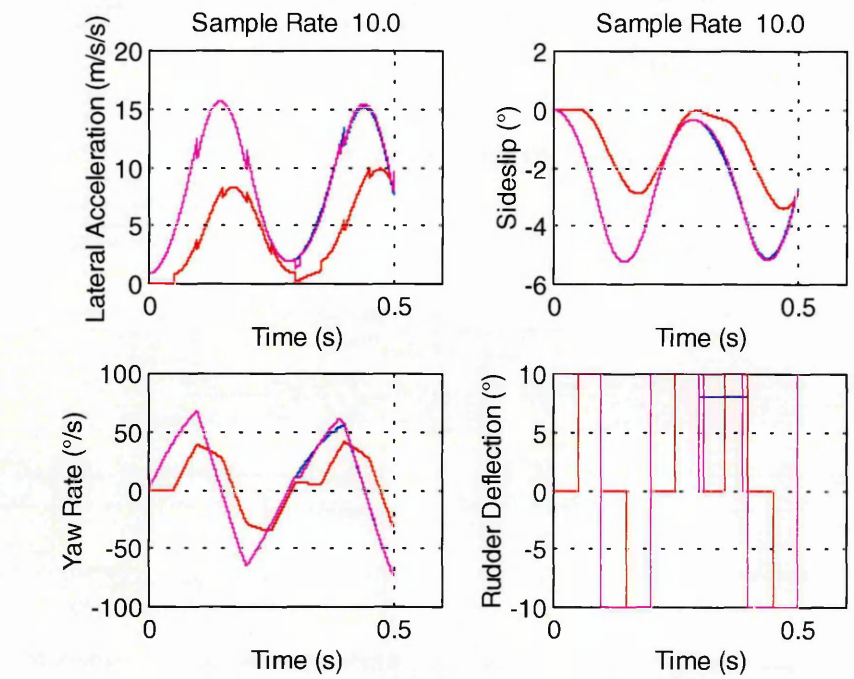

PAM, *PWM (Original Scheme),* *PWM (Zimpfer Scheme)*

Figure 33 Comparison of PAM and PWM Responses (Autopilot Bandwidth = 5Hz)

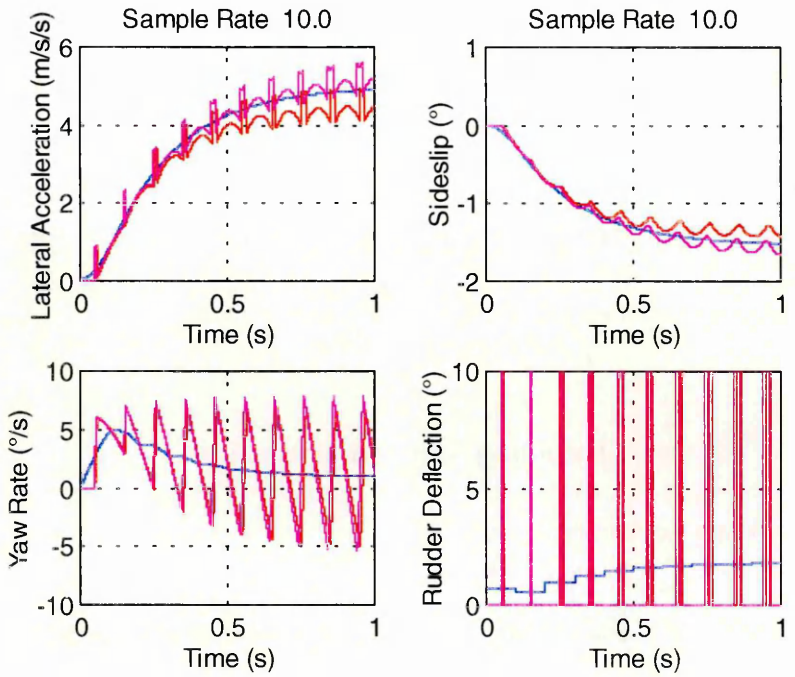

PAM, *PWM (Original Scheme),* *PWM (Zimpfer Scheme)*

Figure 34 Comparison of PAM and PWM Responses (Autopilot Bandwidth = 1Hz)

Referring to Figure 32 it can be seen that in the steady state both of the PWM schemes match the PAM response extremely well. However, the original Bernelli-Zazzera et al[4] scheme does not match the dynamic response well and the Zimpfer et al[43] scheme is clearly superior in this respect. Figure 33 shows that as might be expected the response will become unstable if the sample rate is too low but Figure 34 shows that the autopilot bandwidth and sample rates can be closely matched and a stable response is still obtained.

At first glance it would appear that the Zimpfer et al[43] scheme produces an overshoot in the response in the steady state. However, integrating over the pulse width shows that the area under each pulse is the same in both cases, the result predicted by

equation (72). The graphs may appear misleading because of the output rate obtained from MATLAB.

Since these results show the superiority of the Zimpfer et al[43] scheme this was preferred in subsequent simulations.

2.7.7 Autopilot Response Including Actuator Dynamics

2.7.7.1 Pulse-Wave Form

In order to examine the steady state a PAM input in considered in the steady state, i.e. $\dot{\underline{x}} = 0$, the input to achieve a desired steady state deflection may be found using:

$$\zeta = \frac{a_{y_d}}{\left[D - C.A^{-1}.B\right]} \tag{99}$$

Using the airframe characteristics given in Table 3 the deflection required to achieve a nominal 5 $m.s^{-2}$ lateral acceleration is thus 1.85°. Assuming a relatively long sample period of 0.1s this results in a nominal pulse delay of 0.0516s and a weighting factor of 0.5159. Assuming that the maximum canard deflection is 10° and a second order actuator response, Figure 35 shows the response of an actuator to a pulse input demand.

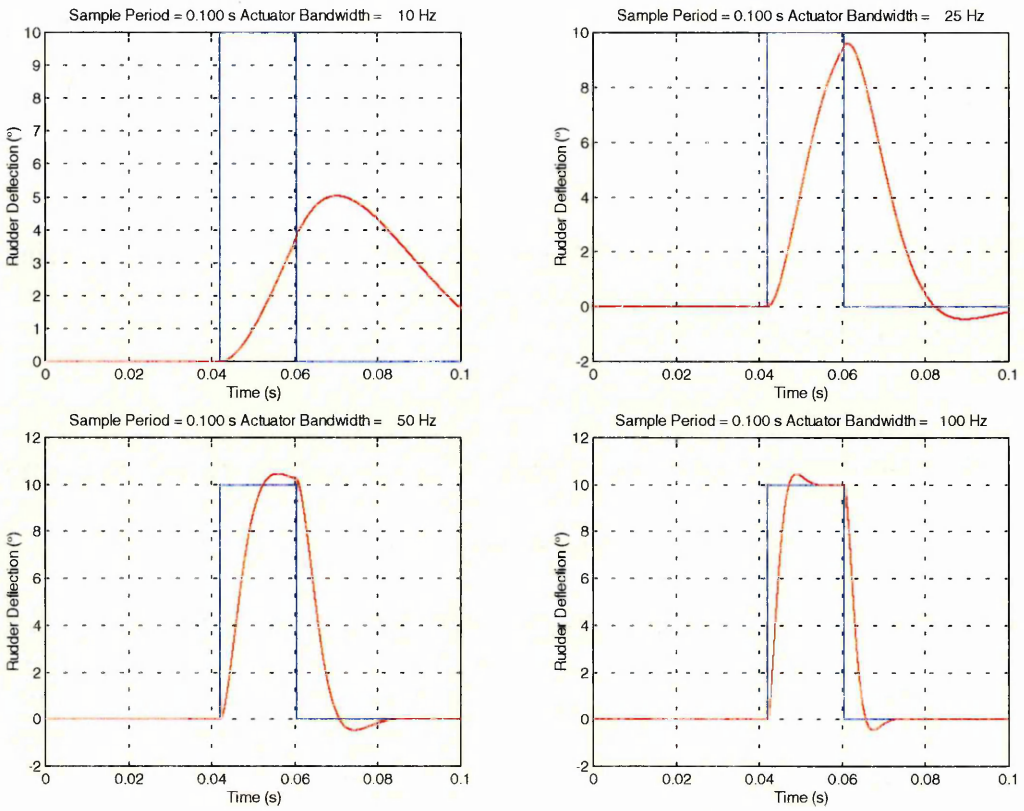

Figure 35 Effect of Actuator Bandwidth Upon Pulse Wave Form

Figure 35 clearly shows that even if the actuator bandwidth is very high (50 Hz or more) the response of the actuator is insufficient to replicate the pulse demand without a significant distortion of the pulse wave form and some phase shift. Note this is at a relatively slow sample rate (10 Hz) and a typical actuator bandwidth for a missile application is of the order of 10-25 Hz.

To examine the impact of actuator dynamics, the autopilot model shown in Figure 31 was modified to include a second order actuator model. The modified block diagram is shown in Figure 36. An actuator bandwidth of 25 Hz was selected as this is typical of high bandwidth missile actuators. A range of acceleration demands was considered in the range 1-10 $m.s^{-2}$ and a typical result is shown in Figure 37. It can

be seen that the response trails the error by about 10-11% and when examined across the range of demands it was found that the trailing error is approximately a fixed percentage of the demand. It is therefore concluded that the error is due to the effects of actuator dynamics, which distort the pulse waveform and do not achieve the required equivalent pulse area.

It is noted that these simulations considered a low sampling rate and even with a high performance actuator system the actuator dynamics result in an error in the autopilot response. Most guidance systems are in fact relatively robust to such errors but the main focus of this autopilot was to achieve a reasonable response using an existing "bang-bang" actuator. It is clear therefore that in order to implement a PWM autopilot design, the actuator dynamics must be included in the design of the control loop.

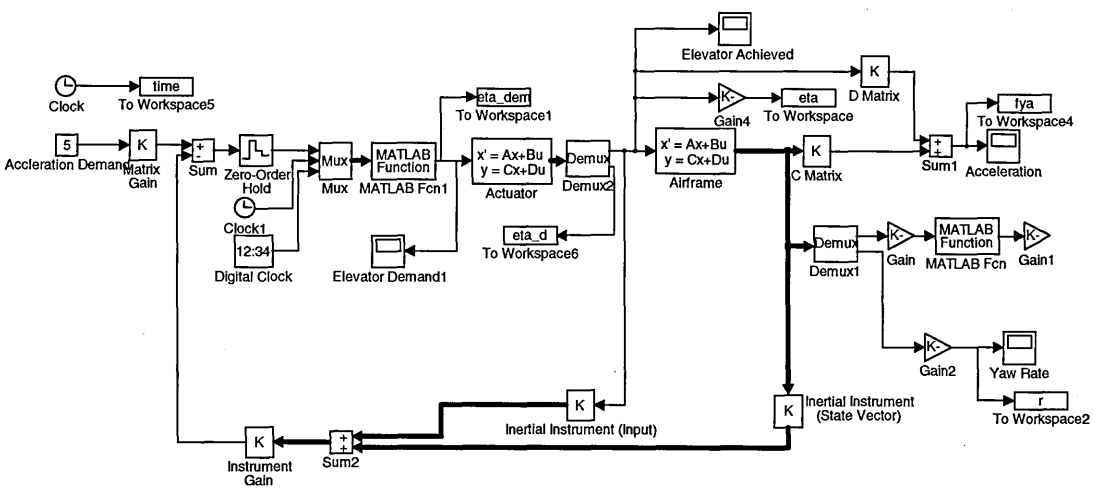

Figure 36 Autopilot Loop Incorporating Actuator Response

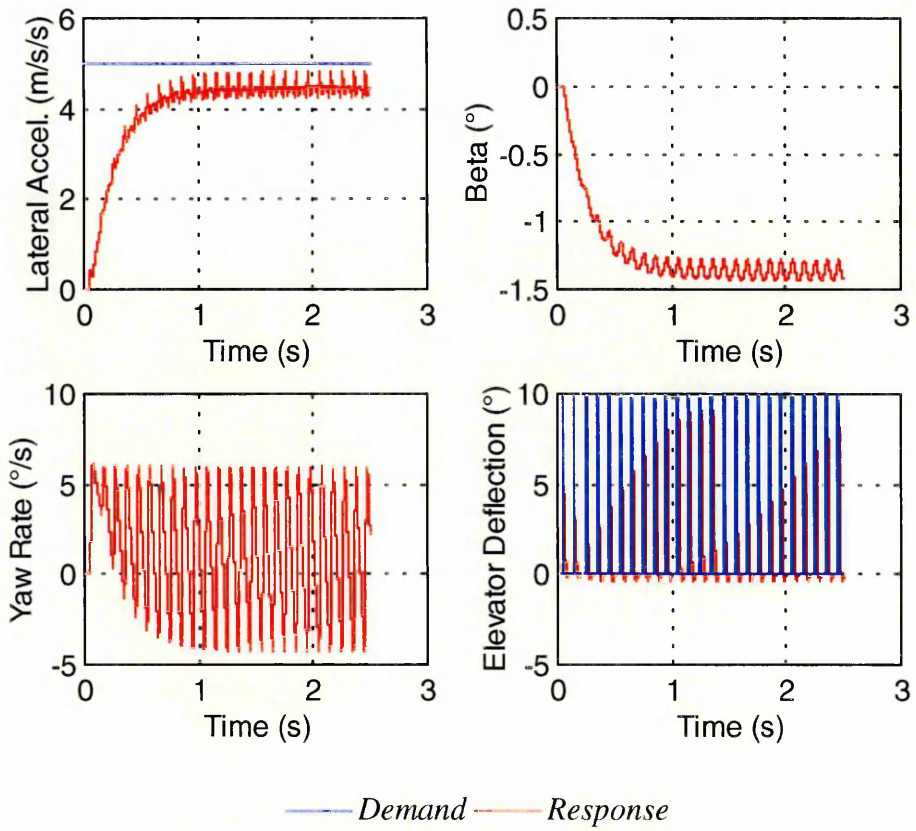

Figure 37 PWM Autopilot Response Including Actuator Dynamics

2.7.7.2 Trapezoidal Wave Form

The idealised waveform for a PWM is rectangular, since the technique used was originally developed for a system incorporating thrusters. These are essentially on-off devices whose rise time is small enough to be neglected, whereas the actuator response includes both the initial rise time and a decay time. Hence, in order to incorporate actuator dynamics in the control design consideration was given to extending the technique by incorporating these effects.

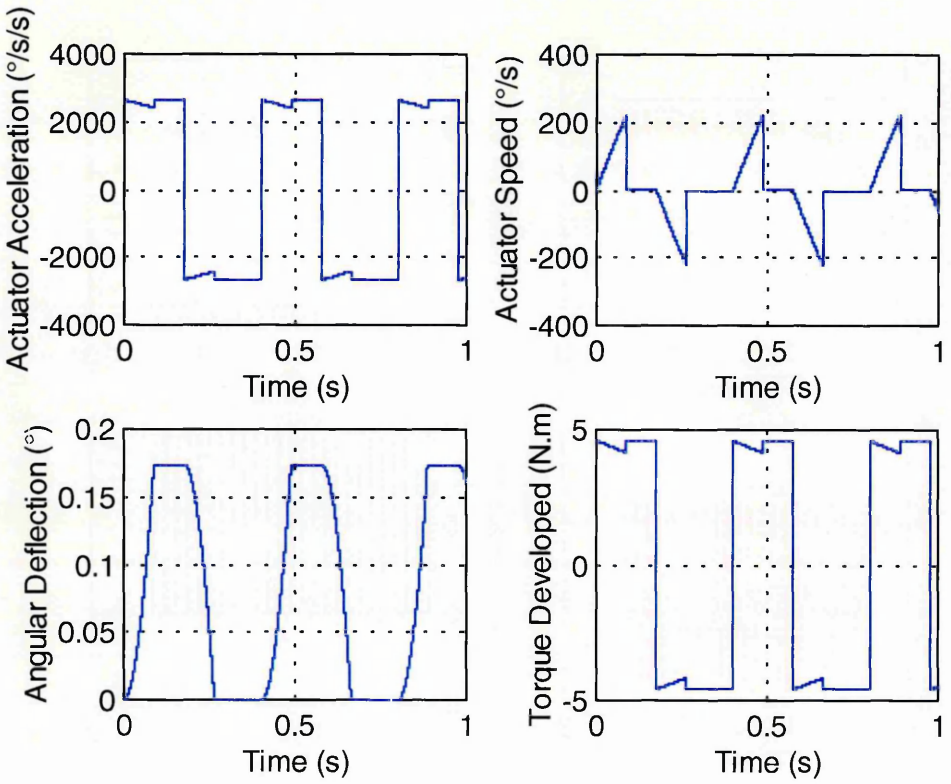

Figure 38 Typical "Bang-Bang" Actuator Response

Figure 38 shows a typical response for a "bang-bang" actuator. An analytical solution of the response to a step input is possible but results in an equation of the form:

$$\theta_A(t) = a_1.t + a_2.\left(1 - e^{-a_3.t}\right) \qquad \textbf{(100)}$$

It is not straightforward to solve this equation to find an analytical solution for the rise time t_1. Instead the pulse waveform is approximated by a trapezoidal waveform and a value for the rise and decay periods was found using simulations in MATLAB/SIMULINK. This work indicated that this assumption introduced a small error in the modelling of the actuator dynamics, numerical simulations indicated this was of the order of 5-6% in the rise time. Given that the error introduced was

comparatively small and the calculation procedure greatly simplified it was concluded this was a suitable approximation to use in modifying the formulation of the demand pulse.

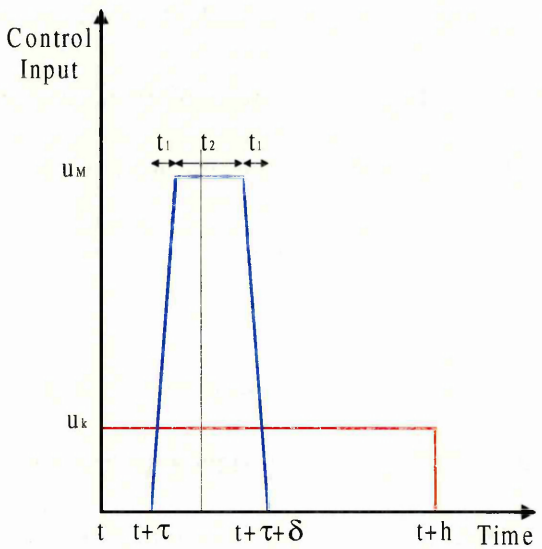

Figure 39 PWM Using Trapezoidal Waveform

Figure 39 shows the trapezoidal waveform assumed for the actuator response, using the principle of equivalent area:

$$u.h = u_m.t_1 + u_m.t_2 \tag{101}$$

Assuming the rise and decay time, t_1, to be constant:

$$t_2 = \frac{u}{u_m}.h - t_1 \tag{102}$$

Noting that the forced response is:

$$\Delta(h) = \int_0^h \Phi(t-\tau).B.\underline{u}(\tau).d\tau \tag{103}$$

Integrating over the pulse period the following is obtained:

$$\Delta(h) = e^{A(h-\tau)}.B.u_m.(t_1 + t_2) \qquad \textbf{(104)}$$

Which is similar to the result previously obtained where $u_m.\delta$ was the pulse area. This result indicates that the previous results obtained for the pulse delay and the weighting factor are still valid. Hence, using the rise time it is simple to modify the basic pulse system to use a trapezoidal pulse.

Before resorting to simulation of a PWM autopilot, the response of the actuator to a repeating sequence was examined. Using data supplied by Litton[25], a simulation was created in SIMULINK to examine the actuator response to a repeating sequence. As shown in Figure 40, this showed that for modest sample rates the ability of the actuator to reproduce the desired waveform was diminished and at low sample rates the actuator can no longer follow the input. At this point the actuator is totally out of phase with the input and clearly the system is unstable. It was found that relatively large sample periods were required (around 0.2 s or more) or the actuator response was unable to reproduce the desired waveform.

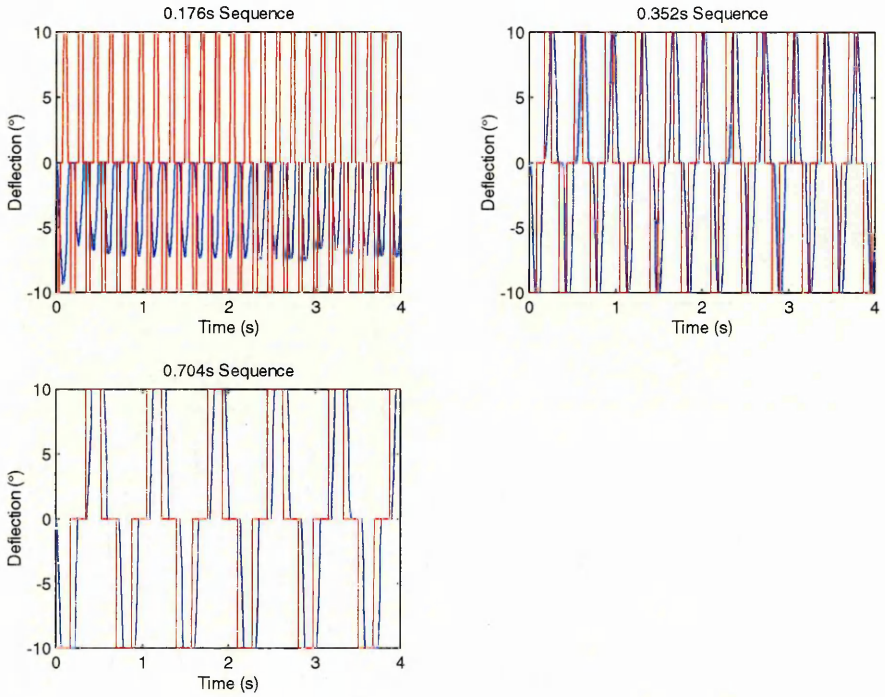

Figure 40 Actuator Response to Repeating Sequence

A simulation was created in SIMULINK using a trapezoidal waveform for the PWM input to the actuator. In order to cope with the low sample rate dictated by the requirement for the actuator to be capable of following the desired wave form the autopilot bandwidth was progressively reduced until finally it was less than 0.5 Hz, Figure 41 shows a typical response.

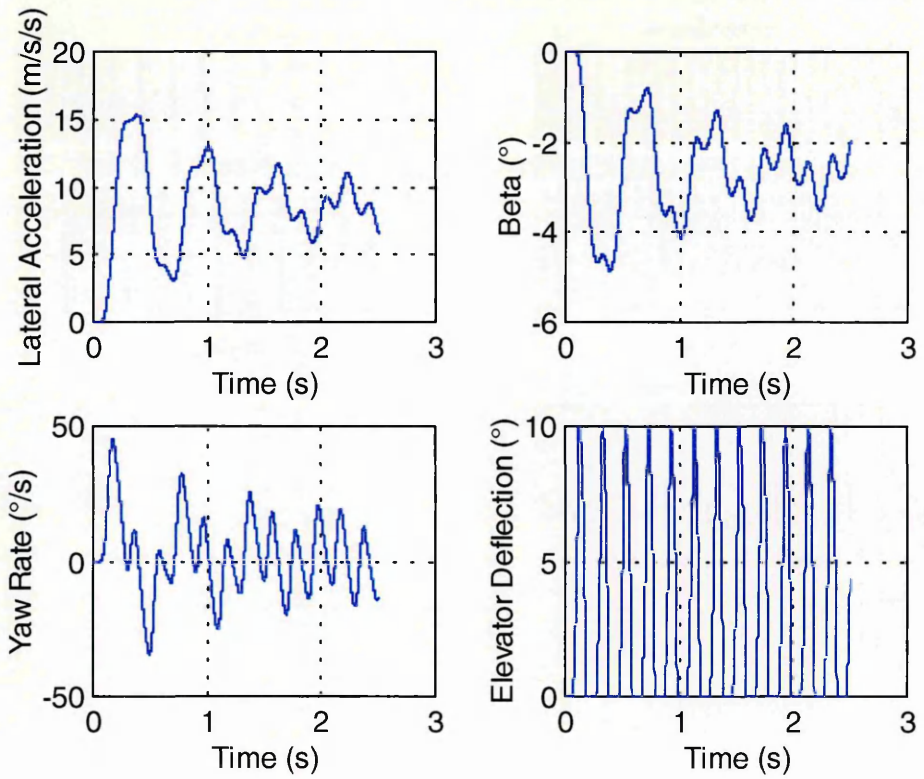

Figure 41 Autopilot Response Using Trapezoidal Pulse Wave Form

Clearly the response is unsatisfactory with a large overshoot and what appears to be a limit cycle about the desired value of 10 ms^{-2}. To some extent this may result from the assumption that the pulse period is small, which is clearly breaking down. It was noted earlier that for large sample periods the pulse delay could be significantly in error. It is also likely that the phase shift introduced by the actuator is to some extent responsible.

Another factor is the assumption used in deriving the technique, the smallest pulse width that can result is double the rise and decay time i.e. t_2 is zero. With a small PAM pulse an error is introduced where the PWM pulse can have a larger pulse area. Smaller pulse-widths could be used but this adds the added complication of the pulse shape. Since the actuator has not yet hit the end stops with small pulses, the

actuator must first stop and then reverse its direction of travel. An analytical solution for this situation is of course possible but the design procedure is becoming ever more complex and reliant upon *a priori* knowledge.

2.7.7.3 Translating Pulses in Time

As noted above there is a lower limit on the pulse area introduced by the assumption of a trapezoidal pulse waveform. This will of course introduce an error for small pulses as the principle of equivalent area is violated. Simply neglecting small pulses also introduces an error, primarily because the principle of equivalent area is once again violated but also because this places a lower limit on the autopilot response below which the control loop cannot respond.

Consideration was therefore given to introducing the concept of translating pulses in time. The concept being that where the PAM pulse was too small to be considered within one sample period it was neglected and compensated for in the next sample period.

Equation **(62)** shows the state space equation in discrete form and can be re-written as:

$$\underline{x}_{k+1} = F.\underline{x}_k + G.\underline{u}_k \qquad \textbf{(105)}$$

Next in the sequence:

$$\underline{x}_{k+2} = F.\underline{x}_{k+1} + G.\underline{u}_{k+1} = F^2\underline{x}_k + F.G.\underline{u}_k + G.\underline{u}_{k+1} \quad \textbf{(106)}$$

Assuming that the PAM amplitude in sequence k was small and neglected, an error of $F.G.\underline{u}_k$ is induced in the state vector for the next sequence. Now further assume the input is modified in sequence k+1 such that the error introduced by neglecting the earlier input is compensated for. Denoting the modified input by $\left[\underline{u}_{k+1}\right]_m$ the response is now

$$\underline{x}_{k+2} = F^2\underline{x}_k + G.\left[\underline{u}_{k+1}\right]_m \quad \textbf{(107)}$$

And the error vector between the desired and achieved response is:

$$\varepsilon = F.G.\underline{u}_k + G.\underline{u}_{k+1} - G.\left[\underline{u}_{k+1}\right]_m \quad \textbf{(108)}$$

The concept is to minimise the error by choosing a suitable value for $\left[\underline{u}_{k+1}\right]_m$ by minimising the norm of the error vector. A minimum is found by differentiating the norm with respect to $\left[\underline{u}_{k+1}\right]_m$. It can be shown that:

$$\begin{aligned}\frac{\partial(\varepsilon'.\varepsilon)}{\partial\left[\underline{u}_{k+1}\right]_m} = 0 = -(F.G)'.G.\underline{u}_k - G'.G.\underline{u}_{k+1} \\ - G'.F.G.\underline{u}_k - G'.G.\underline{u}_{k+1} + 2G'.G.\left[\underline{u}_{k+1}\right]_m\end{aligned} \quad \textbf{(109)}$$

Differentiating again:

$$\frac{\partial^2(\varepsilon'.\varepsilon)}{\partial\left[\underline{u}_{k+1}\right]_m^2} = 2G'.G \quad \textbf{(110)}$$

Which is a positive scalar value and hence equation **(109)** represents a minimum. Noting that G'.G and (F.G)'.G and G'.(F.G) are scalars, equation **(109)** can be re-written as:

$$\left[\underline{u}_{k+1}\right]_m = \underline{u}_{k+1} + \frac{(F.G)'.G + G'.(F.G)}{2G'.G}.\underline{u}_k \qquad \textbf{(111)}$$

Examining the above result it is plain that the effect of delaying the pulse in time can be compensated for by multiplying by a constant scalar factor. Using the airframe characteristics given in Table 3 the size of this factor was calculated using MATLAB and is shown in Figure 42 below.

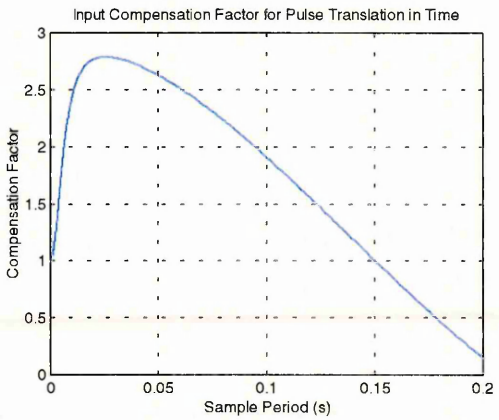

Figure 42 Compensation Factor for Pulse Translation in Time

For small sample periods the factor rises quickly to a value of around 2.8 and then drops to a small value. It can therefore be seen that for sample periods beyond 0.15 s a geometric series will be established where the input will converge to a small value. Beyond this point the concept of translating the pulse from one sample period to the next can no longer compensate the error vector. It is likely that the system will become unstable long before this point is reached since the effect of translating the

pulse in time is to effectively introduce a phase shift. At this point the problem of closed loop stability has not been considered. In a feedback loop, if a small control pulse, u_k, is neglected then the subsequent pulse, u_{k+1}, is in part due to the error introduced.

After considering both the modification to a trapezoidal pulse and modification to compensate for small pulses it was therefore concluded that the actuator dynamics must be included in the design of the control algorithm.

2.7.7.4 PWM Fin Controller Design

First of all consider the state space equation for a "bang-bang" actuator and for the moment ignore the nonlinearities:

$$A=\begin{bmatrix}0 & 1\\ 0 & \frac{K_M^2}{RJ}\end{bmatrix},\ B=\begin{bmatrix}0\\ \frac{K_M^2}{RJ}\end{bmatrix},\ \underline{x}=\begin{bmatrix}\zeta\\ \dot{\zeta}\end{bmatrix},\ \dot{\underline{x}}=A\underline{x}+B\underline{u} \qquad \textbf{(112)}$$

The eigenvalues of the system equation are $\begin{bmatrix}0 & \frac{K_M^2}{RJ}\end{bmatrix}$, or if the state variables are reversed $\begin{bmatrix}0 & 1\end{bmatrix}$.

In both cases the system has a pole in the right hand side of the imaginary axis and is therefore unstable. This could of course have been anticipated since the block diagram in Figure 17 shows that the system has two integrating poles and without position feedback is unstable. In a conventional system a resolver would be used to

provide position feedback and so it was proposed to use an Observer to estimate the system states, including the actuator states and then to use state feedback to close the loop around the actuator making the system stable. Including the IMU[‡], actuator and airframe dynamics in the state equation results in the following system:

$$A=\begin{bmatrix} y_v & (y_r-U) & 0 & y_\zeta \\ n_v & n_r & 0 & n_\zeta \\ 0 & 0 & 1 & 0 \\ 0 & 0 & \frac{K_M^2}{R.J} & 0 \end{bmatrix},\ B=\begin{bmatrix} 0 \\ 0 \\ \frac{K_M}{R.J} \\ 0 \end{bmatrix}, \qquad \textbf{(113a)}$$

$$C=\begin{bmatrix} (y_v+l_x.n_v) & (y_r+l_x.n_r) & 0 & (y_\zeta+l_x.n_\zeta) \\ 0 & 1 & 0 & 0 \end{bmatrix},\ D=[0] \qquad \textbf{113b)}$$

Using the values given in Table 3 the controllability and observability of this system was examined using MATLAB. The system was both controllable and observable with one important exception. If the following condition is satisfied:

$$l_x=-\frac{y_\zeta}{n_\zeta} \qquad \textbf{(114)}$$

The system is unobservable, this position is known as the centre of percussion and a missile designer will typically try to place the IMU as close as possible to this position, precisely because at this point the instruments do not detect the forces and moments induced by a control deflection. In order for the fin states to be *observable*, the instruments must be placed at some other location than the centre of percussion.

[‡] Inertial Measuring Unit

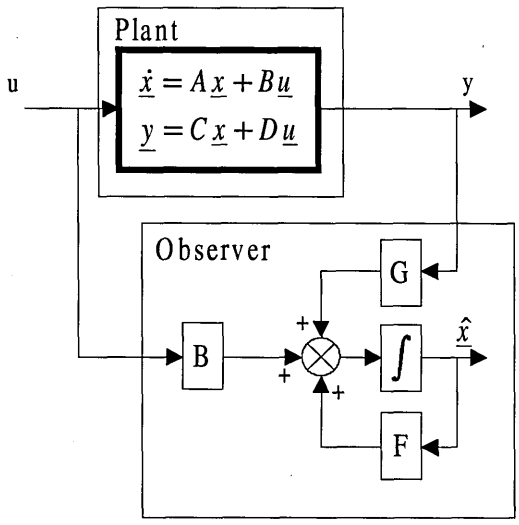

Figure 43 General Form of a State Space Observer

The general form of the Observer used is illustrated in Figure 43; an observer system matrix is defined to have the property:

$$F = A - G.C \tag{115}$$

Where G is the observer gain matrix. The design procedure of Dutton et al[9] was adopted; this selects suitable eigenvalues for the observer state matrix to achieve the desired dynamic performance of the observer. Equation **(115)** was then used to derive the gain matrix G to satisfy the design equation for the observer.

Using the values given in Table 3, the poles of the system are at (-0.91±10.10 i, 0, 1). Since the fastest pole in the system was at -0.9 the locations of the observer poles were placed at approximately –9, allowing suitable separation of the poles of the observer from the poles of the system and the autopilot loop. Moving the poles further to the left would be undesirable since this would start to come into conflict with the poles of the inertial instruments. MATLAB incorporates a function, the

"place" function that enables the design of a suitable observer system matrix by specifying the desired location of the poles. This function does not allow the placement of poles at the same location and so the poles were specified as [-9.1, -9.3, -9.5, -9.6].

Figure 44 shows the design of an autopilot loop that incorporates such an observer to provide state feedback. The error between the desired position and the estimate of the achieved position is used to provide voltage input to the actuator motor via a proportional gain, K_P. The use of an observer fulfils a similar function to that of a resolver allowing a "bang-bang" actuator to be controlled in a proportional manner.

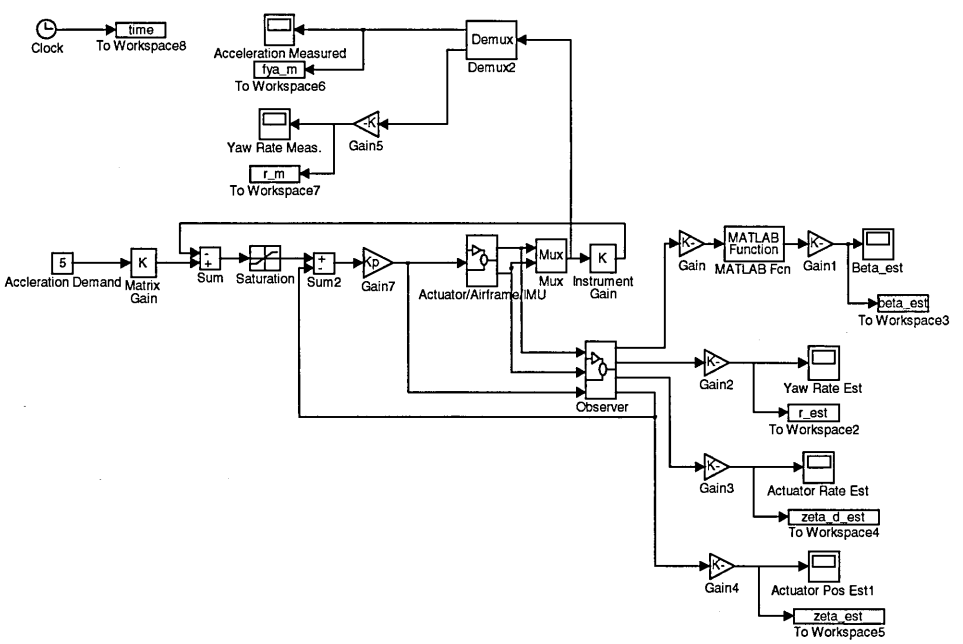

Figure 44 Actuator Feedback using a Linear Observer

Using the characteristics given in Table 3, an assumption of an autopilot bandwidth of 1 Hz and a proportional gain on the actuator, K_P, of 315 a series of simulations were performed. Figure 45 shows the observer response to a step input demand of 5

$m.s^{-2}$. It can be seen that the sideslip velocity and yaw rate estimates quickly converge, whilst the actuator position and actuator rate converge more slowly. Nevertheless the estimated position is suitable for providing feedback and a stable system results. Nevertheless this design is not entirely efficient. There are two direct measurements of the system states provided by the IMU and it would be more computationally efficient to use these states in a reduced order observer.

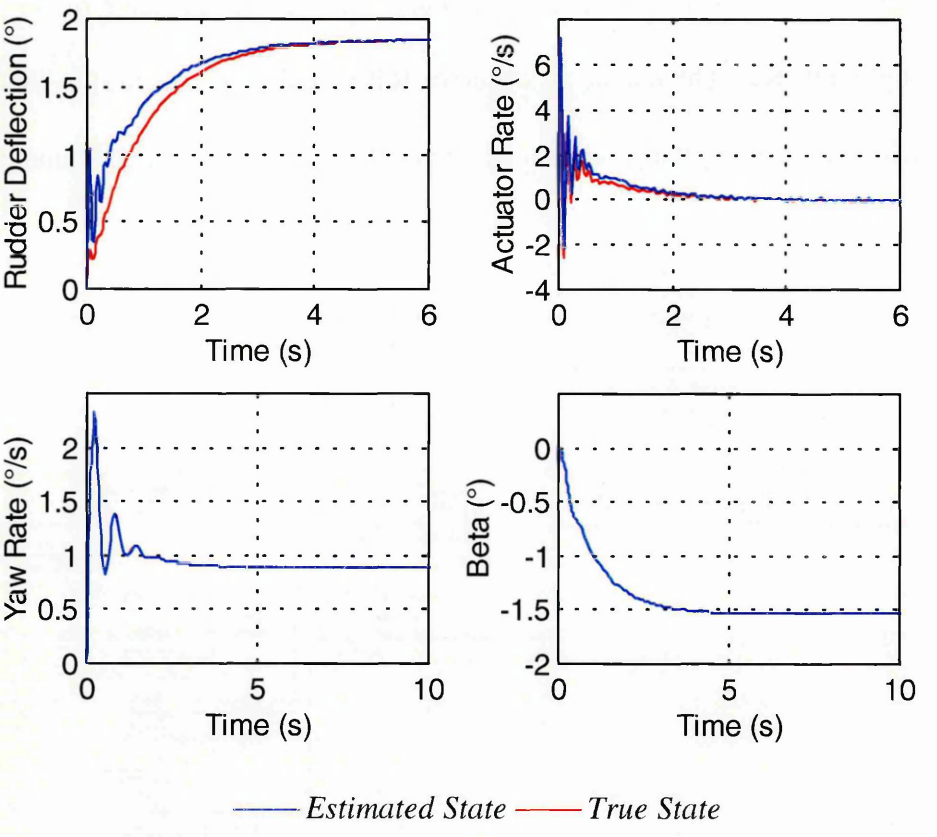

Figure 45 Observer Performance

The block diagram for a reduced order observer is given in Figure 46.

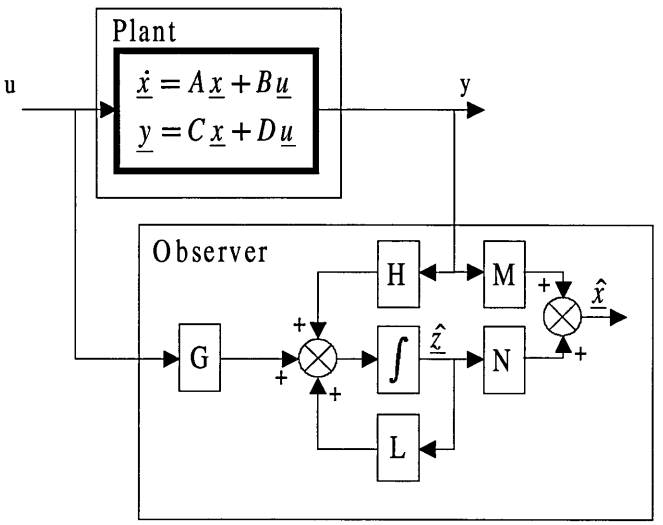

Figure 46 General Arrangement of a State Space Reduced Order Observer

The equations of the reduced order observer are:

$$\dot{\hat{\underline{z}}} = L.\hat{\underline{z}} + G.u + H.\underline{y},\ \hat{\underline{x}} = M.\underline{y} + N.\hat{\underline{z}},\ \hat{\underline{z}} = T.\hat{\underline{x}} \qquad \textbf{(116)}$$

As the system being observed has 4 states and 2 outputs, $\hat{\underline{z}}$ is a [2 x 1] column vector, L a [2 x 2] matrix, G a [1 x 2] matrix, H a [2 x 2] matrix, M and N are [4 x 2] matrices and T a [2 x 4] matrix. The design equations are:

$$T.A - L.T - H.C = 0 \qquad \textbf{(117)}$$

And

$$\begin{bmatrix} M & N \end{bmatrix} = \begin{bmatrix} C \\ T \end{bmatrix}^{-1} \qquad \textbf{(118)}$$

For the moment let the matrices T and H be denoted by:

$$T = \begin{bmatrix} T_{11} & T_{12} & T_{13} & T_{14} \\ T_{21} & T_{22} & T_{23} & T_{24} \end{bmatrix}, \; H = \begin{bmatrix} H_{11} & H_{12} \\ H_{21} & H_{22} \end{bmatrix} \tag{119}$$

Similarly denoting the system matrices by:

$$A = \begin{bmatrix} A_{11} & A_{12} & 0 & A_{14} \\ A_{21} & A_{22} & 0 & A_{24} \\ 0 & 0 & A_{33} & 0 \\ 0 & 0 & A_{34} & 0 \end{bmatrix}, \; C = \begin{bmatrix} C_{11} & C_{12} & 0 & C_{14} \\ 0 & C_{22} & 0 & 0 \end{bmatrix} \tag{120}$$

For convenience write the state estimator equation in modal form, denoting the L matrix as:

$$L = \begin{bmatrix} e_1 & 0 \\ 0 & e_2 \end{bmatrix} \tag{121}$$

Expanding equation **(117)** 8 simultaneous equations in 12 unknowns are obtained. This gives some freedom in the design of T and H.

$$\left(A_{11} - e_1\right).T_{11} + A_{21}.T_{12} = H_{11}.C_{11} \tag{122}$$

$$A_{12}.T_{11} + \left(A_{22} - e_1\right).T_{12} = H_{11}.C_{12} + H_{12}.C_{22} \tag{123}$$

$$\left(A_{33} - e_1\right).T_{13} + A_{43}.T_{14} = 0 \tag{124}$$

$$A_{14}.T_{11} + A_{24}.T_{12} - e_1.T_{14} = H_{11}.C_{14} \tag{125}$$

Due to the manner in which the system matrices have been formulated the simultaneous equations for the second rows in T and H are formulated in an

identical manner to those above with the row indices in T, L and H changed from 1 to 2. For convenience let $T_{13} = T_{23}=1$ and $H_{12} = H_{22} = 1$ and the above equations may now be solved for the matrices T and H.

M and N are now calculated using equation **(118)**. Although this solution is convenient since it permits a computationally efficient means of calculating the observer matrices it does introduce a constraint. If the eigenvalues for L are placed in the same position both rows of T become identical. M and N can no longer be found since the right hand side of equation **(118)** becomes singular.

Finally G is calculated using:

$$G = T.B \qquad \textbf{(126)}$$

The eigenvalues chosen for L were [-10, -11], since this was suitably removed from the system poles but avoided placing the observer poles too close to the other system poles such as those of the IMU. The design technique was implemented in MATLAB to solve for the system matrices and a simulation created in SIMULINK. Superficially the block diagram is identical to Figure 44 but differs in that a reduced order observer is substituted for the full order observer.

The results of repeating the earlier simulations using the reduced order observer are shown in Figure 47. It can be seen that the same result is obtained in a computationally efficient manner using the reduced order observer. Subsequent simulation used the reduced order observer exclusively.

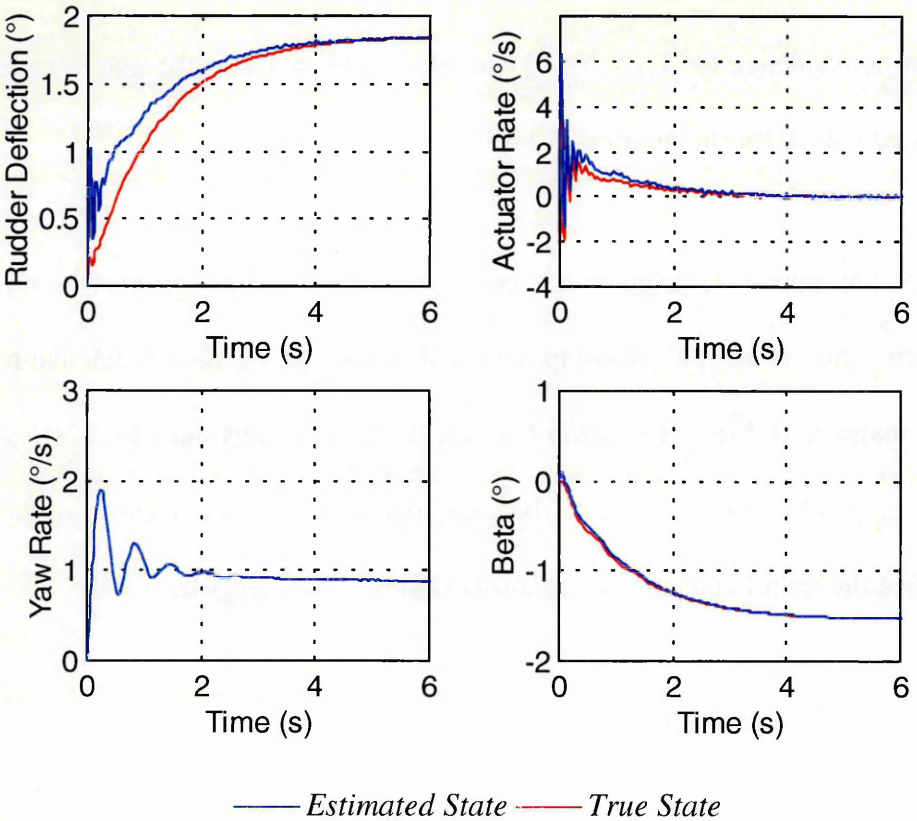

Figure 47 Reduced Order Observer Performance

So far, the simulation using an observer to provide position feedback considered a linear system. Essentially what has been derived is a fin controller to provide motor input in a proportional manner. A "bang-bang" actuator is somewhat different in that the input required is simply an up/down or neutral command. The next stage of the algorithm design was to derive a PAM system from this linear equivalent and hence to derive the PWM input required by the "bang-bang" actuator.

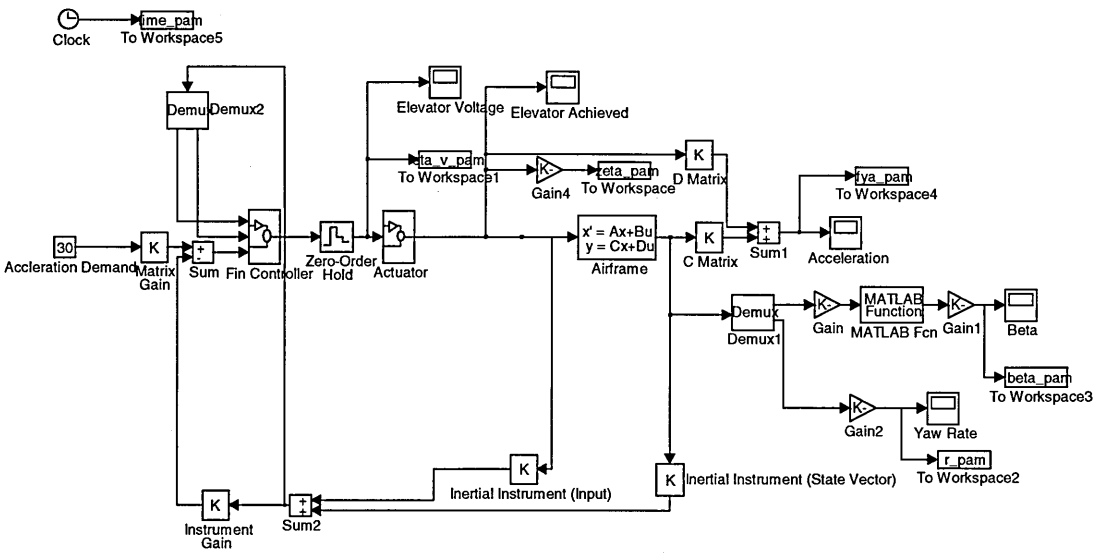

Figure 48 PAM Autopilot Block Diagram

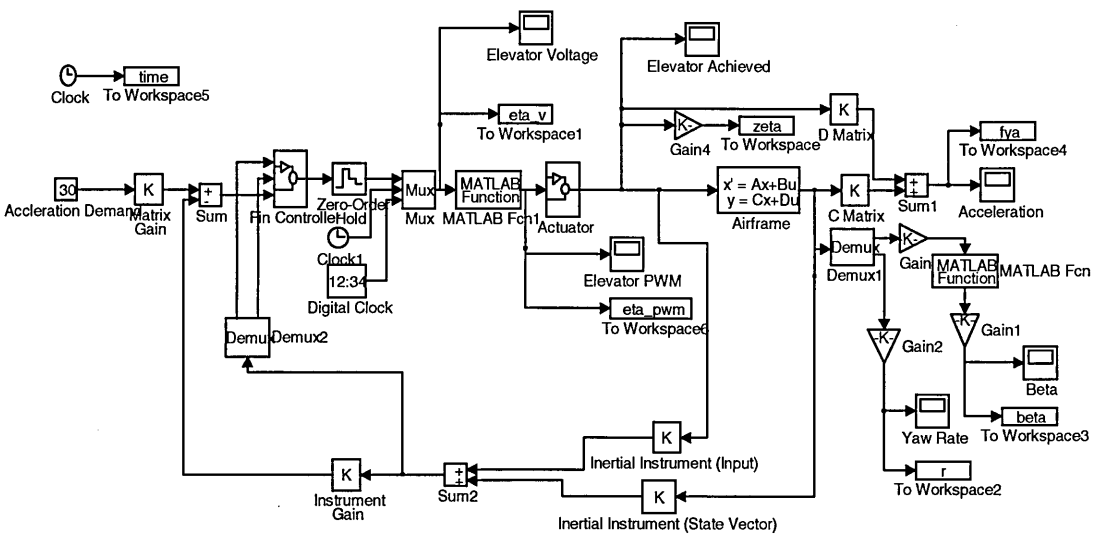

Figure 49 PWM Autopilot Block Diagram

Figure 48 shows the block diagram for a PAM autopilot design, whilst Figure 49 shows the block diagram for the equivalent PWM system. Both designs are similar to the previous block diagrams, the PAM design incorporating a zero order hold sampling device and the PWM design incorporates the MATLAB function described previously. The PWM design used the scheme proposed by Zimpfer et al[43].

2.7.7.5 Simulation Results

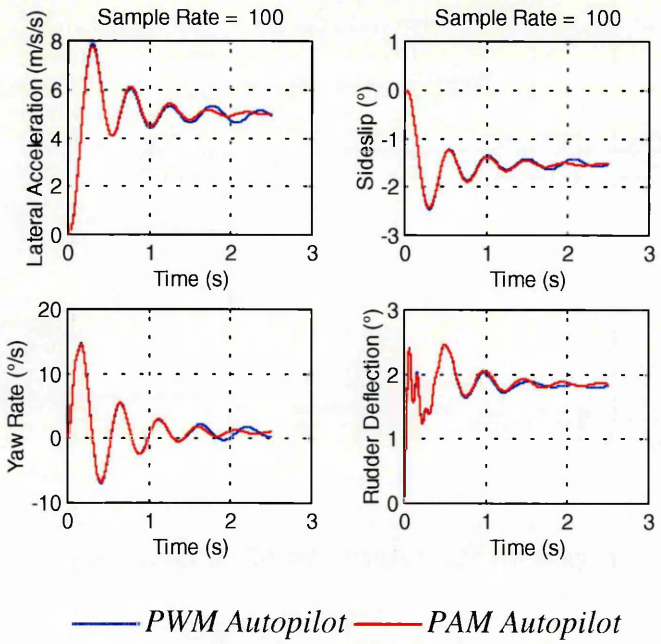

Figure 50 PWM & PAM Autopilot Response 100 Hz Sample Rate 2.5 Hz Autopilot Bandwidth

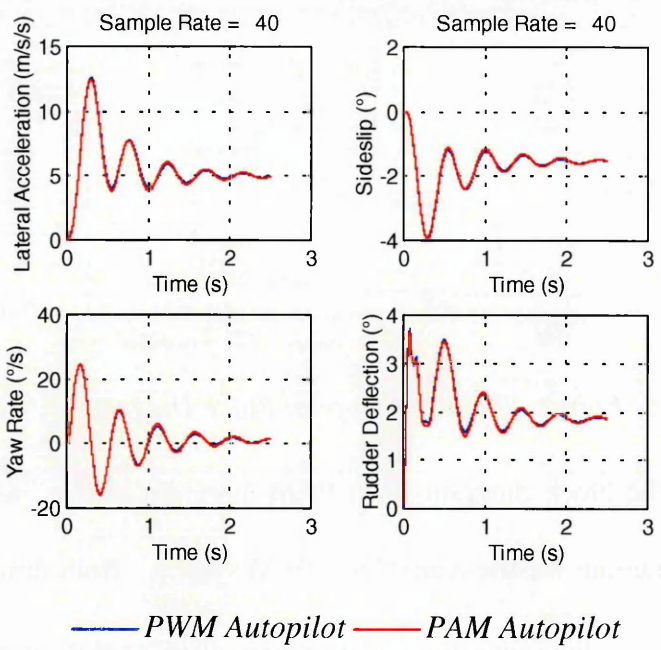

Figure 51 PWM & PAM Autopilot Response 40 Hz Sample Rate 2.5 Hz Autopilot Bandwidth

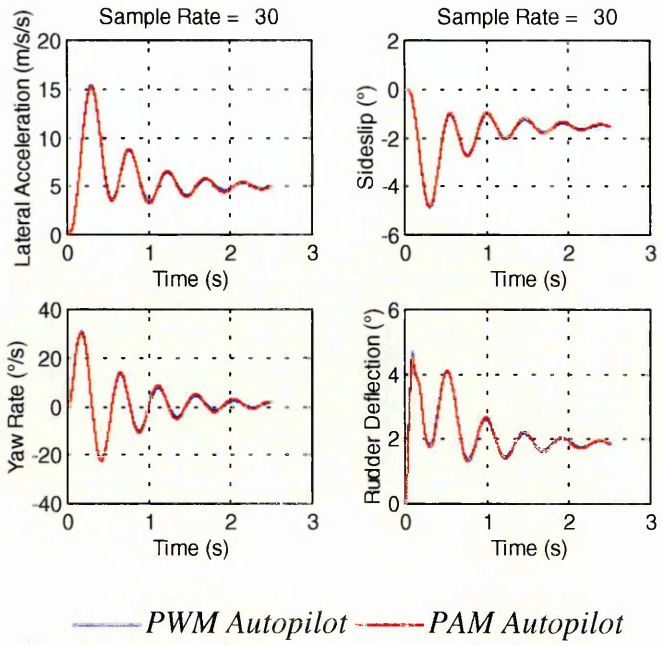

Figure 52 PWM & PAM Autopilot Response 30 Hz Sample Rate 2.5 Hz Autopilot Bandwidth

Figures 50 through 52 show the PAM and PWM responses to a 5 $m.s^{-2}$ acceleration demand, assuming a 2.5 Hz autopilot bandwidth for a variety of sample rates. As the sample rate reduces, the overshoot in the achieved acceleration becomes more pronounced, primarily as a result of the phase shift induced by the low sampling rate. It can be readily observed that the PAM and PWM responses are essentially the same and that the system achieves the design objective of producing a PWM design equivalent to a PAM design.

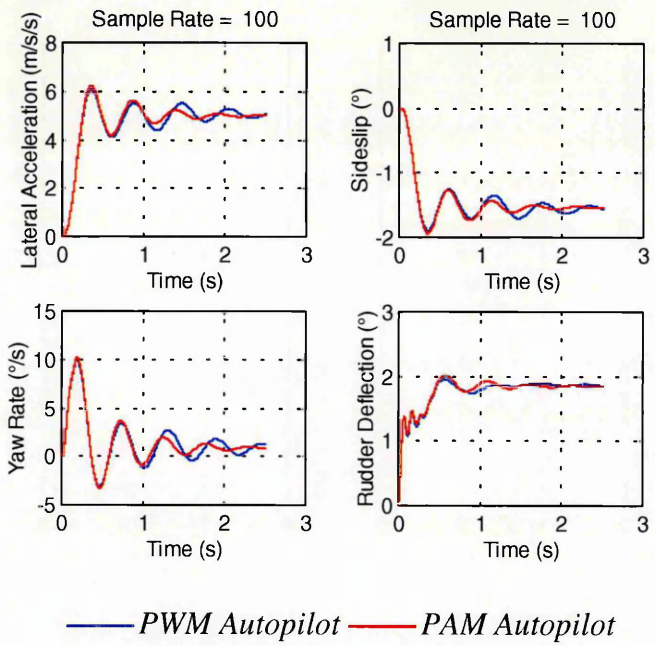

Figure 53 PWM & PAM Autopilot Response 100 Hz Sample Rate 2.0 Hz Autopilot Bandwidth

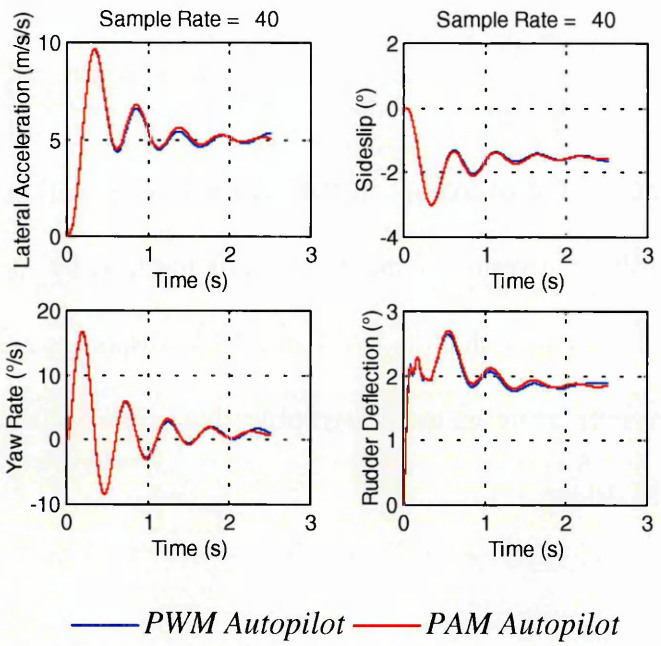

Figure 54 PWM & PAM Autopilot Response 40 Hz Sample Rate 2.0 Hz Autopilot Bandwidth

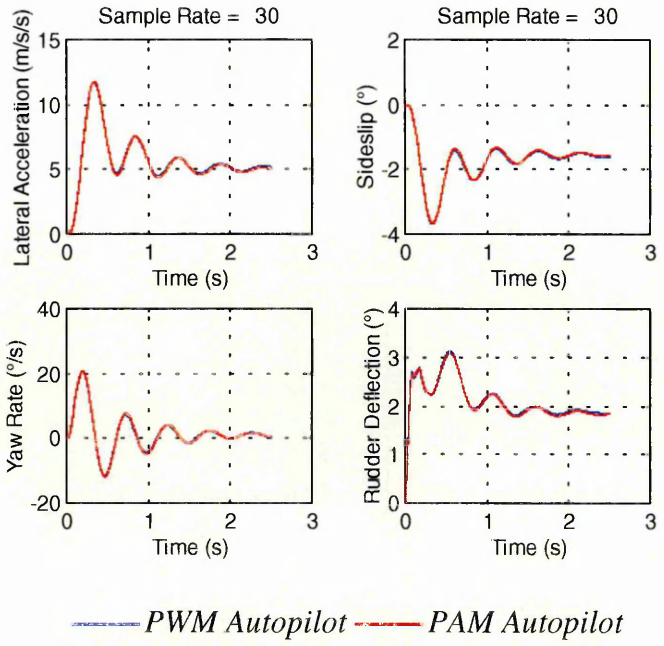

Figure 55 PWM & PAM Autopilot Response 30 Hz Sample Rate 2.0 Hz Autopilot Bandwidth

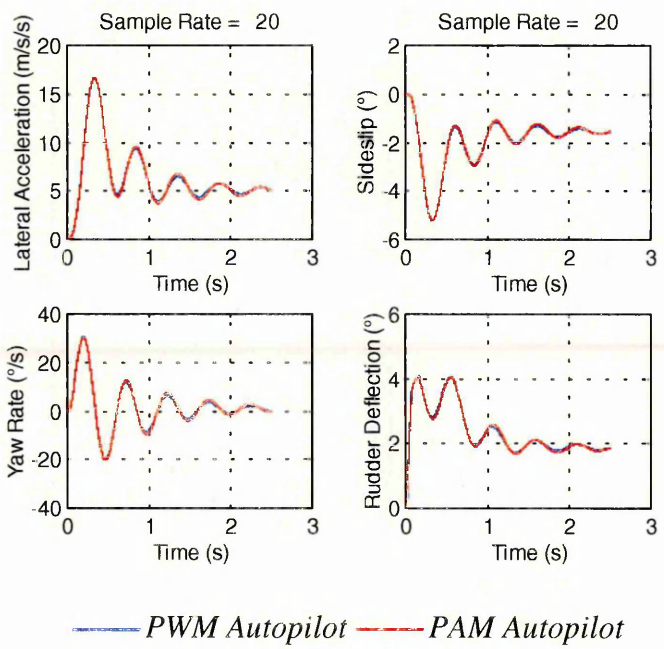

Figure 56 PWM & PAM Autopilot Response 20 Hz Sample Rate 2.0 Hz Autopilot Bandwidth

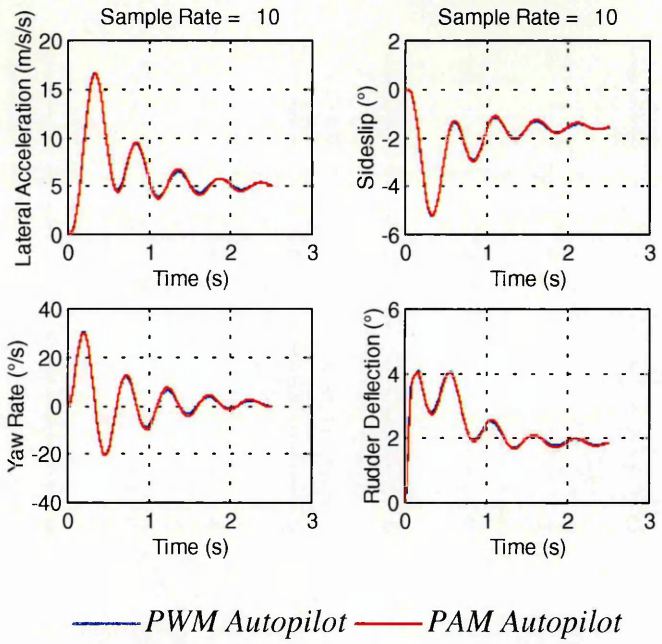

Figure 57 PWM & PAM Autopilot Response 10 Hz Sample Rate 2.0 Hz Autopilot Bandwidth

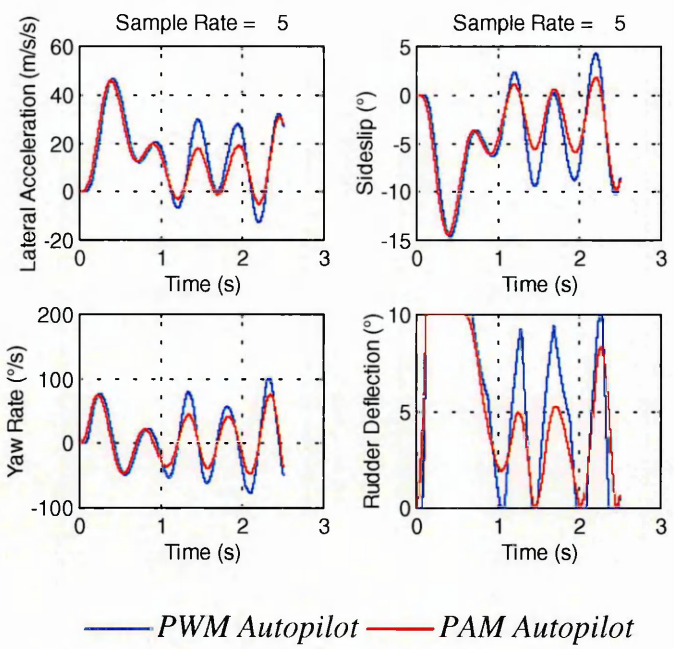

Figure 58 PWM & PAM Autopilot Response 5 Hz Sample Rate 2.0 Hz Autopilot Bandwidth

Figures 53 through 58 show that the overshoot can be reduced by a comparatively modest reduction in the autopilot bandwidth to 2.0 Hz. The figures also show that low sample rates can be achieved and a satisfactory response still results. This is

primarily as a result of the inherent robustness in the autopilot design using both acceleration and rate feedback but also serves to demonstrate that the inherent robustness of the linear design is incorporated into the nonlinear design. At sample rates below 10 Hz the response for both systems becomes unstable, once again the behaviour of the PWM and PAM designs is very similar.

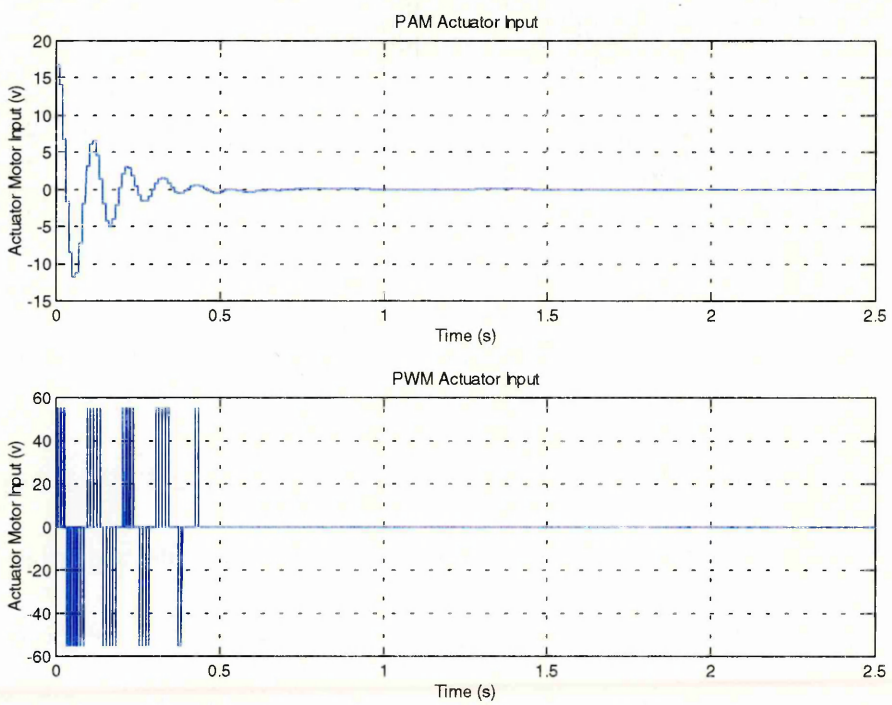

Figure 59 PWM & PAM Actuator Input 100 Hz Sample Rate 2.0 Hz Autopilot Bandwidth

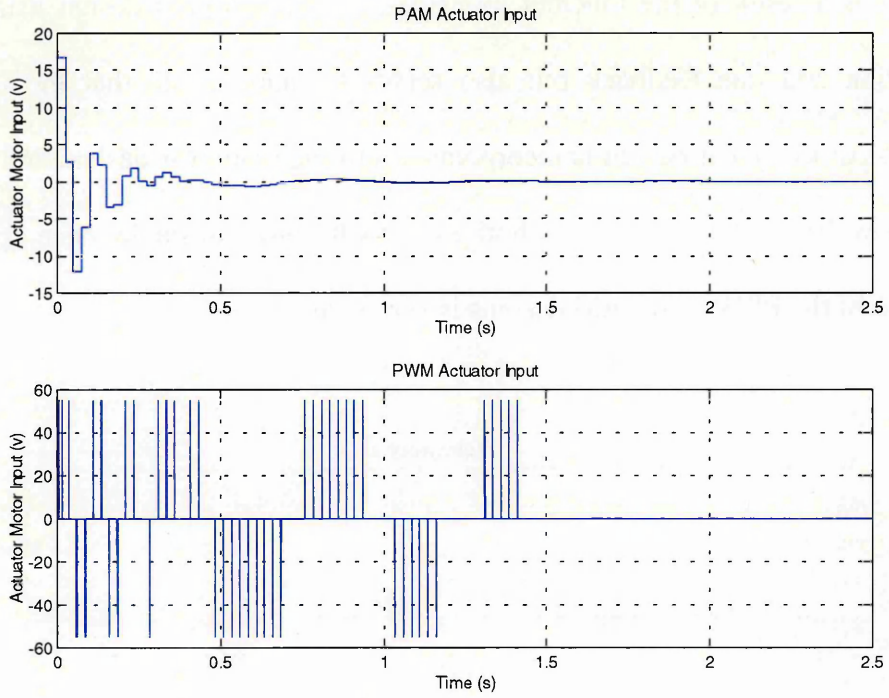

Figure 60 PWM & PAM Actuator Input 40 Hz Sample Rate 2.0 Hz Autopilot Bandwidth

Figures 59 and 60 show the input to the actuator in the PAM and PWM designs for sample rates of 100 Hz and 40 Hz. The main effect of the sample rate appears to be destabilising primarily as a result of the phase shift introduced by sampling. With the lower sample rate, the system input to the actuator takes much longer to decay in comparison with higher sample rates, over twice as long in this particular example.

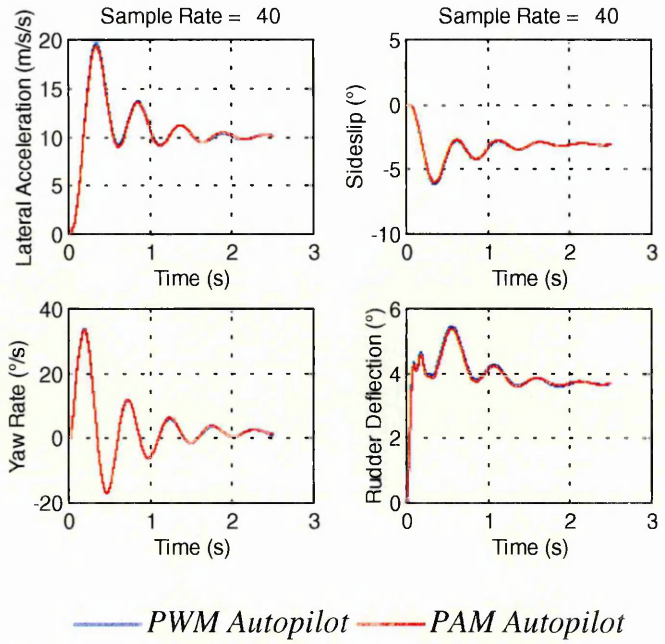

Figure 61 PWM & PAM Autopilot Response 10 m.s^{-2} Demand 40 Hz Sample Rate 2.0 Hz Autopilot Bandwidth

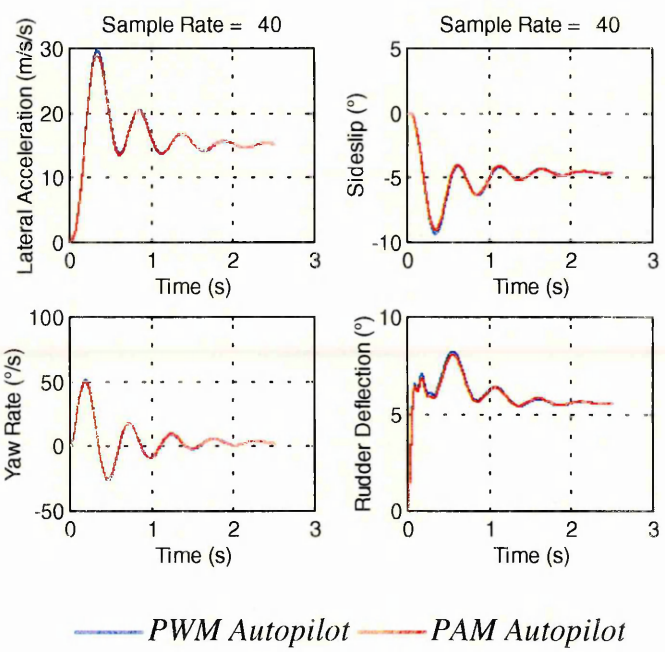

Figure 62 PWM & PAM Autopilot Response 15 m.s^{-2} Acceleration Demand 40 Hz Sample Rate 2.0 Hz Autopilot Bandwidth

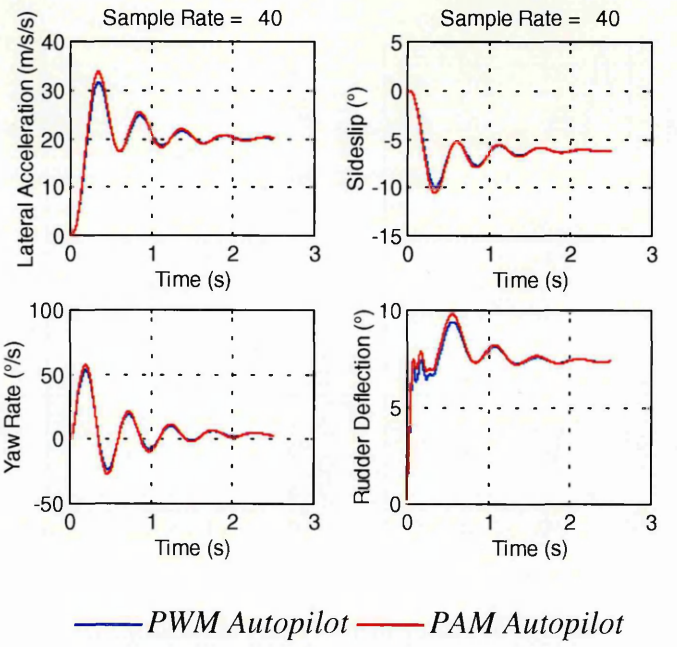

Figure 63 PWM & PAM Autopilot Response 20 m.s^{-2} Acceleration Demand 40 Hz Sample Rate 2.0 Hz Autopilot Bandwidth

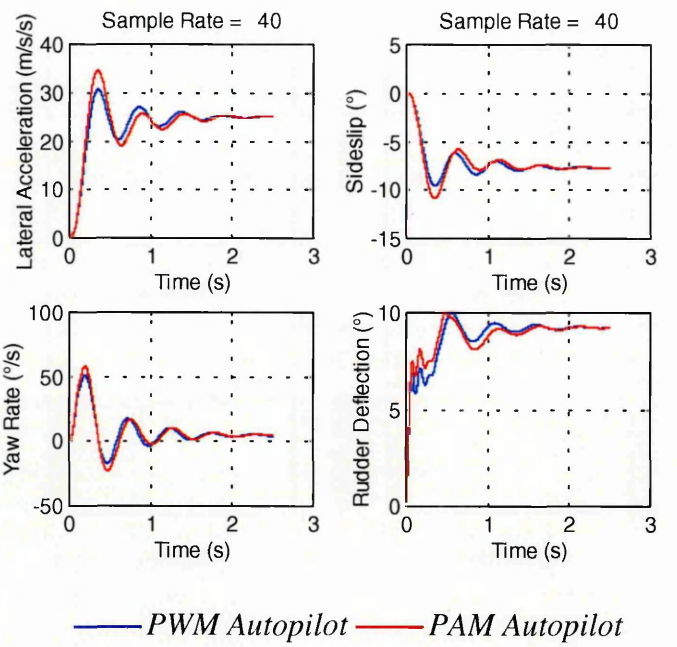

Figure 64 PWM & PAM Autopilot Response 25 m.s^{-2} Acceleration Demand 40 Hz Sample Rate 2.0 Hz Autopilot Bandwidth

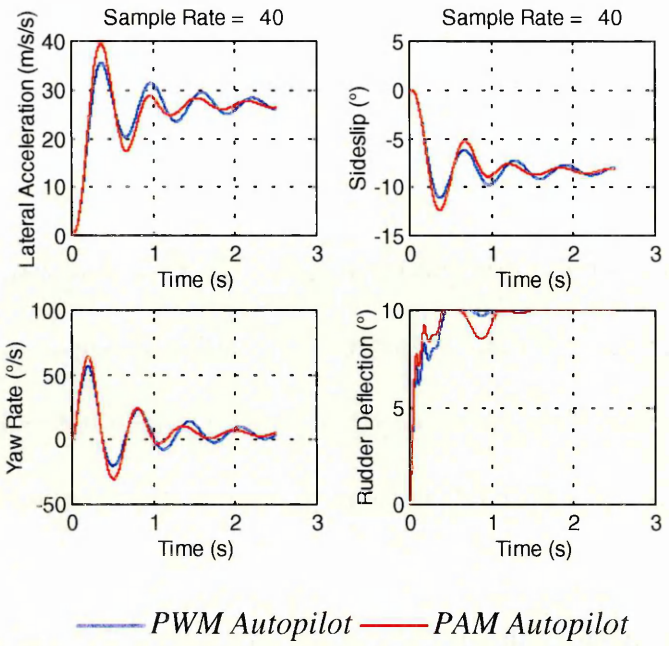

Figure 65 PWM & PAM Autopilot Response 30 m.s^{-2} Acceleration Demand 40 Hz Sample Rate 2.0 Hz Autopilot Bandwidth

Finally Figures 61 through 65 show the effect of various acceleration demands between 10 and 30 m.s^{-2} for a sample rate of 40 Hz and an autopilot bandwidth of 2 Hz. As the maximum deflection is limited to 10° the system could be expected to saturate at demands in excess of 27 m.s^{-2}. The response of both autopilots remains approximately the same for modest to large acceleration demands. As the system is nearly saturated by acceleration demands in the region of 27 m.s^{-2} the response of both systems remains essential the same, although there is a tendency for the overshoot in the PWM system to be slightly less than for the PAM system. This is probably due to the fact that the input to the actuator is constant over a sample period in the PAM system and so the actuator is in constant motion. However, in the PWM system the actuator is driven cyclically and so achieves a slightly smaller deflection as illustrated in Figures 64 and 65.

2.8 Conclusions

The first section of this document demonstrates that existing weapon systems can be enhanced by the use of INS/GPS navigation systems to be enable an all-weather day/night capability. An intuitive guidance design has been demonstrated to be able to enhance these legacy weapons. However, the design example presented retains many of the limitations of the existing system including undesirable features such as reduced impact velocity and a tendency to impact short of the designated target.

Consideration was given to the use of phase-plane analysis to design a nonlinear control system using "bang-bang" actuator controls. However, this technique proved to be unsatisfactory, since it relies entirely on the open loop response of the airframe to control input. As the system is required to consider a wide range of possible Mach numbers and altitudes this is clearly undesirable since the aerodynamic derivatives will vary tremendously. Also relying on the open loop airframe response is unsatisfactory since the airframe bandwidth tends to be low and therefore the response is sluggish. A further consideration is the potential requirement to reduce incidence at impact (a critical factor in the attack of hard targets), since the open loop response typically takes 2-3 s to allow incidence to decay, requiring guidance be shut down at some considerable distance from the target.

A PWM design technique proposed by Bernelli-Zazzera et al[4] was considered and demonstrated to be a suitable technique for designing a PWM autopilot design. Later improvements suggested by Zimpfer et al[43] were considered and demonstrated

to improve the match between the dynamic response of the PAM and PWM control systems.

After some consideration it was concluded that the design of a PWM autopilot must consider the effect of actuator dynamics since these can dominate the response. This complicates the design since a "bang-bang" controller is essentially an open loop device and, therefore, there is no linear equivalent upon which to base the PAM and PWM designs.

The use of an observer to provide state feedback and hence close the control loop around the actuator was considered and shown to be a suitable technique but with some limitations. In a departure from current design practise, the inertial instruments must be placed at a different location from the centre of percussion in order for the fin state variables to be observable.

It has also been demonstrated that a reduced order observer design is possible which reduces the computational overhead of the design. Using a reduced order observer a fin controller design can be generated that can control a "bang-bang" actuator to achieve a proportional response.

Using the observer based fin controller a number of simulations have demonstrated that the PWM design technique proposed by Bernelli-Zazzera et al[4] and later improved by Zimpfer et al[43] is a robust technique and that the PWM response closely matches the PAM response. Both responses remain essentially the same even when

saturation is approached and very low sample rates may be achieved and a stable response will still result.

Using this technique it is concluded that the proportional response required by a guidance system to optimise impact parameters can be achieved using the existing "bang-bang" actuator system. This will, however, require inertial instruments but this is not considered a large overhead since these are required by the INS system.

3. Precision Guidance and Impact Control

3.1 Introduction

This section considers the guidance aspects of an air launched Precision Guided Munition (PGM) for the attack of fixed and moving targets. Initially techniques are considered for the simple interception of the desired target and later the modification of these techniques to tailor the impact conditions to meet specific performance criteria.

Obviously the principle objective of any guidance system is to ensure that the successful interception of the target, however, this is not the only objective. In the engagement of a hard target, such as a command bunker, the weapon is required to impact at a steep angle with aerodynamic incidence at a minimum. This reduces the possibility of ricochet and avoids the phenomenon known as "slap down", where the weapon impacts tail first. The latter can be a significant problem for penetrating warheads, since it can result in a split warhead casing thereby drastically reducing weapon effectiveness. Conversely, infrastructure targets, such as bridges, are best engaged with a shallow angle of impact, thereby concentrating blast effects with the target. Many missile warheads are directional and the guidance system must ensure that the target is engaged within the optimum parameters of the warhead. Examples of such warheads include the shaped charge and the continuous rod.

The origin of air-launched guided weapons is a great deal older than many people would imagine; indeed the very first experiments took place before the First World

War. However, practical guided weapons did not emerge until the Second World War and included among the first examples was the German Hs 293 Glider Bomb; further details may be obtained from Benecke and Quick[3]. This was a 1000 lb. class weapon with a range of over 7.5 miles and employed a form of guidance known as Command to Line of Sight (CLOS). As shown in Figure 66, the concept behind CLOS is extremely simple and essentially involves constraining the missile flight path such that the missile always appears to lie on a path connecting an observer and the intended target. The simplicity of the technique has ensured that it has continued to be used extensively in guided weapons.

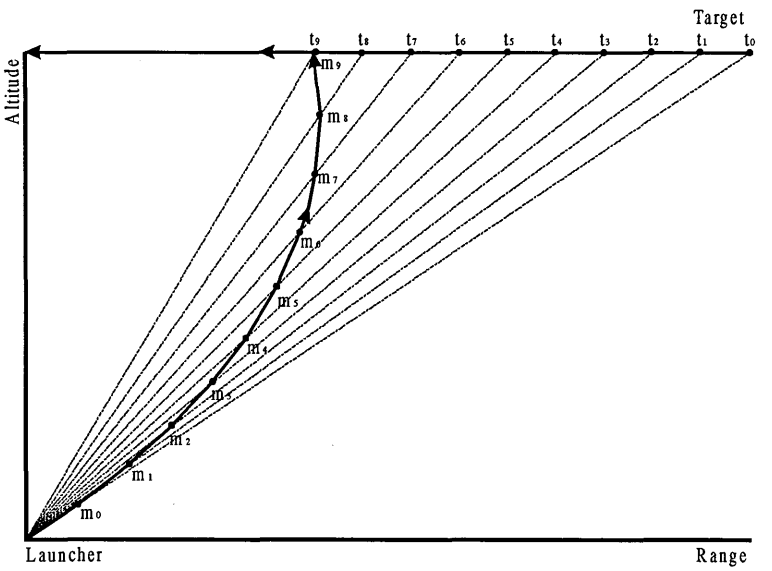

Figure 66 Command to Line of Sight Guidance

Although CLOS is widely used in missile applications it has a number of disadvantages. One of the main operational disadvantages is that it requires the launch vehicle to maintain a line of sight to the target. This not only exposes the launch vehicle to hostile action but damage incurred by the launch vehicle may also preclude a successful engagement.

The technique also imposes a number of constraints on the weapon that can limit the kinematic engagement zone. To illustrate this latter point, consider the curvature of the missile trajectory shown in Figure 66. During the flyout the missile maintains its position along the sightline by generating an acceleration normal to its flight path. However, it is apparent that the instantaneous velocity vector of the missile is, in general, not directed along the line of sight and, furthermore, toward the end of the engagement this angular offset can be quite large. Hence, toward the end of the engagement the increasing angular offset reduces the ability of the missile acceleration to change the sightline leading to increased control demands. Noting the comments above concerning the desirability of controlling the terminal phase of the engagement it can be seen that CLOS is unsuitable for this application. Fortunately there exists another simple and effective guidance law - Proportional Navigation. This section considers the use of Proportional Navigation (PN) guidance and its variants as a guidance strategy for an air launched PGM suitable for the attack of ground targets.

Initially a literature survey was undertaken and identified there is extensive coverage of the basic theory underpinning PN in open literature. What is perhaps surprising is that the coverage of variants of PN, such as angular impact control, is less extensive.

Following on from the literature survey variants of PN that enable control of the impact parameters was identified. These were then studied using a Lyapunov technique to establish the asymptotic stability of the control law and to indicate the constraints on the launch parameters to establish a successful intercept. Although a

useful technique, the Lyapunov method is not suited to establishing the full range of conditions under which an intercept is achievable. Hence, in addition to the use of the Lyapunov method, performance was assessed using six degree-of-freedom simulations.

3.2 Literature Survey

3.2.1 Introduction

There is extensive coverage of the study of PN in the literature and no study of the subject could hope to be completely comprehensive. The available literature falls into a number of broad categories, including qualitative analysis of PN, linearisation of the nonlinear intercept equations, the application of optimal control schemes, as well as general reference works that consider the fundamentals of the guidance strategies.

The basic equations of motion governing PN are highly nonlinear and unsuitable for an analytical solution but many authors attempt to derive such a solution through the use of linearising assumptions. These techniques have limited application due to the assumptions involved but nevertheless offer a useful insight into the use of PN. In a similar vein, many authors use qualitative methods to assess PN that are useful in establishing the launch requirements for a successful intercept.

Exo-atmospheric interception of ballistic missile targets is an interesting application of PN that poses many challenges for the control engineer. The very nature of such intercepts requires the use of divert thrusters by the pursuer and therefore the control

effort expended is of great concern. Fuel required for divert is at a premium and any method to reduce the control effort results in considerable benefits for the weapon design. As a result this particular problem has been singled out for considerable attention in recent years, much of the research concentrating on the use of optimal control methods to minimise control effort.

Finally, many authors report the development of variants of PN guidance laws. This includes the use of state estimators to estimate target motion in augmented PN, variations concerning the direction of the applied acceleration in ideal, true and pure PN, and biased PN in which an angular rate bias is added to the sightline rate.

3.2.2 General References

Garnell and East[10] have produced a general reference work that considers many of the fundamental features of guided weapon control systems. This includes target tracking systems, servo-control mechanisms, missile instruments, aerodynamic transfer functions, autopilot design, CLOS guidance, seekers and proportional navigation. A simple analogy is used to introduce the concept behind Proportional Navigation and to explore the effect of the kinematic gain. Assuming that the target and missile maintain an essentially straight-line course in the final stages of the intercept a simple mathematical model of the intercept is derived using small perturbations about the constant bearing trajectory. This is then used to identify optimum values for the kinematic gain, to show the effect of a heading error, the effect of evasive manoeuvres by the target, angular noise in the seeker head and glint (an apparent shift in the radar centre of a target). It is also shown that in the terminal

part of the engagement many homing systems can become unstable, although in a well designed system the effects of such instability has a limited effect upon the miss distance. Also introduced, is a variant of PN known as acceleration vectored navigation. This includes a component of the acceleration demand that is related to the sightline angle, which compensates for errors due to the axial component of the missile acceleration resulting from the propulsion system. Finally, the integrated form of PN is introduced in which the feedback term is the sightline angle rather than the sightline rate.

Zarchan[42] is acknowledged as an expert in this field and has published a number of papers on this subject. This is a useful reference that covers many aspects of the field. Initially, Zarchan[42] introduces the concept of PN and then develops a simplified engagement simulation for further insight into its effectiveness as a guidance strategy. More detailed simulations show that these simple models are accurate indicators of the system performance, in spite of the simplicity of the closed form solutions derived. The method of adjoints is introduced; a technique that has been used by many authors to establish the performance of PN and its derivatives. Also introduced is the concept of augmented proportional navigation, in which estimates of the target motion are used to compensate for the destabilising effect of evasive manoeuvres. The subject of noise and its effect upon the guidance system is covered extensively and methods to establish accurate estimates of miss distances are introduced. Later chapters discuss Kalman filters and other forms of tactical guidance such as Lambert guidance and gravity turn manoeuvres for strategic missiles.

Rogers[28] considers the use of PN for an air-launched inertially guided missile for the attack of ground targets. Using vector algebra, Rogers[28] derives the rate of change of the sightline as a function of the relative motions of target and missile. This expression is then used to demonstrate that a normal acceleration by the missile can be used to change the sightline rate. Using simplifying assumptions of a stationary target and a constant missile speed optimal control theory is used to derive an optimal value for the kinematic gain. Rogers[28] also derives a variant of proportional navigation that can be used to approach the target along a predefined approach vector. Finally, Rogers[28] considers an alternative method of gravity compensation that steers the missile onto a ballistic interception trajectory.

3.2.3 Classification of Proportional Navigation

Due to its importance as a guidance law, considerable effort has been expended in the analytical study of PN. However, such analysis has been hampered by the highly nonlinear nature of the intercept equation, even if the analysis is simplified by constraining the intercept to lie within a plane. Attempts to solve the PN equations have concentrated on two separate approaches, the main difference between these approaches being in the formulation of the guidance demand. In Pure PN (PPN), the acceleration demand is formulated normal to the pursuer velocity vector, whereas in True PN (TPN), the acceleration demand is formulated normal to the instantaneous line of sight. A further variation of TPN is the so-called Generalised TPN, in which the acceleration vector is not normal to the line of sight but has a fixed angle relative to it. Depending on the nature of the intercept, these subtle definitions in the formulation of PN can have a significant effect.

Shukla and Mahapatra[30] consider a review of the existing literature and compare PPN, TPN and GTPN. It is noted that PPN has only been solved in a closed form for the interception of a non-manoeuvring target with a fixed and discrete value of the kinematic gain. This is represented by the special case when the kinematic gain is either unity or two. These values are not particularly useful; a value of unity is equivalent to CLOS guidance, where it is known that excessive guidance demands can result in the terminal stages of the intercept. A value of two results in an intercept, where the pursuer maintains a constant acceleration throughout the intercept; hardly an optimal solution. On the other hand TPN is mathematically tractable and it is noted that several papers have been published containing solutions of the TPN problem. Similarly GTPN was introduced as a technique for solving the PN equations and since GTPN is a generalisation of TPN, the same techniques used to solve GTPN can be extended to solve TPN. However, since the technique for solving GTPN involves a change of variable, it is less useful for obtaining a meaningful physical insight into PN. In the special case of a tail chase, it is demonstrated that there is little to choose between the two forms of PN, since for a given kinematic gain both require a similar amount of control effort. However, as the line of sight diverges from the tail chase, TPN requires an ever-greater control effort. In the example contained in the paper, TPN requires a control effort some 27% greater than PPN when the sightline is at 60° from the tail chase. Using PPN an intercept is always possible except for one definite direction and then only when the kinematic gain is less than two; a value that would be unusually low. Therefore, in general, this is not a practical limitation. TPN on the other hand can only achieve a successful intercept provided certain constraints on the initial geometry are

imposed. In PPN, the lateral acceleration is a decreasing function of the time to go provided the pursuer has a speed advantage and a suitably high kinematic gain. Once again for practical systems this is not a meaningful limitation, whereas with TPN the boundedness of the acceleration demands is a function of the initial geometry. It is demonstrated that PPN is more robust and requires less control effort than TPN.

3.2.4 Pure Proportional Navigation

Guelman[13,14,15] appears to have been one of the first authors to consider a qualitative approach to studying PPN and has published a number of papers on the subject. Previous researchers had tended to approach the subject by the use of simplifying assumptions. These reduce the nonlinear differential equations that describe the pursuit of the target into a linear differential equation solvable in a closed form. These were generally limited in application and were often limited to the terminal phases of the engagement. Guelman[13,14,15] successfully demonstrated that qualitative methods could be used to obtain a general solution of a planar pursuit of a target. Initially he considered the special case of a non-manoeuvring target and demonstrated that a missile would always reach the target, with the exception of a finite number of initial conditions. Furthermore, he demonstrated that the missile would always arrive at the target travelling along a straight line, the angle of which was determined by the initial conditions. The boundedness of the rate of change of the sightline was established and the initial conditions under which the rate of change was diminishing at the end of the engagement were identified. This technique was later extended to a manoeuvring target, where the concept of dividing

the plane of pursuit into classes of sectors defined by the relative motion of the missile and target was introduced. This enabled the conditions to be established, under which the missile would reach the target for any given initial state. This work also enabled the boundaries of missile acceleration to be established based upon cases where the missile lay in pre-assigned regions of the pursuit plane. A later paper extends this work for more general cases.

Ha et al[16] introduce the concept of a Lyapunov like function for the qualitative study of PPN, although they neglect to demonstrate that the function they suggest is a Lyapunov function. Nevertheless the method they suggest appears to be extremely powerful and is used to demonstrate that a short-range homing missile can always intercept a target manoeuvring randomly with time varying normal acceleration provided the kinematic gain is large enough. Song et al[32] use this concept further in the analysis of PPN guidance in three-dimensional space.

Ghawghawe and Ghose[11] examined the use of the Lyapunov technique to determine the capture zones for a missile but found that the method demarcates a small element of the capture region. This is perhaps understandable since many different Lyapunov functions are possible and no single function can be considered valid over the entire region. It is noted in the earlier paper, Ha et al[16], that some of the conditions imposed by the function they suggest are quite weak and that capture can still occur outside of the region suggested. Instead the method pioneered by Guelman[13,14,15] is extended to derive representative conditions for capture, which can demarcate almost the whole of the capture region. It is demonstrated that a time

varying target manoeuvre changes the capture region but does not reduce it drastically and that the worst case capture region is that defined by a constant target manoeuvre at the extreme of the manoeuvre envelope. Some bounds on missile acceleration are also obtained for a limited subset of regions of the engagement plane.

3.2.5 True Proportional Navigation

Murtaugh and Criel[26] were one of the first authors in the open literature to propose PN in the TPN form. In this paper, the application of TPN for the exo-atmospheric interception of a satellite is considered, although the guidance theory presented is in effect generic and can be applied to the interception of a non-manoeuvring airborne target. Murtaugh and Criel first present the basic theory of proportional navigation, then derive the equations of motion for an intercept using TPN. This is underpinned by an example using a space vehicle with an infinitely variable rocket motor and an attitude control system to orientate the thrust axis. Further variants of PN are also introduced, firstly, Biased PN (BPN) is considered, in which a constant rate bias is added to the sightline rate. Also considered is PN with a dead band at low sightline rates. Using the intercept equation, the effect of the kinematic gain is considered and it is demonstrated that for a kinematic gain less than two, the sightline rate and acceleration demand tend to infinity as time to go diminishes. A singular solution results for a kinematic gain equal to two and this represents an intercept with a constant acceleration demand. A kinematic gain between two and three results in the sightline rate tending toward infinity as time to go diminishes. However, for values in excess of three the equations are well behaved and the sightline rate and

acceleration demands remain bounded throughout the engagement. In the proposed BPN scheme acceleration demands are commanded only when the sightline rate exceeds some positive bias value. The effect of the bias rate is to null the system response at low sightline rates, removing the tendency of the system to respond to noise signals. The bias term also reduces the sightline rate and, hence, the commanded acceleration is smaller. However, the reduction in the control effort for a given sightline rate requires a greater overall control effort, since the sightline rate continues to grow and larger demands result. Although in the example quoted BPN required a greater propellant mass than TPN, the required throttle range of the rocket motor was reduced. PN with a dead space is essentially identical to TPN unless the sightline rate falls below the threshold value. In the absence of control effort once the sightline rate is reduced below this value, the sightline rate will continue to grow once more and drift back outside of the dead band. This in turn will cause the control system to respond and drives the sightline rate back into the dead band. Thus it can be seen that a limit cycle is produced with the sightline rate oscillating about zero. Once again due to the cyclical nature and the lack of response at low sightline rates, a greater overall control effort is required in comparison with TPN. However, the additional control effort is smaller than with BPN and the throttle range is further reduced.

Yuan and Chern[38] give a brief literature review of TPN and its solutions. The work first introduced by Murtaugh and Criel[26] is introduced and the qualitative approach used by Guelman[13,14,15] to study TPN is described. It is noted that Guelman[13,14,15] obtained a closed form solution of the TPN intercept equation through the use of

certain simplifying assumptions. A refinement of Guelman[13,14,15]'s solution was then obtained by Yuan and Chern[38] that eliminated many of these assumptions. In this paper a further variation of the formulation of PN is proposed, Ideal PN (IPN), in which the commanded acceleration is applied in a direction normal to the relative velocity vector and it's magnitude is a function of the sightline rate and the closing velocity. This proposed scheme is, in effect, a variation upon GTPN in which the bias angle of the acceleration demand varies with the relative velocity vector. A closed form solution is presented for both manoeuvring and non-manoeuvring targets, the impact on the capture area considered, as well as the overall control effort required. The main drawback of TPN is that the forward velocity varies as a function of time. In the proposed scheme, this drawback is eliminated. As a result IPN has many of the features of PPN but can easily be obtained in a closed form solution. In a later paper Yuan and Hsu[40] present a closed form solution of GTPN for a manoeuvring target and examine the characteristics of GTPN such as the capture zone and the control energy cost function. As may be expected it is demonstrated that target manoeuvres reduce the capture zone and increase the cost function. Yuan and Hsu[39] further refine this solution and demonstrate that TPN is an optimal form of GTPN.

3.2.6 Augmented Proportional Navigation

Zarchan[42] considers a further variant of PN, known as Augmented PN, in which knowledge of the target behaviour is used to enhance the guidance law. In augmented PN, the commanded acceleration is not only a function of the sightline rate but also includes a term related to the target acceleration. Garnell and East[10]

and Zarchan[42] both demonstrate that a timely target acceleration can result in a large miss distance. Introducing the concept of the Zero Effort Miss (ZEM) Zarchan[42] develops the concept behind Augmented PN using a simplified heuristic argument. Zarchan[42] then introduces an example using the adjoint technique and demonstrates that Augmented PN can result in small miss-distances, reduced overall control effort and that, under certain circumstances, Augmented PN is an optimal control law. However, when a lag is introduced into the system the performance advantage of Augmented PN is reduced and, whilst Augmented PN has the advantage in short range engagements, PN has the advantage for longer-range engagements.

Ha et al[16] study a similar guidance law, where the target acceleration is modified by the sightline angle. Using the modified law Ha et al[16] demonstrate through simulation that the guidance demands are reduced in comparison with PPN. Assuming a scale factor error in the measurement of the target acceleration the effects of estimation accuracy are explored. This demonstrates that errors in the estimation can have a significant effect upon the guidance algorithm. The authors conclude that in addition to stochastic study of the target acceleration estimate, a deterministic estimation method needs to be explored.

3.2.7 Biased Proportional Navigation

As noted above, Murtaugh and Criel[26] considered the use of BPN for the exo-atmospheric interception of a satellite target. In this case, the bias return resulted in a greater overall control demand but reduced the throttle range of the divert motor.

In a later paper, Brainin and M^{c}Ghee[6] consider a similar problem, the exo-atmospheric interception of a target moving with a constant acceleration. It is noted that in an earlier paper by Ho et al[17] had demonstrated that under certain conditions PN was an optimum guidance law provided both the interceptor and target had perfect knowledge of the dynamic states and strategy of both participants. Brainin and M^{c}Ghee[6] demonstrate that when the interceptor knowledge of the target is reduced then PN is no longer optimal but that this could be improved with the addition of a correctly formulated rate bias term. The case considered is limited to a fixed target acceleration and it is further assumed that the interceptor has knowledge of the target capabilities. Hence, the interceptor can use this additional information to calculate a suitable rate bias term. The performance index chosen was the integral of the acceleration demand, since this is directly related to the divert propellant consumed and propellant mass is at a premium for this type of interceptor. After consideration of the equations of motion a nonlinear equation is solved numerically to find the optimum value of the rate bias. It is found that for values of the kinematic gain greater than four, the bias term asymptotically approaches a value defined by a simple function of the kinematic gain. In the case where the target manoeuvre capability is unknown a partially biased PN law is proposed where the bias term is a function of the time to go, the initial sightline rate and the initial sightline acceleration. A further simplification of this law is proposed where only the initial sightline rate is used to formulate the bias term. Although this latter scheme is less efficient, it is demonstrated to be more efficient than PN alone. Note that this result appears to contradict the earlier result reported by Murtaugh and

Criel[26], however, they did not consider a manoeuvring target, neither did they consider the formulation of the bias term as an optimal control problem.

Shukla and Mahapatra[30] also present an analytical study of the optimisation of the rate bias term, resulting in a similar conclusion that the rate bias term can improve the efficiency of BPN over PN alone. It is demonstrated that BPN has greater control efficiency for a range of target manoeuvres and in the presence of higher target accelerations. The optimum bias is derived from a simple algebraic equation, obtained using the assumption of small perturbations about a collision course. In the special case of a kinematic gain equal to 3, an optimum value for a collision course, the bias term is explicitly obtained from a simple quadratic equation. The benefits of BPN are demonstrated for a tactical air-to-air missile and for an exo-atmospheric interception. In the latter case, it is demonstrated that a significant reduction in divert propellant can result from the use of an optimal BPN scheme.

3.2.8 Impact with Angular Constraints

As noted in the introduction, there are often additional constraints applied to the guidance system other than the obvious requirement of hitting the target. An angular constraint is often applied to ensure that a weapon does not ricochet from a hard target or encounter an effect known as "slap down". The latter occurs when the weapon impacts with a high angle of attack and as a result a tail-first impact results. This results in an enormous turning moment and a violent side impact results. This can split the warhead casing, a particular problem with cast bombs, result in a fuze failure or simply failure to penetrate the target.

In addition to these concerns there are target effects to be considered. The attack of hard targets is generally best achieved with impact at a high angle to minimise the penetration requirement, a typical such target being a command bunker. Conversely other hard targets can require a shallow impact angle to achieve the same effect; an example of such a target would be a tunnel complex fitted with armoured blast doors. Many infrastructure targets, such as bridges, require a shallow angle of impact thereby concentrating the blast effects of the warhead within the target.

It is also noted that the effects of many warheads are directional in nature. Shaped charge warheads designed for the defeat of armour require impact at zero angle of attack to be effective. These warheads are also more effective when engaging the thinner turret armour, thereby imposing an additional angular requirement. A number of anti-armour weapons have been deployed using an EFP (Explosively Formed Projectile) warhead that can impose similar constraints on impact. Large shaped charges are also being deployed for the attack of hard targets, in this application a large pre-cursor shaped charge warhead makes the initial penetration, which is then followed by the main hard target penetrator warhead.

Noting that the desire to impose an angular constraint upon impact is driven by the features of many weapon systems, it was surprising to find that coverage of the subject in the open literature was limited. Although undoubtedly much of the research remains either classified or commercially sensitive, PN has nevertheless been the subject of extensive coverage in open literature.

Kim and Grider[22], in what appears to be pioneering research in to this subject, consider a terminal guidance system for a re-entry vehicle with a constraint on the attitude at impact. The guidance algorithm is formulated as a state space problem using state space feedback, with optimal control theory used to derive the feedback matrix. In this formulation, the guidance algorithm is divided between state estimation and the optimal control problem, although the state estimation procedure is the subject of a separate paper. Initially, the intercept equations are expressed in a nonlinear form as a function of the miss distance and the attitude angle. These are then linearised around the operating point and the optimal control problem is formulated using a performance index derived from the miss distance, impact angle and overall control effort. Solving the Riccati equation a linear function of the state variables is used to formulate the feedback matrix and simulation used to assess the performance of this control law. It was found that without a constraint on the control input the algorithm could successfully achieve the guidance requirements in terms of miss distance and angular constraint. However, the required control effort was excessive and with a constraint applied the guidance algorithm became unsatisfactory. It is also noted that the algorithm is particularly sensitive to errors in the estimation of the time to go. Reformulating the problem as a more conventional PN problem using the sightline rate was more successful.

York and Pastrick[37] consider a similar problem, namely the attack of armoured targets using anti-armour weapons; in this example a high angle of impact is required to engage the thinner turret armour. The paper is an extension of the work of Kim and Grider[22] and considers the effect of the autopilot lag and the angle of

attack of the missile upon the guidance solution. In the revised formulation, the lag is included in the formulation of the guidance algorithm. As the autopilot bandwidth becomes infinite, the solution tends toward the solution derived earlier by Kim and Grider and at low autopilot bandwidths, the control algorithm can become unstable. The practical implementation of the control law was briefly investigated to examine whether the states could be established from physically realisable measurements, with a linear function approximating the feedback gains. It was found that performance was sensitive to the error introduced by the linear function and even with an increasing number of breakpoints there was no improvement. Noting that the angle of attack is an important factor in the terminal part of the engagement, a reformulation of the control law including the angle of attack is presented. However, the control law that results does not readily lend itself to a closed form solution and is not considered further. Finally, the control law was reformulated to impose an angular constraint at impact. Through suitable choice of the weighting factors in the performance index it is asserted that the control law can achieve any arbitrarily demanded impact angle, however, although some results are presented the technique used to select the weighting factors is not reported.

As noted above, Rogers[28] presents a PN variant in which the target approach direction can be specified. As originally formulated the control law is designed so that an inertially guided missile is able to approach a target from any given bearing. However, since the approach direction is specified as a unit vector in space axes, the technique can equally well be applied to control the attitude angle at impact. The technique requires knowledge of both the sightline vector and the relative velocity

vector and so assumes that an Inertial Navigation System (INS) is present. This is typically available on the latest class of weapons but older weapons may use an autopilot based upon displacement gyroscope technology.

Kim et al[23] propose a BPN guidance law for an impact with angular constraint that utilises a time varying rate bias to achieve the desired impact angle. The algorithm was derived using the Lyapunov technique pioneered by Ha et al[16] and is developed as a generic technique with a wide variety of applications. Among the applications proposed include heavyweight torpedoes and anti-tank weapons. As formulated the guidance law does not require a time-to-go estimation, although a time-to-go estimation is in fact implicit in the formulation of the bias term. Also as the nonlinear intercept dynamics are implicit in the scheme, some guidelines are proposed as to the release parameters required to ensure a successful intercept. Noting the comments of Ghawghawe and Ghose[11] these are likely to be conservative and will not fully delineate the capture zone. The size of the capture zone is examined using simulation and is demonstrated to be considerably larger than using the scheme proposed by Kim and Grider[22]. However, such an assertion should be treat with caution as Kim and Grider[22]'s scheme was sensitive to errors in the time-to-go estimation and the simulations used by Kim et al[23] use an approximate value for time-to-go. It is also noted during the simulations a successful intercept with angular constraint could still be achieved even when some of the assumptions used in deriving the guidance law are violated. These results indicate that while the Lyapunov technique is useful as an analysis tool, it's ability to establish performance parameters are perhaps exaggerated by the authors. Assuming a collision course and

small angle approximations the optimality of the proposed guidance law is examined and an indication of the optimal values of the kinematic gain and the weighting factor for the rate bias term are obtained. The authors suggest that the system requires an active seeker in conjunction with a weapon INS for the implementation of the control law. However, further consideration of the control law as part of this study has shown that the control law can be implemented with just the weapon seeker and a relatively simple autopilot using displacement gyroscopes.

3.2.9 Effect of Target Motion

Zarchan[41] considers the effect of weaving targets on miss distance for a generic PN guidance law. Weave manoeuvres are a common countermeasure to PN guidance, since it is known that periodic manoeuvres can induce large miss-distances. Previous results indicating that the missile will always intercept the target had been derived on the basis that both the airframe and autopilot responses were zero lag. These assumptions are broadly applicable through much of the engagement but break down in the terminal phase. Assuming a simplified single time constant model of a PN guidance system, Zarchan[41] obtains closed form solutions for miss-distance as a function of the effective navigation ratio, guidance system time constant and the weave manoeuvre in terms of the magnitude and frequency of the weaving motion. Noting that the simple model of a single time constant underestimates the miss distance a higher order system is used to develop normalised miss distance design curves using normalisation factors from the simple simulations. As in previous work it is demonstrated that the manoeuvre advantage of the pursuer is a key factor in determining system performance. It is noted that many of the

insights obtained from the simpler model also apply in the higher order model and both models can be used to improve overall system performance.

Hough[18,19] has studied the use of optimal control and nonlinear estimation techniques for the interception of non-manoeuvring targets subject to aerodynamic drag and a ballistic missile target under acceleration during the boost phase. The main focus of Hough[18,19]'s research is orientated toward the interception of ballistic missile targets using a small Kinetic Kill Vehicle (KKV). As a KKV relies upon kinetic energy as the defeat mechanism, the guidance system is required to ensure extremely small distances in what is an extremely challenging interception problem. The first paper considers the implementation of simple, yet accurate optimal guidance and estimation algorithms. An optimal guidance algorithm is developed using the calculus of variations, initially assuming that there is three axis control of the acceleration command and later assuming two axis control using divert thrusters. An Extended Kalman (EKF) is developed, based upon the relative equations of motion of the interceptor and target and theoretical limits on miss-distance are assessed. This approach is extended in the second paper to include the effects of target motion.

3.2.10 Optimal Control

As noted previously many authors have used optimal control techniques in the study of various aspects of the guidance problem. In a brief paper Nazaroff[27] considers an optimal terminal guidance law using optimal control theory. Using the relative equations of motion simplified using small angle assumptions, a performance index

is formulated using the miss distance and the control effort. Using the Algebraic Matrix Riccati Equation (AMRE) an optimal control law is derived. This is then simplified for implementation in an airborne application.

Glizer[12] considers the closed-form solution of planar interceptions with prescribed end conditions using a performance index derived from the time of capture penalised by the control input. An optimal control solution is obtained by solving the nonlinear intercept equation involving elliptic integrals.

Ben-Asher and Yaesh[2] note that in recent years ideas from linear quadratic optimisation theory have been extensively applied in guidance problems. This reference introduces new guidance laws based upon one-sided optimisation theory and differential game theory. Initially, the classic problems in guidance theory are assessed using LQ methods and later more complex problems are examined including the effects of sub-system dynamics and manoeuvring targets. Also included are approaches to robust design using H_∞ methods.

3.3 Proportional Navigation

Proportional Navigation (PN) was apparently known to German scientists and engineers at Peenemunde but was not used in a weapon application during World War II. In parallel, PN was studied in the US under a naval programme that resulted in the Lark surface-to-air missile (SAM), one of the first practical systems. Initially it was derived using heuristic arguments and later subjected to more rigorous mathematical examination.

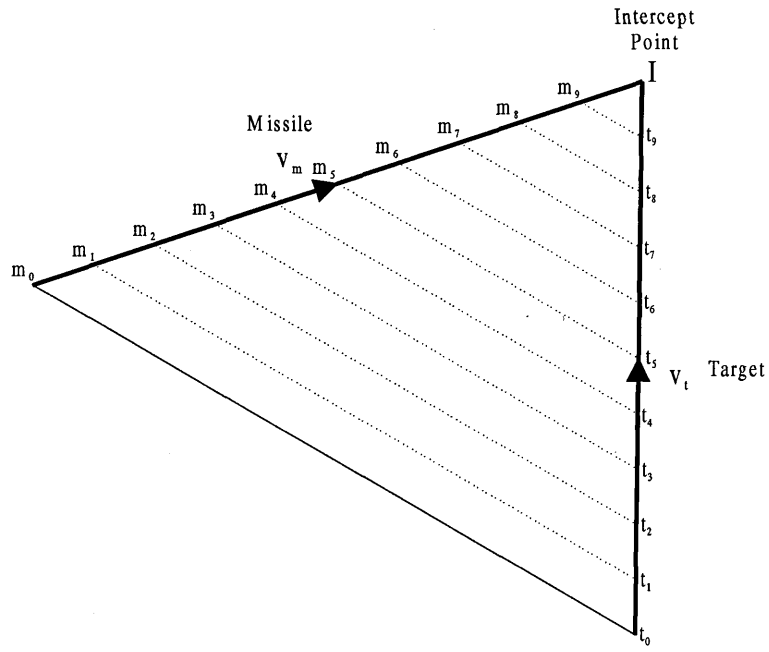

Figure 67 Collision Course at Intercept

The fundamental principle behind PN is not a new idea and in fact has nautical origins. Before embarking on a rigorous mathematical demonstration of PN it is useful to illustrate the intercept problem by means of a simple example. Consider the planar engagement shown in Figure 67 in which the missile and target are travelling at constant speed toward an intercept at point I. Next consider equal intervals of time Δt and the sightline from the missile to the target. It is clear that at each time interval the intercept triangle is similar, each successive sightline is parallel to the original sightline and, hence, the sight line angle remains constant. Clearly if the sightline does not rotate then the missile and target are on a collision course. This principle was well known to mariners, if the bearing to an approaching ship remained constant then avoiding action had to be taken. PN turns this principle on its head and attempts to force the sightline rate to zero by changing course in proportion to the rate of change of the sightline angle i.e.

$$\dot{\psi} = K.\omega_S \tag{127}$$

Where K is a constant known as the kinematic gain. Further insight can be gained by considering the very simple planar mathematical model of the intercept developed by Rogers[28].

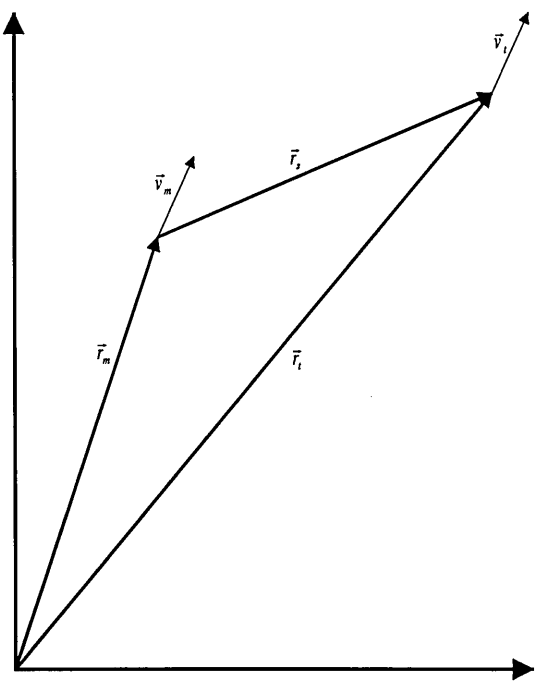

Figure 68 General Intercept Geometry

Referring to Figure 68, the position of the missile and target are denoted in a fixed frame of reference by two position vectors $\vec{r}_m$ and $\vec{r}_t$ respectively. Their velocities are given by:

$$\vec{v}_m = \dot{\vec{r}}_m,\ \vec{v}_t = \dot{\vec{r}}_t \tag{128}$$

The sightline vector and it's rate of change are therefore:

$$\vec{r}_s = \vec{r}_t - \vec{r}_m,\ \dot{\vec{r}}_s = \vec{v}_t - \vec{v}_m \tag{129}$$

If $\dot{\vec{r}}_s$ is entirely in the direction $\vec{r}_s$ then an intercept is inevitable, however, any component normal to the sightline will cause a miss. The normal component is equivalent to a rotation of the sightline given by:

$$\vec{\omega}_s = \frac{\vec{r}_s \times [\vec{v}_t - \vec{v}_m]}{\vec{r}_s \cdot \vec{r}_s} \tag{130}$$

Assuming that the target is moving with a constant velocity, i.e. $\dot{\vec{v}}_t = 0$, the sightline rate obtained by differentiating equation **(130)** is:

$$\dot{\vec{\omega}}_s = \frac{\dot{\vec{v}}_m \times \vec{r}_s}{\vec{r}_s \cdot \vec{r}_s} - 2\frac{\vec{r}_s \cdot (\vec{v}_t - \vec{v}_m)}{\vec{r}_s \cdot \vec{r}_s}\vec{\omega}_s \tag{131}$$

Equation **(131)** demonstrates that the sightline rate can be modified by the missile acceleration. As noted in equation **(127)**, in PN this is equivalent to:

$$\dot{\vec{v}}_m = K\vec{\omega}_s \times (\vec{v}_m - \vec{v}_t) \tag{132}$$

Hence, equation **(131)** becomes:

$$\dot{\vec{\omega}}_s = -(K-2)\frac{\vec{r}_s \cdot (\vec{v}_m - \vec{v}_t)}{\vec{r}_s \cdot \vec{r}_s}\vec{\omega}_s \tag{133}$$

In the closing stages of the intercept, the flight-path is virtually rectilinear, then:

$$\frac{\vec{r}_s \cdot (\vec{v}_m - \vec{v}_t)}{\vec{r}_s \cdot \vec{r}_s} \approx T - t \tag{134}$$

I.e. the time of flight remaining. Hence, equation **(133)** reduces to:

$$\dot{\vec{\omega}}_s = -(K-2)\frac{\vec{\omega}_s}{T-t} \tag{135}$$

Which has the solution:

$$\vec{\omega}_s = \vec{\omega}_0\left(1-\frac{t}{T}\right)^{K-2} \tag{136}$$

Where $\vec{\omega}_0$ is the initial sightline rate.

Referring to equation **(136)** it can be seen that the sightline rate reduces to zero provided the kinematic gain is greater than two.

The choice of the kinematic gain, K, depends on a number of factors. However, a simple example of a procedure for selection of the kinematic gain may be obtained using a performance index derived from the integral of the missile acceleration. Such a performance index could be:

$$I = \int_0^T \dot{\vec{v}}_m . \dot{\vec{v}}_m dt \tag{137}$$

Using the sightline history developed from the equations developed by Rogers[28], it is possible to demonstrate approximations for the optimum value of the kinematic gain. A stationary target is assumed and the missile velocity remains constant

throughout the engagement. Using equation **(132)** and noting that the vectors are orthogonal, equation **(137)** can be re-written as:

$$I = K^2 v_m^2 \int_0^T \vec{\omega}_s . \vec{\omega}_s \tag{138}$$

Using equation **(136)** and integrating results in:

$$I = \frac{K^2 v_m^2 \omega_0^2 T}{2K-3} \tag{139}$$

Differentiating with respect to K and equating to zero results in:

$$\frac{dI}{dK} = \frac{2K v_m^2 \omega_0^2 T}{2K-3} \cdot \left(1 - \frac{K}{2K-3}\right) = 0 \tag{140}$$

Which has the solutions, $K = 0$ and $K = 3$. Noting that equation **(136)** indicates that $K > 2$ solution $K = 0$ is rejected. Differentiating equation **(140)** results in:

$$\frac{d^2 I}{dK^2} = v_m^2 \omega_0^2 T \cdot \left\{ \begin{array}{l} \left(\frac{2}{2K-3} - \frac{4K}{(2K-3)^2}\right) \cdot \left(1 - \frac{2K}{2K-3}\right) + \\ \frac{2K}{2K-3} \cdot \left(-\frac{1}{2K-3} - \frac{2K}{(2K-3)^2}\right) \end{array} \right\} \tag{141}$$

Substituting $K = 3$ into equation **(141)** results in:

$$\frac{d^2 I}{dK^2} = 2/3 \, v_m^2 \omega_0^2 T \tag{142}$$

Hence, it has been shown for the particular case under consideration $K=3$ minimises the acceleration demands of the pursuer.

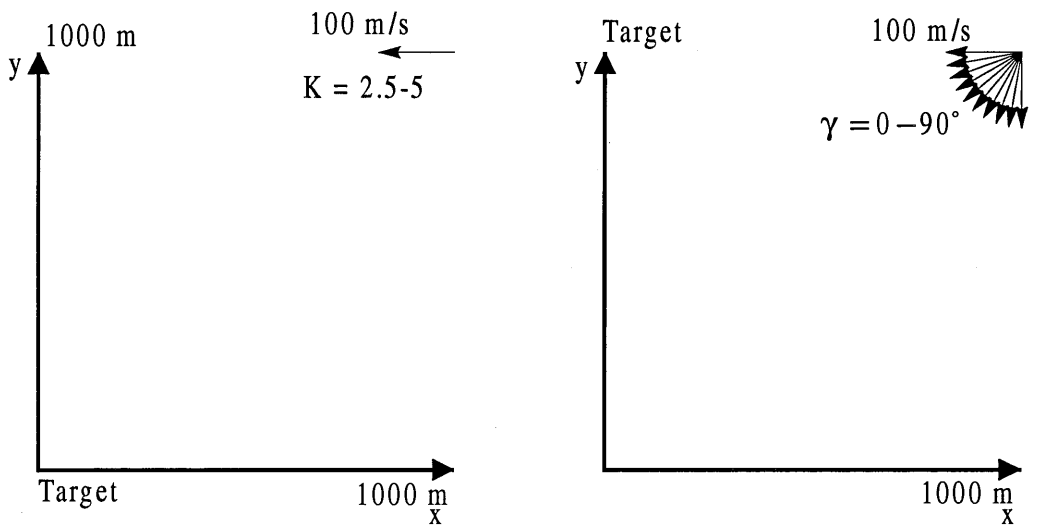

Figure 69 Initial Geometry Assumed in Simulations

Equation **(136)** may also be used to demonstrate the effect of the kinematic gain upon the commanded acceleration. Assuming a non-dimensional time base, t/T, and an initial missile/target geometry as shown in Figure 69, Figure 70 shows the commanded acceleration as a function of time. Note that a kinematic gain of 2 corresponds to the case where the missile maintains a constant acceleration throughout the engagement. Note also that a large kinematic gain has the effect of a large initial acceleration but that demands reduce throughout the engagement such that at the end of the engagement a reduced acceleration demand results. Integration of the acceleration time profile confirms that the performance index in equation **(137)** is at a minimum when the kinematic gain is 3. A similar procedure can be used to demonstrate the effect of an initial heading error as shown in Figure 71. As might be expected the larger the initial heading error the greater the commanded acceleration. However, for larger heading errors the increment in acceleration

demand diminishes since the initial sightline rate is related to the sine of the heading error.

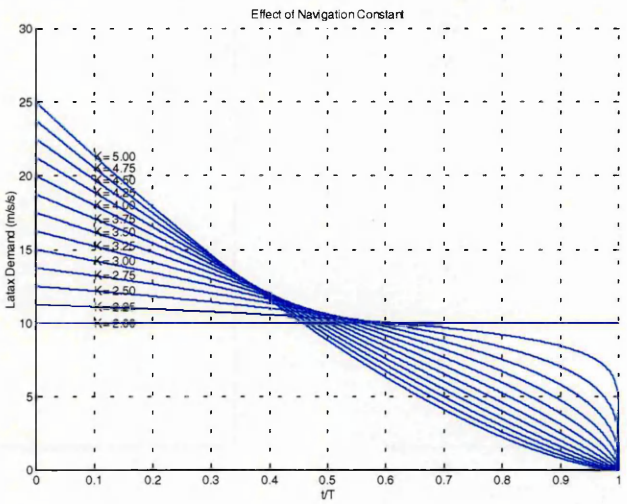

Figure 70 Effect of Kinematic Gain Upon Commanded Acceleration

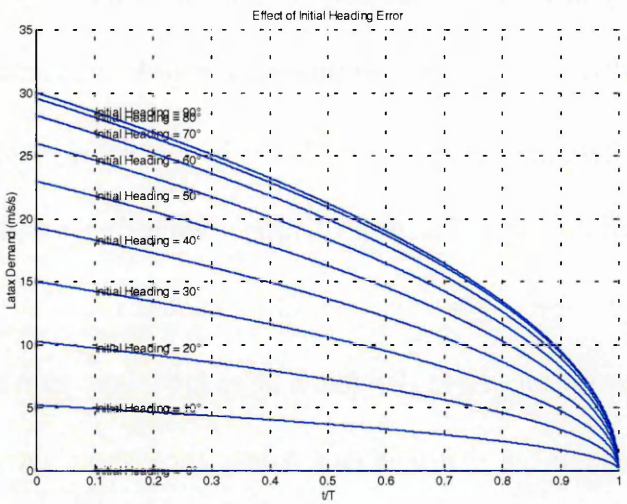

Figure 71 Effect of an Initial Heading Error Upon Commanded Acceleration

3.4 Linearisation About a Collision Course

The previous example shows how with a few simplifying assumptions a simple mathematical model of the PN intercept equations may be constructed. One of the

simplest techniques used by many authors is to linearise the equations of motion about a constant bearing trajectory i.e. a collision course. The method presented here is that of Ben-Asher and Yaesh[2].

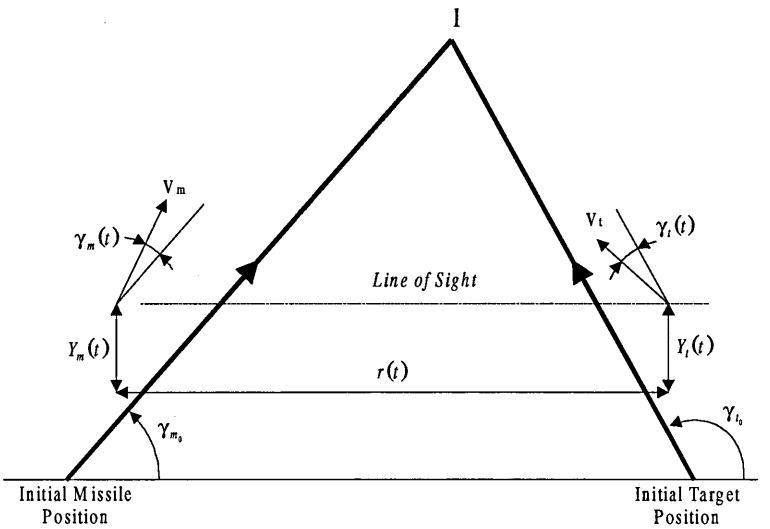

Figure 72 Two-Dimensional Engagement Geometry for Linearisation

It is assumed that the motion is constrained to a single plane and the speeds of the missile and target remain constant. It is further assumed that the trajectories of both missile and target may be linearised about a collision triangle as shown in Figure 72 above. The condition for a collision course requires that:

$$V_m \sin(\gamma_{m_0}) - V_t \sin(\gamma_{t_0}) = 0 \tag{143}$$

The nominal closing velocity is given by:

$$V_c = -\dot{r} = V_m \cos(\gamma_{m_0}) - V_t \cos(\gamma_{t_0}) \tag{144}$$

And, hence, the nominal time of flight is:

$$t_f = r(0)/V_c \tag{145}$$

Denoting the relative separation of the missile and target by $y(t)$, i.e.:

$$y(t) \equiv Y_t(t) - Y_m(t) \tag{146}$$

The relative separation of the missile and target may be defined as a differential equation:

$$\begin{aligned} \dot{y}(t) &= \dot{Y}_t(t) - \dot{Y}_m(t) \\ &= V_t \sin\left(\gamma_{t_0} + \gamma_t(t)\right) - V_m \sin\left(\gamma_{m_0} + \gamma_m(t)\right) \end{aligned} \tag{147}$$

Using small angle approximations and equation **(143)** this may be simplified to:

$$\dot{y}(t) = \dot{Y}_t(t) - \dot{Y}_m(t) = V_t \cos\left(\gamma_{t_0}\right)\gamma_t(t) - V_m \cos\left(\gamma_{m_0}\right)\gamma_m(t) \tag{148}$$

Denoting the sightline angle by $\sigma(t)$ and assuming without loss of generality that $\sigma(0) = 0$. Once again using the small angle assumption the sightline angle is defined by:

$$\sigma(t) = y(t)/r(t) \tag{149}$$

Hence, differentiating equation **(149)** with respect to time, the following equation for the sightline rate is obtained:

$$\dot{\sigma}(t)=\frac{d}{dt}\left(\frac{y(t)}{r(t)}\right)=\frac{y(t)}{V_c\left(t_f-t\right)^2}+\frac{\dot{y}(t)}{V_c\left(t_f-t\right)} \tag{150}$$

Figure 73 shows a simplified block diagram of a generic guidance system using the linearising assumptions. In this example, the relative acceleration between the missile and target is integrated twice to obtain the relative position, which at the end of the flight is of course the miss-distance. Using equation **(149)** the small angle assumption is used to yield an approximation of the sight-line angle. Differentiation of the sightline angle yields the sightline rate that is processed by the guidance system into an acceleration demand. The flight control system implements the guidance demand.

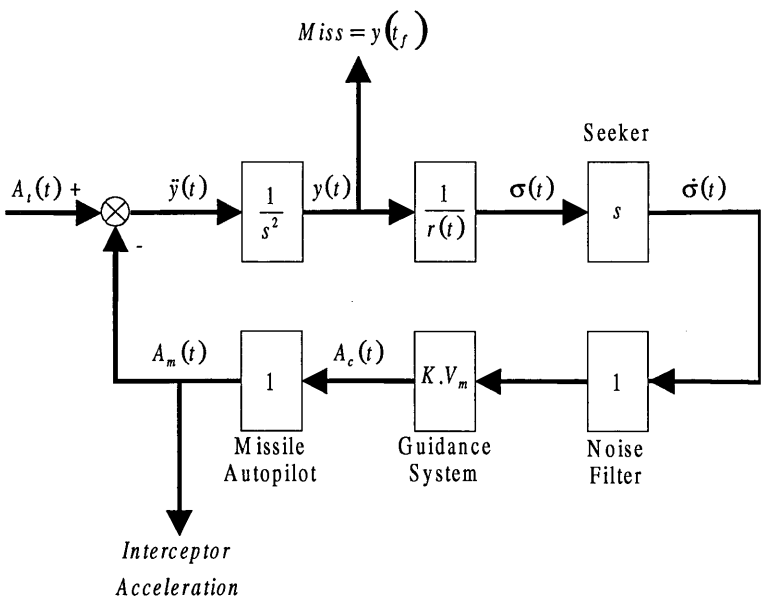

Figure 73 Simplified Block Diagram of PN Simulation

3.5 Integrated Proportional Navigation

One of the main advantages of PN is that it can be implemented in an integrated form and the two forms of PN are equivalent. This is particularly useful in weapons

where the inertial instruments are in the form of displacement gyroscopes and the guidance demand is formulated as an Euler angle demand. The equivalence of the two forms of PN is shown easily with a simple example.

Integrated PN uses a guidance law of the form:

$$\gamma_m(t) = K\left(\gamma_m(t) - \sigma(t)\right) \tag{151}$$

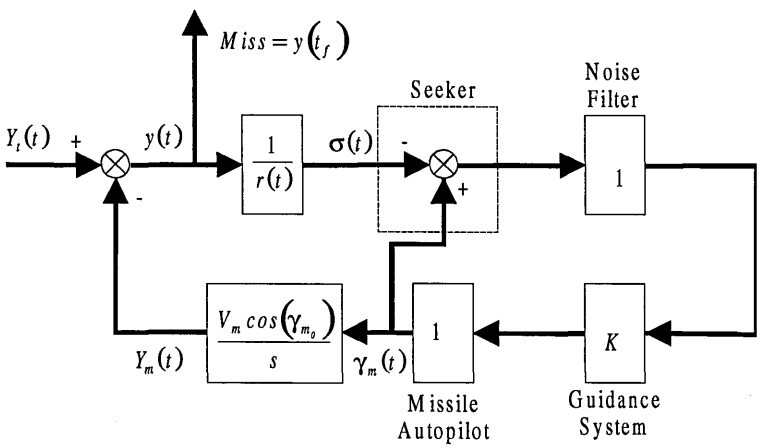

Figure 74 Simplified Block Diagram for Integrated PN

Figure 74 above shows a simplified block diagram of a generic guidance system using integrated PN. Comparing Figures 73 and 74 it can be seen that the guidance loop now contains one integration rather than a double integration following by a differentiation. Hence, at a superficial level the two forms of PN are in fact equivalent. In practise, problems can occur in matching the seeker characteristics to the inertial instrument characteristics.

3.6 Lyapunov Stability

3.6.1 Proportional Navigation Against a Randomly Manoeuvring Target

A previous section has shown via a simple linearised example that the kinematic gain is a vital factor in the optimality of PN. However, the utility of this example is fairly limited since once the linearising assumptions are violated then the system becomes sub-optimal.

Ha et al[16] introduce the use of Lyapunov methods to directly examine the stability of PN. The method is of some benefit since it may be applied directly to the nonlinear equations governing the intercept dynamics. Its principle disadvantage is that many Lyapunov functions are possible and the technique does not necessarily fully delineate the capture region.

The basic method of Ha et al[16] has been examined and expanded. Expanding this technique further, the method of Kim et al[23] in constraining the impact angle has been revisited.

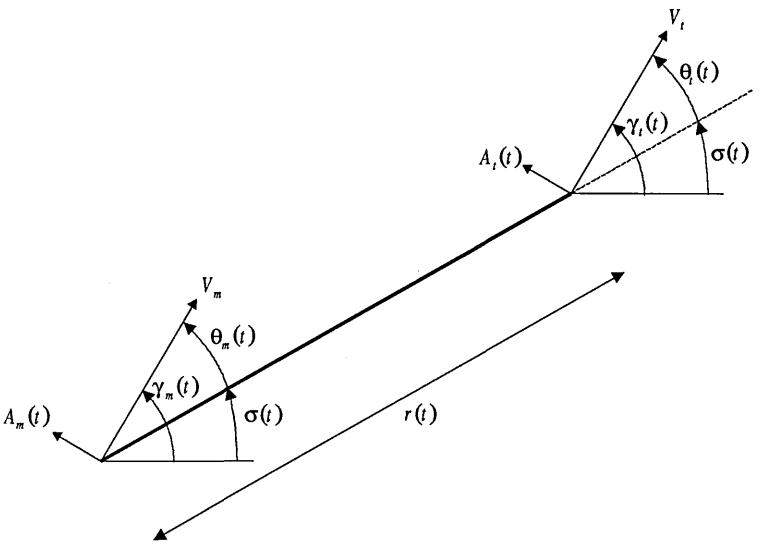

Figure 75 Simplified Intercept Geometry

In order to demonstrate the method a number of simplifying assumptions have been made. Figure 75 shows the basic intercept geometry for a planar interception of the target by the missile. Constraining the intercept in a single plane, both target and interceptor move at constant speed. The interception may be described using the following nonlinear equations:

$$\dot{\gamma}_t(t) = A_t(t)/V_t\,,\ \dot{\gamma}_m(t) = A_m(t)/V_m \tag{152}$$

$$\dot{r}(t) = V_m \cdot (\rho \cdot \cos\theta_t(t) - \cos\theta_m(t)) \tag{153}$$

$$r(t) \cdot \dot{\sigma}(t) = V_m \cdot (\rho \cdot \sin\theta_t(t) - \sin\theta_m(t)) \tag{154}$$

Where θ_t, θ_m and ρ are defined by:

$$\theta_t(t) = \gamma_t(t) - \sigma(t),\ \theta_m(t) = \gamma_m(t) - \sigma(t),\ \rho = V_t/V_m \tag{155}$$

Assuming that the missile acceleration response is instantaneous, i.e. neglecting the autopilot and airframe responses, and assuming the missile acceleration is normal to the velocity vector and varies according to:

$$A_m(t) = K \cdot V_m \cdot \dot{\sigma}(t) \tag{156}$$

Implicit in equation **(156)** is the assumption that the interceptor is significantly faster than the target i.e.:

$$V_m >> V_t \tag{157}$$

Equation **(157)** simply indicates that the interceptor velocity dominates the closing velocity. It is assumed that the target will manoeuvre in an unknown manner but that the target acceleration is a continuous function of time and is upper bounded by a known value, α.

$$|A_t(t)| \leq \alpha \tag{158}$$

Finally, it is assumed that at the start of homing, the intercept geometry is subject to the following constraints:

$$|\rho \cdot \sin\theta_t(0) - \sin\theta_m(0)| < \beta\,,\ |\theta_m(0)| < \pi/2 \tag{159}$$

Where β is a positive constant, $\beta \in (0, 1-\rho)$.

This condition is actually quite a weak constraint, it simply implies that the target is within the field of view of most practical seekers and that at the start of homing the missile is heading toward the target. Applying this constraint to an air-to-ground weapon system is not particularly onerous; however, this may be of some concern for an air-to-air missile. In the latter situation, the missile may be launched under inertial guidance toward an off-bore-sight target and obviously these constraints may well be violated.

Noting the range rate equation, equation **(153)**, it is assumed for now that equations **(152)** to **(154)** are satisfied if:

$$\left|\rho \cdot \sin\theta_t(t) - \sin\theta_m(t)\right| < \beta\,,\ t_0 < t < t_1 \qquad \textbf{(160)}$$

Where $t_1 \in (0,\infty)$.

This implies that:

$$\left|\theta_m(t)\right| < \sin^{-1}(\rho+\beta) \qquad \textbf{(161)}$$

This can be proven by first of all considering from equation **(160)** that:

$$\left|\sin\theta_m(t)\right| < \rho+\beta < 1 \qquad \textbf{(162)}$$

Defining the sets Ω_1, Ω_2 by:

$$\Omega_1 = \{\theta \in R : |\theta| < \sin^{-1}(\rho + \beta)\} \tag{163a}$$

$$\Omega_2 = \{\theta \in R : |\theta - \pi| < \sin^{-1}(\rho + \beta)\} \tag{163b}$$

Solving equation **(160)** for $\theta_m(t)$ gives:

$$\theta_m(t) \in \Omega_1 \cup \Omega_2, \; t_0 < t < t_1 \tag{164}$$

However, these results together with the initial condition defined by equation **(159)** implies that:

$$\theta_m(t_0) \in \Omega_1 \tag{165}$$

Noting that the sets Ω_1, Ω_2 are not path connected and that $\theta_m(t)$ is continuous in t, hence:

$$\theta_m(t) \in \Omega_1, \; t_0 < t < t_1 \tag{166}$$

This with equation **(160)** implies that:

$$|\sin\theta_m(t)| < \beta + \rho \cdot |\sin\theta_t(t)| \tag{167}$$

Also, since $\theta_m(t) \in \Omega_1, \; t_0 < t < t_1$, it is noted that:

$$\cos\theta_m(t) > 0 \tag{168}$$

This with equation **(167)** implies that:

$$\cos\theta_m(t) > \sqrt{1-\{\beta+\rho\cdot|\sin\theta_t(t)|\}^2} \tag{169}$$

This together with equation **(153)** implies that:

$$\dot{r}(t) < V_m\cdot\left(\rho\cdot\cos\theta_t(t)-\sqrt{1-\{\beta+\rho\cdot|\sin\theta_t(t)|\}^2}\right) \tag{170}$$

Defining $f(\theta)$ as:

$$f(\theta)=\rho\cdot\cos\theta-\sqrt{1-\{\beta+\rho\cdot|\sin\theta|\}^2} \tag{171}$$

Differentiating with respect to θ the following is obtained:

$$f'(\theta)=-\rho\cdot\sin\theta+\frac{\rho\cdot\cos\theta\cdot(\beta+\rho\cdot|\sin\theta|)}{\sqrt{1-\{\beta+\rho\cdot|\sin\theta|\}^2}} \tag{172}$$

$f'(\theta)=0$ has the solutions:

$$\sin\theta=\frac{\beta}{1-\rho},\ \cos\theta=\sqrt{1-\left(\frac{\beta}{1-\rho}\right)^2} \tag{173}$$

Differentiating equation **(172)** with respect to θ results in:

$$f''(\theta) = -\rho \cdot \cos\theta - \frac{\rho \cdot |\sin\theta| \cdot (\beta + \rho \cdot |\sin\theta|)}{\sqrt{1 - \{\beta + \rho \cdot |\sin\theta|\}^2}} + \frac{\rho^2 \cdot \cos^2\theta}{\sqrt{1 - \{\beta + \rho \cdot |\sin\theta|\}^2}} - \frac{\rho^2 \cdot \cos^2\theta \cdot (\beta + \rho \cdot |\sin\theta|)^2}{\sqrt[3]{1 - \{\beta + \rho \cdot |\sin\theta|\}^2}} \tag{174}$$

Substituting the solution given in equation **(173)** results in:

$$f''(\theta) = -\rho \cdot \left[\begin{array}{l} (1-\rho) \cdot \left\{ 1 - \left(\frac{\beta}{(1-\rho)} \right)^2 \right\}^{1/2} \\ + (1+\rho) \cdot \left(\frac{\beta}{(1-\rho)} \right)^2 \cdot \left\{ 1 - \left(\frac{\beta}{(1-\rho)} \right)^2 \right\}^{-1/2} \end{array} \right] \tag{175}$$

$$\Rightarrow f''(\theta) < 0$$

Assuming that the constraint implied by equation **(160)** to be correct, the solution of equation **(172)** represents a maximum value and, therefore, using equation **(170)** the upper bounds on range rate may be expressed as:

$$\dot{r} < -V_m \cdot \sqrt{(1-\rho)^2 - \beta^2} \tag{176}$$

It is now assumed that:

$$|\theta_m(t)| \leq \sin^{-1}(\rho + \beta) \tag{177}$$

Furthermore, it is also assumed for now that:

$$\dot{r}(t) < -V_m \cdot \sqrt{(1-\rho)^2 - \beta^2}\ ,\ t_0 < t < t_2 \tag{178}$$

Where $t_2 \in (0,\infty)$. Noting that a constraint on the initial conditions is imposed and defined by equation **(159)** it holds that at t_0:

$$\dot{r}(0) < -V_m \cdot \sqrt{(1-\rho)^2 - \beta^2} \tag{179}$$

Now if equation **(178)** is invalid, this with the continuity of $\dot{r}$ implies that there exists a time $t_3 \in t_2$ such that:

$$\dot{r}(t) < -V_m \cdot \sqrt{(1-\rho)^2 - \beta^2}\ ,\ t_0 < t < t_3 \tag{180a}$$

$$\dot{r}(t_3) = -V_m \cdot \sqrt{(1-\rho)^2 - \beta^2} \tag{180b}$$

However, as the result of equation **(177)** it is noted that:

$$\cos\theta_m(t) > \sqrt{1-(\rho+\beta)^2} \tag{181}$$

A candidate Lyapunov function is suggested as:

$$V(t) = \tfrac{1}{2}(r(t)\cdot\dot{\sigma}(t))^2 \tag{182}$$

Differentiating with respect to time results in:

$$\dot{V}(t) = r(t)\cdot\dot{\sigma}(t)\cdot[\dot{r}(t)\cdot\dot{\sigma}(t) + r(t)\cdot\ddot{\sigma}(t)] \tag{183}$$

Similarly, differentiating equation **(154)** with respect to time results in:

$$r(t)\cdot\ddot{\sigma}(t)=-2r(t)\cdot\dot{\sigma}(t)+A_t\cdot\cos\theta_t(t)-A_m(t)\cdot\cos\theta_m(t) \tag{184}$$

Noting equation **(156)** these two results may be combined resulting in:

$$\dot{V}(t)=V_m\cdot r(t)\cdot\dot{\sigma}(t)^2\cdot\{-\rho\cdot\cos\theta_t(t)+(1-K)\cdot\cos\theta_m(t)\}+ r(t)\cdot\dot{\sigma}(t)\cdot A_t(t)\cdot\cos\theta_t(t) \tag{185}$$

Lyapunov stability implies that $\dot{V}(t)<0$, $t_0<t<t_1$. Applying this constraint to the above equation and re-arranging implies the kinematic gain must satisfy the following inequality:

$$K\cdot\cos\theta_m(t)>-\frac{\dot{r}}{V_m}+\frac{A_t(t)\cdot\cos\theta_t(t)}{V_m\cdot\dot{\sigma}(t)} \tag{186}$$

Noting that a constraint upon $\cos\theta_m(t)$ is indicated by equation **(181)**, that the target manoeuvre capability is upper bounded by the limit α and a constraint on $\dot{r}$ is indicated by equation **(176)**; assuming for now that the assumption implied by equation **(160)** to be true. Substituting these values into equation **(186)** the lower bounds on the kinematic gain to ensure our candidate function is a Lyapunov function is defined by:

$$K>\left(\frac{1-\rho+\beta}{1+\rho+\beta}\right)^{1/2}+\frac{\alpha\cdot r(0)/\beta\cdot V_m^2}{\sqrt{1-(\rho+\beta)^2}} \tag{187}$$

Considering the term in the right hand bracket and noting that, the upper and lower bounds can be expressed as:

$$\beta = 0 \Rightarrow \left(\frac{1-\rho}{1+\rho}\right)^{1/2} < 1,\ \beta = 1-\rho \Rightarrow (1-\rho)^{1/2} < 1 \qquad \textbf{(188)}$$

Differentiating this term with respect to β indicates the term is monotonic $\beta \in (0,1-\rho)$. Hence, it is noted that:

$$\left(\frac{1-\rho+\beta}{1+\rho+\beta}\right)^{1/2} < 1,\ \beta \in (0,1-\rho) \qquad \textbf{(189)}$$

Hence, equation **(187)** can be written in a more convenient form as:

$$K > 1 + \frac{\rho + \alpha \cdot r(0)/\beta \cdot V_m^2}{\sqrt{1-(\rho+\beta)^2}} \qquad \textbf{(190)}$$

Substituting into equation **(185)** the upper limit on the rate of change of the Lyapunov function may be defined as:

$$\dot{V}(t) < -\frac{2\alpha \cdot V(t)}{\beta \cdot V_m} + \alpha \cdot [2V(t)]^{1/2} \qquad \textbf{(191)}$$

This result implies that:

$$V(t)^{1/2} < \frac{\beta \cdot V_m}{\sqrt{2}} + \left[V(0)^{1/2} - \beta \cdot V_m / \sqrt{2}\right] \cdot e^{-\alpha \cdot t / \beta \cdot V_m} \qquad \textbf{(192)}$$

Noting equations **(154)** and **(159)** it is observed that:

$$\left[V(0)^{1/2} - \beta \cdot V_m / \sqrt{2}\right] < 0 \qquad \textbf{(193)}$$

Therefore it follows from equation **(192)** that:

$$\left|\rho \cdot \sin\theta_t(t) - \sin\theta_m(t)\right| < \beta\,,\ t_0 < t < t_3 \qquad \textbf{(194)}$$

Hence, using the result obtained previously it follows that:

$$\dot{r}(t) < -V_m \cdot \sqrt{(1-\rho)^2 - \beta^2}\,,\ t_0 < t \le t_3 \qquad \textbf{(195)}$$

This result contradicts equation **(180b)**, which is itself contradictory to the initial assumption and hence equation **(178)** holds. Hence, it is also concluded that the assumption implied in equation **(160)** also holds.

Returning now to equation **(192)**. This indicates that provided the kinematic gain satisfies the constraint in equation **(186)** then proportional navigation against a randomly manoeuvring target is Lyapunov stable and, furthermore, is exponentially stable and, therefore, asymptotically stable. It is therefore concluded that although the basic PN guidance law is generally formulated assuming that the target maintains a rectilinear flight, it remains a robust and stable guidance algorithm in the presence of target manoeuvres. Hence, intrinsically the PN algorithm itself does not generate a miss-distance, in effect a zero lag PN system will always result in zero miss-distance as shown in the simple example from the previous section.

In practical systems, miss-distance results from a number of the simplifying assumptions that were made in order to examine the basic properties of PN itself. One of these assumptions is that the effect of the autopilot and airframe responses of

the missile can be neglected. Throughout much of the engagement this assumption does not introduce a significant error. However, in the final stages of the engagement this assumption breaks down, as their time constant becomes significant. This is considered further in a later section.

3.6.2 Impact With Angular Constraint

The previous section has considered the stability of the conventional PPN guidance algorithm against a manoeuvring target. This section will now consider an extension of this guidance law to tailor the engagement to meet an angular constraint at impact. In order to simplify the development of the algorithm it is initially assumed that the target does not manoeuvre and both missile and target maintain a constant velocity.

It is assumed that the impact angle requirement will be achieved using a time-varying rate bias, noting that Murtaugh and Criel[26] indicate that a rate bias can be used to shape a trajectory. Ignoring for the moment the formation of the rate bias term it is assumed that the acceleration demand is formulated according to:

$$A_m(t) = K \cdot V_m \cdot (\dot{\sigma}(t) - \dot{\sigma}_b(t)) \qquad \textbf{(196)}$$

Where $\dot{\sigma}_b(t)$ is a time varying rate bias term.

Before considering the development of the algorithm, assuming that γ_t and γ_D are given let the desired sightline angle, σ_D, be a solution of the trigonometric equation:

$$\rho \cdot \sin(\gamma_t - \sigma_D) - \sin(\gamma_D - \sigma_D) = 0 \qquad \textbf{(197)}$$

Subject to the constraint that:

$$|\gamma_D - \sigma_D| < \pi/2$$

Expanding equation **(197)** and re-arranging leads to the following expression:

$$\sigma = \tan^{-1}\left(\frac{\rho \sin\gamma_t - \sin\gamma_D}{\rho \cos\gamma_t - \cos\gamma_D}\right) \qquad \textbf{(198)}$$

Which has a unique solution with the trivial exception of the indeterminate form:

$$\rho \sin\gamma_t - \sin\gamma_D = 0 \wedge \rho \cos\gamma_t - \cos\gamma_D = 0 \qquad \textbf{(199)}$$

Next assuming that γ_t and σ_D are given, it is trivial to demonstrate that there is a single unique solution, γ^*, of equation **(197)**. In this case σ_D acts as a common phase angle and so without loss of generality it may be assumed that $\sigma_D = 0$. Noting that with the applied constraint $\sin\gamma^*$ is monotonic, hence, there must be a single unique solution for γ^*.

As in the previous case it is assumed that the initial geometry satisfies the following constraint:

$$\left((\rho \sin\theta_t(0) - \sin\theta_m(0))^2 + \eta(\sigma_D - \sigma(0))^2\right)^{1/2} < \beta \qquad \textbf{(200)}$$

Where η is a positive constant and σ_D defines the desired approach angle.

Noting that equation **(200)** is a subset of the condition implied by equation **(159)** it is assumed for now that equation **(160)** remains valid leading to the upper limit on the range rate implied by equation **(176)**. A candidate Lyapunov function is suggested as:

$$V(t)=\frac{1}{2}\left((r(t)\cdot\dot{\sigma}(t))^2+\eta V_m^2(\sigma_D-\sigma(t))^2\right) \tag{201}$$

Equation **(200)** may now be expressed as:

$$V(0)<\tfrac{1}{2}V_m^2\beta^2 \tag{202}$$

Differentiating $V(t)$ with respect to t implies results in:

$$\begin{aligned}\dot{V}(t)=V_m\cdot r(t)\cdot\dot{\sigma}(t)^2\{&-\rho\cos\theta_t(t)+(1-K)\cos\theta_m(t)\}\\&+K\cdot V_m\cdot\dot{\sigma}_b(t)\cdot\cos\theta_m(t)\cdot r(t)\cdot\dot{\sigma}(t)\\&-\eta\cdot V_m^2\cdot(\sigma_D-\sigma(t))\cdot\dot{\sigma}(t)\end{aligned} \tag{203}$$

In order to ensure Lyapunov stability the guidance must ensure that $\dot{V}(t)<0$, $t_0<t<t_1$, noting that $V_m\cdot r(t)\cdot\dot{\sigma}(t)^2>0$, this can be achieved if the following inequalities are satisfied:

$$-\rho\cos\theta_t(t)+(1-K)\cos\theta_m(t)<0 \tag{204a}$$

$$K \cdot V_m \cdot \dot{\sigma}_b(t) \cdot \cos\theta_m(t) \cdot r(t) \cdot \dot{\sigma}(t) - \eta \cdot V_m^2 \cdot (\sigma_D - \sigma(t)) \cdot \dot{\sigma}(t) \leq 0 \quad \textbf{(204b)}$$

Re-arranging equation **(204a)** implies the following constraint on the kinematic gain:

$$K > 1 - \rho \frac{\cos\theta_t(t)}{\cos\theta_m(t)} \quad \textbf{(205)}$$

Applying the earlier constraint identified by equation **(181)** implies a lower limit on the kinematic gain of:

$$K > 1 + \frac{\rho}{\sqrt{1-(\rho+\beta)^2}} \quad \textbf{(206)}$$

For small values of β this is a weak constraint since, as shown earlier, the kinematic gain must be greater than 2 or the acceleration demands grow according to a power law. Thus in most practical applications this constraint will be satisfied. However, as $\beta \to (1-\rho)$, $\sqrt{1-(\rho+\beta)^2} \to 0$ and $K \to \infty$. Nevertheless this condition represents the extreme edge of the boundary defined by equation **(200)** and for smaller values of β, K rapidly reduces below 2.

It is more difficult to define a condition that ensures the second inequality is satisfied since the sightline rate may be either positive or negative. However, the effect of this term can be removed if the sightline bias rate is formulated as:

$$\dot{\sigma}_b(t)=\frac{\eta \cdot V_n \cdot (\sigma_D - \sigma(t))}{K \cdot \cos\theta_m(t) \cdot r(t)} \tag{207}$$

Applying this constraint ensures that the requirement to control attitude does not affect the rate of change of $V(t)$ and the previous constraint ensures that $\dot{V}(t)<0$, $t_0 < t < t_1$. Hence, the time derivative of $\dot{V}(t)<0$ may now be expressed as:

$$\dot{V}(t)=V_m \cdot r(t) \cdot \dot{\sigma}(t)^2 \{-\rho \cos\theta_t(t)+(1-K)\cos\theta_m(t)\} \tag{208}$$

Hence, it has been shown that $V(t)$ is a Lyapunov function; this together with equation **(202)** can be used to prove by contradiction that equation **(160)** remains valid. In the previous example for a manoeuvring target it was trivial to show that $V(t)$ was a logarithmic function, indicating both exponential and asymptotic stability. Lyapunov stability by itself does not automatically imply asymptotic stability and the modifications to the suggested Lyapunov function mean that it is no longer possible to re-arrange $V(t)$ into a convenient logarithmic form. The proof of asymptotic stability is more complex in this example.

Before proceeding to the proof of asymptotic stability, the following lemmas, Buck[7], are introduced:

> Lemma 1. If $f(t)$ is bounded and monotone over the open interval $a<t<b$ then $\lim_{t\to a} f(t)$ and $\lim_{t\to b} f(t)$ exists.

Lemma 2. Let $f(t) \geq 0$ and $g(t) \geq 0$ over the open interval $a < t < b$ and let $\lim_{t \to b} f(t)/g(t) = L$, where $0 < L < \infty$. Then the integrals:

$$\int_a^b f(t)dt, \int_a^b g(t)dt$$

are either both convergent or both divergent.

Ideally, asymptotic stability would imply that the guidance algorithm fulfils the requirements of minimising the miss distance and ensuring that the weapon approaches along the desired trajectory path. This implies that there is a finite time of impact, t_f, where:

$$r(t_f) < \varepsilon_r, \left|\gamma_m(t_f) - \gamma_D\right| < \varepsilon_\gamma$$

Where ε_r and ε_γ represent small finite errors in the guidance solution at impact. Considering first of all the range equation, equation **(176)**, it is assumed that there exists a finite time, t_f', such that:

$$\lim_{t \to t_f'} r(t) = 0 \text{ and } r(t) > 0, \; t \in (0, t_f') \qquad \textbf{(209)}$$

If equation **(209)** does not hold, noting equation **(176)**, there exists a limit $\delta > 0$ such that:

$$r(t) \geq \delta,\ 0 \leq t \leq \hat{t}\text{, where } \hat{t} = r(0)/V_m\sqrt{(1-\rho)^2 - \beta^2} \qquad \textbf{(210)}$$

Integrating equation **(176)** over the interval $(0,\hat{t})$ it holds that $r(\hat{t}) < 0$, which contradicts the above result and hence the earlier assumption, equation **(160)**, is true. In order to prove that the impact angle approaches the desired impact angle it is necessary to consider two cases:

Case 1. $\lim_{t \to t_f'} \sigma(t)$ exists and is finite.

Case 2. $\lim_{t \to t_f'} \sigma(t)$ does not exist or is infinite.

First of all considering Case 1, noting the range rate equation, equation **(153)**, it is obvious that:

$$\dot{r}(t) \leq -V_m(1+\rho) \qquad \textbf{(211)}$$

Integrating equation **(211)** over (t,t_f'), noting the definition of ρ, the following is obtained:

$$0 < r(t) \leq (V_m + V_t)\cdot(t_f' - t) \qquad \textbf{(212)}$$

Noting that:

$$\lim_{t \to t_f'} \int_{t_5}^{t} \frac{1}{(V_m + V_t)\cdot(t_f' - \tau)} d\tau = \infty,\ t_5 \in (0, t_f')$$

Implies that the following improper integral is divergent:

$$\lim_{t\to t_f'} \int_{t_5}^{t} \frac{1}{r(\tau)} d\tau \tag{213}$$

If the assumption that $\lim_{t\to t_f'} \sigma(t)$ exists and is finite is correct, then these results together with the fact that that $V(t)$ has been shown to be a Lyapunov function, Lemma 1 implies that $\lim_{t\to t_f'} r\cdot\dot{\sigma}(t)$ exists and is finite. This together with equation **(154)** implies that $\lim_{t\to t_f'} \gamma_m(t)$ exists and is finite. Denoting these limits by:

$$\lim_{t\to t_f'} \sigma(t)=\sigma_0,\ \lim_{t\to t_f'} \gamma_m(t)=\gamma_0 \tag{214}$$

The existence of $\lim_{t\to t_f'} \sigma(t)$ implies that the following improper integral exists and is finite:

$$\begin{aligned} &lim_{t\to t_f'}\ \sigma(t)-\sigma(0)=lim_{t\to t_f'} \int_0^t \dot{\sigma}(\tau)d\tau \\ &=lim_{t\to t_f'} \int_0^t \frac{V_m\cdot\left(\rho\, sin(\gamma_t-\sigma(\tau))-sin(\gamma_m(\tau)-\sigma(\tau))\right)}{r(\tau)} d\tau \end{aligned} \tag{215}$$

Defining the functions:

$$f(t)=\frac{V_m\cdot(\rho\sin(\gamma_t-\sigma(t))-\sin(\gamma_m(t)-\sigma(t)))}{r(t)} \tag{216a}$$

$$g(t)=\frac{1}{r(t)} \tag{216b}$$

Let $\lim_{t\to t_f'}[\rho\sin(\gamma_t-\sigma(t))-\sin(\gamma_m(t)-\sigma(t))]=L$, with $0<L<\infty$. Lemma 2 and equation **(213)** implies that the following improper integral is divergent:

$$\lim_{t\to t_f'}\int_{t_t}^{t} f(\tau)d\tau \tag{217}$$

However, this contradicts equation **(215)** and hence L cannot lie in the interval $(0,\infty)$ and by a similar argument cannot lie in the interval $(-\infty,0)$. Hence it is concluded that L=0, which can be written as:

$$\begin{aligned} &lim_{t\to t_f'}\left[\rho\, sin(\gamma_t-\sigma(t))-sin(\gamma_m(t)-\sigma(t))\right] \\ &=\rho\, sin(\gamma_t-\sigma_0)-sin(\gamma_0-\sigma_0)=0 \end{aligned} \tag{218}$$

The rate of change of the missile flight path may be expressed as:

$$\begin{aligned} \dot{\gamma}_m &= \frac{A_m(t)}{V_m} \\ &= K\cdot(\dot{\sigma}(t)-\dot{\sigma}_b(t)) \\ &= K\cdot V_m\cdot\left\{\frac{(\rho\sin(\gamma_t-\sigma(t))-\sin(\gamma_m(t)-\sigma(t)))}{r(t)}-\frac{\eta\cdot(\sigma_D-\sigma(t))}{K\cdot r(t)\cdot\cos(\gamma_m(t)-\sigma(t))}\right\} \end{aligned} \tag{219}$$

Hence, the existence of $\lim_{t\to t_f'}\gamma_m(t)$ implies that the following improper integral exists and is finite:

$$\lim_{t\to t_f'} \gamma_m(t)-\gamma_m(0)=\lim_{t\to t_f'} \int_0^t \dot{\gamma}_m(\tau)d\tau$$

$$=\lim_{t\to t_f'} K\cdot V_m \int_0^t \frac{(\rho\sin(\gamma_t-\sigma(\tau))-\sin(\gamma_m(\tau)-\sigma(\tau)))-}{r(\tau)} \frac{\eta\cdot(\sigma_D-\sigma(t))/K\cdot\cos((\gamma_m(\tau)-\sigma(\tau)))}{r(\tau)} d\tau \quad \textbf{(220)}$$

Hence, using the same argument used to prove equation **(218)**, it follows that:

$$\lim_{t\to t_f'}\left[\begin{matrix}(\rho\sin(\gamma_t-\sigma(\tau))-\sin(\gamma_m(\tau)-\sigma(\tau)))-\\ \eta\cdot(\sigma_D-\sigma(t))/K\cdot\cos((\gamma_m(\tau)-\sigma(\tau)))\end{matrix}\right]=0 \quad \textbf{(221)}$$

Which implies that $\sigma_0=\sigma_D$ and, hence, since it has been shown that equation **(218)** has a single unique solution, it follows that $\gamma_0=\gamma_D$.

Turning now to Case 2, it is trivial to demonstrate that $\sigma(t)$ is bounded and not infinite. It has been demonstrated that the suggested Lyapunov function, which is a quadratic function of $\sigma(t)$, is stable in the sense of Lyapunov. Hence, if $\sigma(t)$were unbounded, there would exist a time, t_6, where:

$$V(t_6)>V(0) \quad \textbf{(222)}$$

But the function suggested is a Lyapunov function and, hence, it has the property of being negative semi-definite, which is contradictory to equation **(222)**. Hence, $\sigma(t)$ is bounded over $(0,t_f')$. A constant, t_7, is chosen such that:

$$0<r(t)<\varepsilon,\ t\in(t_7,t_f'),\ t_7\in(0,t_f')$$

If $\lim_{t\to t'_f}\sigma(t)$ does not exist it is asserted that there must exist a series of maxima and minima, τ_i, where $\tau_i \in (t_7, t'_f)$ such that:

$$\sigma(x)\geq\sigma(y),\ \sigma(\tau_0)>\sigma(\tau_1) \text{ if } y>x \text{ and } x,y\in(\tau_0,\tau_1)$$

$$\sigma(x)\leq\sigma(y),\ \sigma(\tau_1)<\sigma(\tau_2) \text{ if } y>x \text{ and } x,y\in(\tau_1,\tau_2)$$

...

$$\sigma(x)\geq\sigma(y),\ \sigma(\tau_i)>\sigma(\tau_{i+1}) \text{ if } y>x \text{ and } x,y\in(\tau_i,\tau_{i+1})$$

$$\sigma(x)\leq\sigma(y),\ \sigma(\tau_{i+1})<\sigma(\tau_{i+2}) \text{ if } y>x \text{ and } x,y\in(\tau_{i+1},\tau_{i+2})$$

Otherwise the boundedness and monotone nature of $\sigma(t)$ would guarantee that $\lim_{t\to t'_f}\sigma(t)$ does exist. As each point represents either a maxima or minima, $\dot{\sigma}(\tau_i)=0$, and:

$$V(\tau_i)=\frac{1}{2}\eta\cdot V_m^2\cdot(\sigma_D-\sigma(t))^2 \tag{223}$$

Noting that $\dot{V}(t)<0$ it is obvious that:

$$V(\tau_i)>V(\tau_{i+1}) \tag{224}$$

And, hence, noting that $\sigma(\tau_i)$ is either a maxima or a minima:

$$(\sigma_D-\sigma(\tau_i))\cdot(\sigma_D-\sigma(\tau_{i+1}))<0 \tag{225}$$

The continuity of $\sigma(t)$ implies there must exist a time, λ_i, where $\lambda_i \in (\tau_i, \tau_{i+1}) \subset (t_7, t_f')$ such that:

$$\sigma(\lambda_i) = \sigma_D \tag{226}$$

In addition, the following condition must apply to the sightline rate:

$$\dot{\sigma}(\lambda_i) \cdot \dot{\sigma}(\lambda_{i+1}) \leq 0 \tag{227}$$

Hence, it follows from equations **(154)**, **(226)** and **(227)** that:

$$\begin{aligned} &\left\{\rho \cdot sin(\gamma_t - \sigma_D) - sin(\gamma_m(\lambda_i) - \sigma_D)\right\} \cdot \\ &\left\{\rho \cdot sin(\gamma_t - \sigma_D) - sin(\gamma_m(\lambda_{i+1}) - \sigma_D)\right\} \end{aligned} \leq 0 \tag{228}$$

Noting that there is a unique solution, γ^*, of equation **(197)**, the constraint imposed by equation **(200)**, then the continuity of $\theta(t)$ implies that:

$$\{\gamma_m(\lambda_i) - \gamma_D\} \cdot \{\gamma_m(\lambda_{i+1}) - \gamma_D\} \leq 0 \tag{229}$$

The continuity of $\gamma_m(t)$ implies that there exists a time, ς_i, where $\varsigma_i \in (\lambda_i, \lambda_{i+1}) \subset (t_7, t_f')$ such that:

$$\gamma_m(\varsigma_i) = \gamma_D \tag{230}$$

Hence, in both cases 1 and 2 the guidance law guarantees that the impact angle is asymptotic toward the desired values. It is therefore concluded that the guidance law

with the imposition of an angular constraint is both Lyapunov and asymptotically stable.

3.6.3 Further Development of the Guidance Law

The guidance law as currently formulated requires knowledge of the missile speed and attitude, the range to the target and the target's speed and attitude. An Inertial Navigation System (INS) can provide details of the missile's speed and attitude, whilst an active seeker can provide measurements of the range and bearing of the target. Target velocity and attitude may be estimated using a tracking system based on measurements from the INS and seeker. Such information should be available in a modern guided missile.

In cases where the missile has a large speed advantage over the target or where a static target is engaged, it can be assumed that the sightline equation, equation **(154)**, reduces to:

$$r(t)\cdot\dot{\sigma}(t) \approx -V_m \sin\theta_m(t) \tag{231}$$

And hence, substituting equation **(231)** into equation **(207)**, the acceleration demand may be formulated as:

$$A_m(t) = K\cdot V_m\cdot\dot{\sigma}(t)\cdot\left\{1+\frac{2\eta\cdot(\sigma_D-\sigma(t))}{K\cdot\sin 2\theta_m(t)}\right\} \tag{232}$$

Utilising the fact that PN may be implemented in an integrated form, equation **(232)** can be re-written in an integrated form as:

$$\gamma_m(t) = \gamma_{m_0} + \int_0^t K \cdot \dot{\sigma}(t) \cdot \left\{ 1 + \frac{2\eta(\sigma_D - \sigma(\tau))}{K \cdot sin2\theta_m(\tau)} \right\} d\tau \qquad \textbf{(233)}$$

Intuitively on inspection, equations **(232)** and **(233)** do not look to be a suitable formulation of a guidance law. Whilst they may be mathematically valid it could be expected that in a typical engagement that $\theta_m(t)$ may become zero and a singularity may result. Also, as shown in the previous section, the guidance law is asymptotically stable and, hence, as $t \to t_f, \sigma(t) \to \sigma_D$ and an indeterminate form would result. However, when this guidance law was implemented in a six degree-of-freedom trajectory simulation program it was found that it was surprisingly stable and well-behaved. Clearly more work is required to understand the behaviour of this development of the guidance law.

3.6.4 Simulation Results

The guidance laws as presented so far have considered a simple case where the target and missile maintain constant speeds and motion is constrained to a single plane. In order to assess the guidance laws in a practical application, the guidance laws were implemented in a six-degree of freedom trajectory simulation program. An existing Hunting Engineering Ltd (HEL) trajectory simulation program was modified to simulate guided trajectories for a typical air launched guided weapon. The simulations considered a guided mission with the target placed at the nominal

ballistic impact point. Release conditions were straight and level flight from an altitude of 20,000 ft, Mach 0.85.

The guidance laws implemented were standard PN, equation **(156)**, an augmented PN guidance law to control impact angle, equation **(196)**, and, finally, the modified guidance law described in the previous section, equation **(232)**. In order, to compare the various guidance laws a performance index is defined as:

$$I = \int_0^{t_f} A_m^2(\tau)d\tau \tag{234}$$

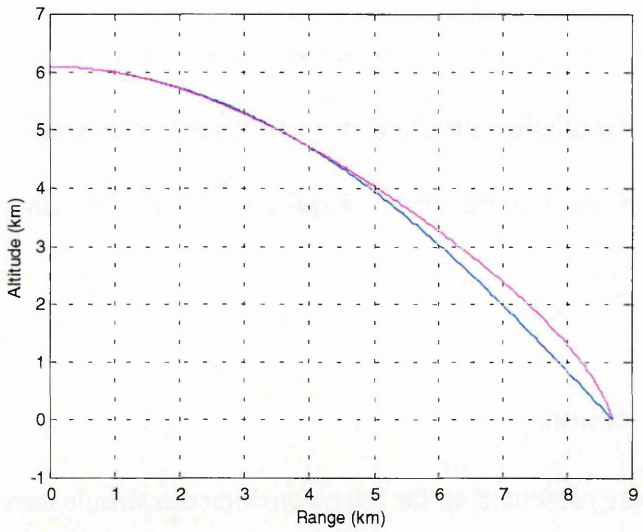

Conventional PN *Augmented PN* *Modified Augmented PN*

Figure 76 Guided Trajectories Using Various PN Guidance Laws (75° Impact Angle)

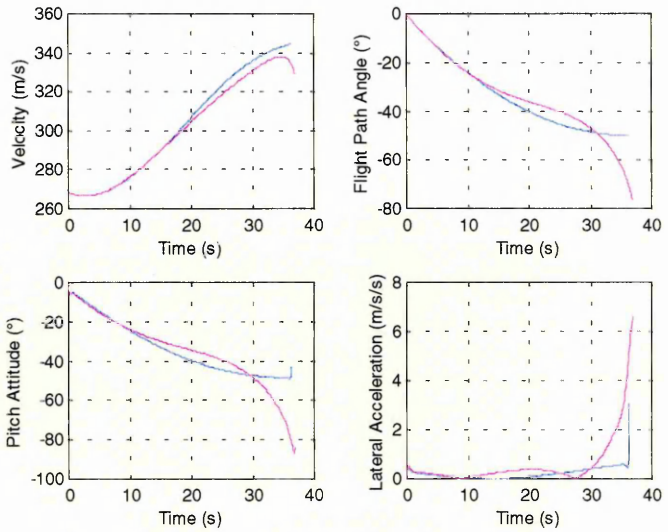

Conventional PN *Augmented PN* *Modified Augmented PN*

Figure 77 Control Response to Various PN Guidance Laws (75° Impact Angle)

Figures 76 and 77 show the results of simulations with conventional PN and the biased PN algorithms. The introduction of the impact angle requirement results in a small performance penalty, a modest reduction in the impact velocity. However, the biased PN guidance laws result in a significantly greater control effort, which is reflected in the performance index, Figure 82. Nevertheless it should be noted that the performance index defined by equation **(234)** has the effect of emphasising the control effort, since it is a function of the square of the lateral acceleration. Bearing in mind the comments in the previous section, it is noted that there is no evidence of any problems with the guidance algorithm resulting in an indeterminate form. Furthermore, it is also noted that the performance of the modified bias PN is virtually identical to that of the original algorithm.

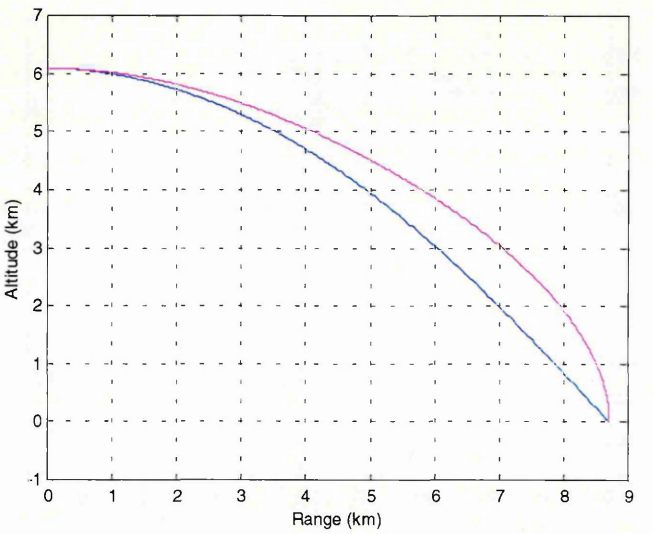

Conventional PN *Augmented PN* *Modified Augmented PN*

Figure 78 Guided Trajectories Using Various PN Guidance Laws (90° Impact Angle)

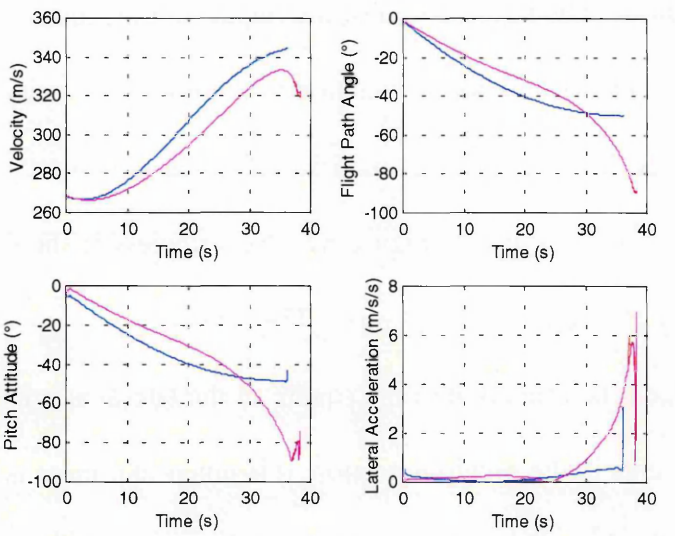

Conventional PN *Augmented PN* *Modified Augmented PN*

Figure 79 Control Response to Various PN Guidance Laws (90° Impact Angle)

Figures 78 and 79 show the results of simulations with an impact angle demand of 90°, i.e. a vertical impact. In comparison with the previous result, impact velocity is only slightly reduced but there is a large increase in the overall control effort.

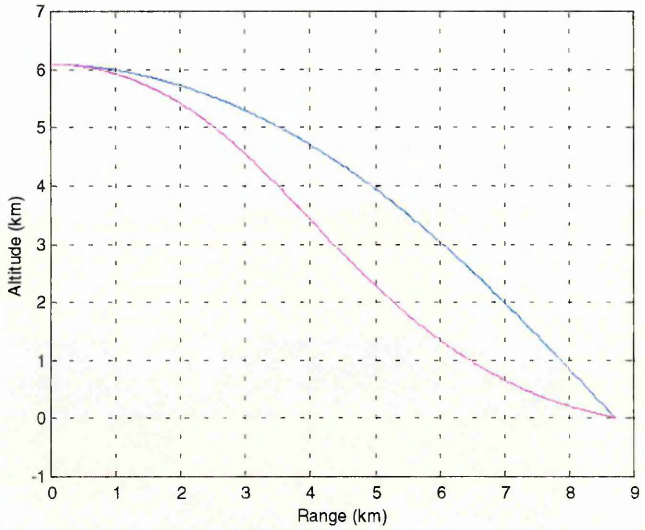

Conventional PN *Augmented PN* *Modified Augmented PN*

Figure 80 Guided Trajectories Using Various PN Guidance Laws (20° Impact Angle)

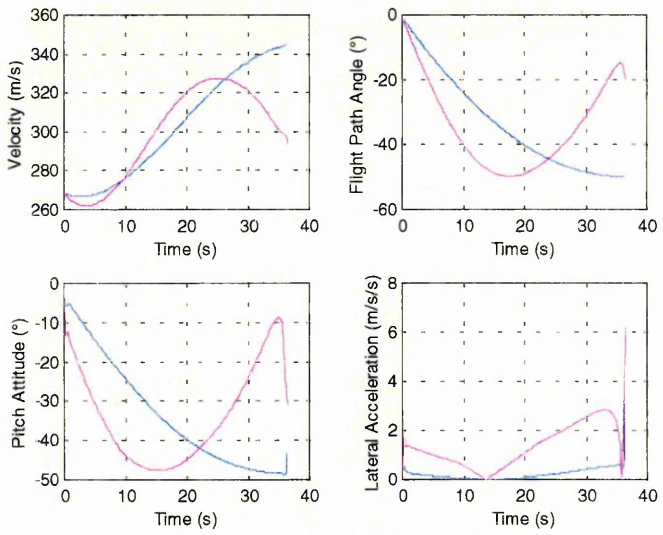

Conventional PN *Augmented PN* *Modified Augmented PN*

Figure 81 Control Response to Various PN Guidance Laws (20° Impact Angle)

These simulations were repeated with impact angle demands of 20°, the results are shown in Figures 80 and 81. In this case the impact velocity is significantly reduced. This result might be expected since the shallow angle demand effectively

means that the weapon must maintain a shallow glide angle in the terminal phase. This is inefficient since it requires the weapon to maintain an aerodynamic incidence to generate lift, which in turn increases drag. This is reflected in the performance index, which shows that these simulations resulted in the highest control effort.

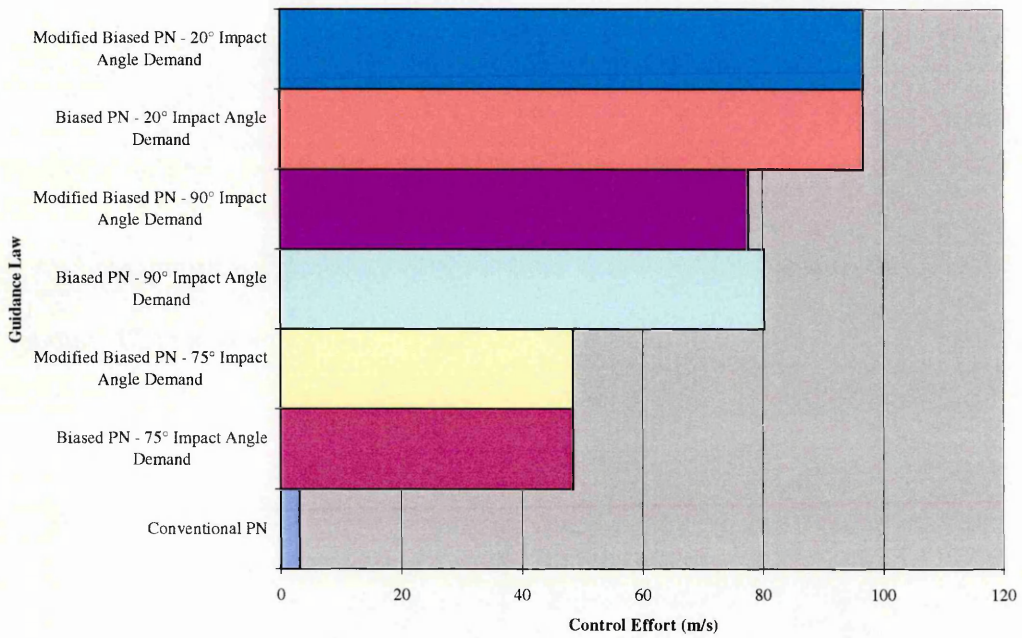

Figure 82 Control Effort for Various PN Guidance Laws

Referring to Figure 77, it is noted that the conventional PN algorithm results in a nominal impact angle of approximately 50°. Noting Figure 82, it is apparent that a comparatively modest impact angle change requires a substantial additional control effort. This has performance implications in that the extra control effort results in additional drag and reduces range performance.

However, the impact on range performance should be traded against the additional performance benefits for the weapon. Using a conventional PN algorithm, the impact angle conditions are a function of the initial conditions at release and the

kinematic gain, Guelman[13,14,15]. This requires the weapon to be released under specific conditions to meet the impact angle criteria and reduces the operational flexibility of the weapon. There are various weapons currently in service that permit various guidance modes that allow some control over the impact conditions but these weapons still dictate the conditions under which they must be released to ensure a successful engagement. As noted previously, many weapon systems have warheads that are directional in nature, the ability to precisely control the impact conditions has significant benefits.

3.6.5 Miss Distance

The previous sections have demonstrated that the PN algorithm itself is inherently robust. Although the algorithm is generally derived with the assumption that the target maintains a rectilinear path, it has been shown that provided the pursuer has sufficient manoeuvre advantage then zero miss-distance will result. This has been developed further and an algorithm has been developed that results in zero miss-distance along a demanded direction of approach. However, as noted previously, miss-distance is a feature of practical systems as the result of lags within the control loop. This is a subject that has received considerable attention within the literature and so will not be considered in detail within this work. Some details are included based upon the work of Zarchan[42] and Garnell and East[10].

The approach adopted in both cases is to consider small perturbations about a constant bearing trajectory. Zarchan[42] uses an adjoint technique to solve the resulting set of equations; this enables miss-distance performance to be evaluated as

a function of flight time and has the additional benefit that many inputs can be considered in a single computer run. Zarchan[42] also provides Matlab software to solve the equations that result and some examples of this are used to illustrate this section. Garnell and East[10]'s approach is similar but differs in the technique used to solve the linearised intercept equations. A summary of the linearised PN equations is given earlier in this document.

The principal sources of miss-distance in practical systems includes:

a. **Sub-System Dynamics.** In deriving the model of the PN algorithm used in the preceding section it is assumed that the response of the various elements within the system was instantaneous. This is a reasonable assumption in most cases but breaks down in the end-game. In most tactical missile systems the acceleration demand is achieved using normal force generated by the lifting surfaces. Inherent in this system is a lag between the input from the control system, generally aerodynamic surfaces, and the achievement of the acceleration demand. The control surfaces themselves are driven by servos that may exhibit rate or acceleration limits. Finally, feedback of the airframe response is achieved via inertial instruments that have their own response characteristics. Figure 83 shows the miss-distance as a function of time to go where the sub-system dynamics are represented by a first order lag with a time constant of 1s.

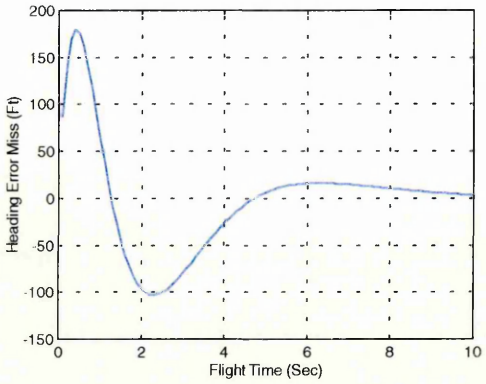

Figure 83 Miss-Distance Due to a Heading Error

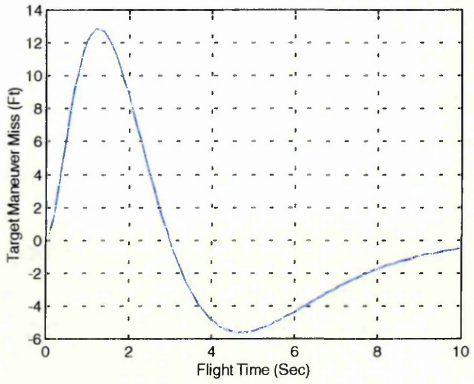

Figure 84 Miss-Distance Due to a Target Manoeuvre (3 'g')

b. **Target Lateral Manoeuvres.** As shown earlier, provided the pursuer has a significant manoeuvre advantage then the PN algorithm remains robust. However, in cases where a very small miss-distance is required or where the pursuer does not enjoy a significant manoeuvre advantage then target manoeuvres will defeat PN. In addition, as a result of the sub-system dynamics if the target manoeuvres a finite time before impact then the system cannot respond in a timely manner and a miss results. Figure 84 shows the miss-distance as a function of time-to-go as the result of a 3 'g' target manoeuvre. The sub-system dynamics are represented by a first order lag with a time constant of 1s.

c. **Angular Noise.** The missile seeker derives a sightline rate measurement that is corrupted by noise. Zarchan[42] notes that noise results in a miss-distance that is proportional to the closing velocity, the square root of the power spectral density of the noise and inversely proportional to the dominant lag in the sub-system dynamics. Poor damping of the dominant response also has a catastrophic effect due to the effects of noise.

3.7 Conclusions

A literature survey has been conducted and indicates that there is a wealth of literature devoted to the study of Proportional Navigation. However, there appears to be a gap in the literature concerning the development of guidance laws to meet impact angle criteria. This is perhaps surprising since many warheads are directional in nature and the ability to tailor the terminal stages of an engagement to optimise warhead performance is an obvious requirement. The gap in the literature is possibly due to the requirements of commercial or military confidentiality.

A simple mathematical model of PN has been presented and used to illustrate the importance of the kinematic gain. Using this simple model the optimality of PN has been examined and an optimum value of the kinematic gain derived for a simple engagement model. Simulations using the model confirm that the control effort is minimised with a gain of 3.

The linearised PN intercept equations have been used to demonstrate by analogy that both PN and integrated PN algorithms are equivalent.

Using the method pioneered by Ha et al[16], Lyapunov methods have been used to examine the stability of the PN intercept equation. Although PN is usually derived based upon the assumption of a non-manoeuvring target it is demonstrated that provided the kinematic gain is large enough PN remains an asymptotically stable algorithm. Effectively, provided the missile has a significant manoeuvre advantage over the target, PN guarantees that the missile will hit the intended target.

The method is then applied to the problem first studied by Kim et al[23] and extended to show that Lyapunov methods may be used to modify the PN algorithm to meet certain performance criteria. In this case, a time varying rate bias is defined to meet impact angle criteria.

It has been claimed that the Lyapunov method may be used to delineate the capture region for the algorithm. However, it is considered that this over emphasises the use of Lyapunov methods, since the method is only valid over the region in which the suggested Lyapunov function remains valid. No single Lyapunov function has been suggested that is suitable for the entire capture region and it is noted that there are some constraints, albeit weak constraints, on the initial conditions. As noted by other authors, most notably Ghawghawe and Ghose[11], the capture zone defined by these constraints nevertheless may delineate only a small part of the capture zone.

Lyapunov methods have been used to demonstrate that the PN algorithm is asymptotically stable i.e. the basic algorithm itself does not result in a miss-distance. Miss-distance is demonstrated to result from a number of factors, principally sub-system dynamics and noise. As a result of these factors, a timely target manoeuvre can be used to increase miss-distance or even defeat PN.

A further refinement of the guidance law to control impact angle has been suggested, although it is recognised that the law suggested may have undesirable features. However, it has been found by simulation that the law appears to be relatively robust.

The guidance laws have been implemented in a six degree-of-freedom trajectory simulation program. Simulation has shown that the modified guidance laws require a greater control effort. The effect of the guidance law on the impact velocity is a function of the impact angle demand. As might be expected shallow impact angles have a large penalty on velocity, whereas the penalty with higher impact angles is negligible.

4. Final Conclusions

The studies underpinning this thesis have focused upon the application of nonlinear control theories in the design of control systems for weapon applications. It is clear that nonlinear systems can offer significant advantages in terms of reducing cost and complexity.

As an example consider the design of the Paveway II LGB, noting that the principles behind the guidance system are described in Section 2.3. The weapon does not use a conventional lateral autopilot but relies upon an open loop strategy with the control surfaces modulated by the signal from the laser seeker. A conventional lateral autopilot requires inertial instruments for rate feedback, resolvers on the control actuators for position feedback and a guidance computer to formulate the guidance demand. Inertial instruments must be initialised before release, which places a requirement on the release aircraft to supply power and a datalink. The strategy behind the Paveway II guidance system eliminates the need for a complex interface with the aircraft, eliminates the inertial instruments and resolvers (which typically represent a significant element of the unit cost) and a much simpler guidance computer is required. Hence, the design adopted is simpler and cheaper but, as shown in Figure 6, a performance penalty results.

As the systems under study were nonlinear, traditional linear approaches to control system design were inappropriate. Indeed, the major hurdle to the use of nonlinear systems is that, despite extensive research, there is no single analysis technique that

has been developed to replace traditional linear approaches to control system design. As a result, design techniques are often developed for specific applications and it is difficult to apply them to other problems. The main techniques used in nonlinear control design include phase plane analysis, Lyapunov theory and the describing function.

An example of an original application specific design is given in Section 2.3.1. This seeks to mimic the operation of the Paveway II system but uses positional information rather than seeker output to modulate the control surfaces. The design was successfully implemented in a six degree-of-freedom trajectory simulation program, showing that positional information, such as that from INS/GPS, could be used to successfully guide the weapon. However, the performance limitations of the existing design were retained. The remainder of Section 2 considers the design of a nonlinear autopilot to remove these deficiencies. The aim of the autopilot design was to control a weapon employing "bang-bang" actuators to achieve a pseudo-proportional response.

Phase-plane analysis was considered first, since a lateral autopilot was developed by Rogers[29] using this technique. Rogers[29] considered a conventional lateral autopilot augmented by pulsed thrusters at the centre-of-gravity and demonstrated that phase plane analysis could be used to design a controller for the thruster system. Initially, a technique suggested by Zarchan[42] was considered and found to be unsatisfactory. However, the phase-plane design demonstrated a performance improvement. This illustrates a common problem in nonlinear systems, in that the advantages and

disadvantages of controller designs are often non-intuitive and the design has a major impact on the success, or otherwise, of the system.

However, attempting to use phase plane analysis to design a suitable nonlinear controller proved to be somewhat of a "blind alley". A number of designs were postulated and all proved to be unsatisfactory. It was concluded that the lack of success stemmed from the dependence of the designs upon the open loop response of the airframe. The bandwidth of the airframe response is low and the response varies widely as a function of Mach number and altitude. Indeed, the main driver behind the development of lateral autopilots was to overcome the unsatisfactory response of typical weapon airframes. Hence, it was concluded that this was an unsatisfactory approach for this particular problem.

After conducting a number of numerical experiments using a lateral autopilot loop it was concluded that a Pulse-Width Modulated (PWM) control scheme offered a potential solution. A literature survey was conducted and identified a number of PWM approaches to nonlinear autopilot design. However, many of these related to spacecraft design and considered pulsed thrusters; it appears that there is a gap in the literature relating to techniques used in weapon systems. As noted above, many of the techniques identified proved to be application specific and difficult to adapt to this particular problem. Nevertheless the method of Bernelli-Zazzera et al[4] was identified as a generic technique that could be applied to a wide range of problems. The details of the scheme included in the original paper were limited and it was necessary to perform some original work to reproduce the results suggested by

Bernelli-Zazzera et al[4]. It was demonstrated that the technique proposed could indeed offer a solution and, furthermore, the improvements suggested by Zimpfer et al[43] enhanced the controller design.

The main limitation of the Bernelli-Zazzera et al[4] design technique is that it requires a linear equivalent upon which to base the PWM controller. After considering the response of the "bang-bang" actuator it was concluded that actuator dynamics must be included in the design. This complicates the design of the controller, since the actuator is nonlinear by nature and there was no equivalent linear design. An observer was proposed as a solution to provide state feedback to linearise the response of the actuator. Using simulation this was demonstrated to result in a satisfactory response but the technique had some limitations. The technique requires that inertial instruments are not located at the centre of percussion, otherwise the fin state variables are unobservable.

Simulation was used to demonstrate that the PWM controller design was robust over a range of sample rates, autopilot bandwidths and guidance demands. A satisfactory response was achieved even when the system approached saturation and low sample rates could be tolerated.

Section 3 considered the use of nonlinear control theory in assessing guidance laws in weapon applications. A literature survey identified that, whilst there is a wealth of technical literature devoted to the study of Proportional Navigation (PN), there appears to be a gap in certain areas of the literature. It is noted that many of the

warheads fitted in weapon systems are directional in nature and that performance of weapon systems would be enhanced if the weapon can control the direction of approach to the intended target. However, it was found that there was little information in the literature related to guidance laws of this nature.

A simple model of the intercept originally developed by Rogers[28] was presented and later used to demonstrate the optimality of PN. Using a simple linearised model of the intercept it was demonstrated that the optimum value for the kinematic gain is 3. Later using the linearised approach to the intercept suggested by Ben-Asher and Yaesh[2], it is demonstrated by analogy that both PN and its integrated form are equivalent.

Ha et al[16] pioneered the use of Lyapunov methods to examine the stability of the PN intercept equations. Although the PN intercept equations are generally formulated around the assumption of a non-manoeuvring target it is demonstrated that provided the kinematic gain is large enough and the missile has sufficient manoeuvre advantage PN will ensure that the missile will hit the intended target. Ha et al[16] describe their technique as using a Lyapunov like function and derive conditions on the kinematic gain based on inspection of the suggested Lyapunov function. In this thesis this technique is expanded upon and using the rate of change of the Lyapunov function, conditions on the kinematic gain are derived to ensure that it remains a positive definite function.

Kim et al[23] expanded on the technique proposed by Ha et al[16] and showed that Lyapunov methods can be used to modify the PN equations to control the direction of approach to the target. This results in a time varying rate bias that modifies the flight path to ensure the target is approached at the defined angle. Once again Kim et al[23] defined the constraints on the kinematic gain from inspection of the suggested Lyapunov function. This was expanded in this thesis by considering the rate of change of the Lyapunov function and deriving a constraint on the kinematic gain and rate bias to ensure the Lyapunov function remains positive definite.

Further refinements to the guidance law of Kim et al[23] were developed, which, although mathematically correct, were perceived to have undesirable features. These refinements eliminated the need for an active seeker, which should reduce cost. When implemented in a six degree-of-freedom simulation, it was found that the proposed refinements resulted in a satisfactory intercept. Nevertheless it is concluded that the proposed guidance law requires further work to ensure that it is a viable algorithm for a weapon application.

After defining a performance index and comparing against a PN baseline it was concluded that modified guidance laws required considerably more control effort to meet the angular constraint applied at impact. This did not have a major impact on impact velocity in most of the high impact angle simulations. However, if a shallow angle of impact was demanded the performance penalty was significant due to gravitational effects.

Both Ha et al[16] and Kim et al[23] suggest that their Lyapunov technique could be used to delineate the capture zone of the proposed guidance laws. After considering the use of Lyapunov methods this was concluded to be an inappropriate use of the technique. Lyapunov methods by their very nature include a measure of "trial and error" and even if a suggested Lyapunov function proves to be unsatisfactory it does not mean that the system is unstable. Several authors note that the technique delineates a small part of the capture zone and it is impossible to demonstrate that a particular Lyapunov function would remain valid over the entire capture region. Indeed, both Ha et al[16] and Kim et al[23] demonstrate successful simulations of interceptions when their suggested constraints on the initial conditions are violated. It is concluded that a combination of simulation and other techniques is a more suitable approach.

5. Recommendations for Further Work

Section 2 considers the use of a reduced order observer to provide position feedback in a PWM autopilot. It would be a useful extension of this work to examine the noise budget in a typical weapon application to confirm that these states could be recovered in a practical application. A related topic of further research would be to examine the use of a Kalman filter in a similar application.

The guidance system is based upon an INS coupled with a GPS receiver. An obvious topic of further research would be to examine the error propagation in such a system and the effect upon guidance stability. In particular, the guidance system requires knowledge of the roll orientation and it has been suggested that guidance could be achieved using a GPS receiver and a roll gyro only. In an air-launched weapon, transfer alignment is of particular importance.

The guidance work in this thesis did not consider the effect of the weapon seeker upon the guidance algorithm. As noted by Garnell and East[10] and Zarchan[42], sub-system dynamics have a major impact upon miss-distance. It would be useful to extend the work in this thesis to include the effects of sub-system dynamics in order to assess their impact on guidance stability.

The technique developed by Bernelli-Zazzera et al[4] is a general-purpose technique that has the potential to be used in a number of applications. A useful extension of

this thesis would be to apply this technique to other nonlinear devices including impulse thrusters, thrusters and pulsed thrusters.

The simulation of the nonlinear autopilot design presented in this thesis has been conducted for a limited range of conditions and the simulations assume that the aerodynamic derivatives remain constant. It would be useful to examine the performance of the autopilot across a broad range of conditions by the use of six degree-of-freedom simulation.

A design procedure has been developed for the linear autopilot using a conventional design process derived using a state-space approach. In the design process a number of simplifying assumptions were made. An improved autopilot design could consider nonlinear effects, for example including the effects of cross-coupling.

In this thesis the actuator model is derived from a simulation of a brushless DC motor. Many of the older generations of weapon use a pneumatic system and it would be useful to extend the work to consider different actuator types.

Ieko et al[21] present a further refinement of the basic technique of Bernelli-Zazzera et al[4]. It has not been possible within the scope of this study to examine their work in detail. Future work may benefit from examining the refinements proposed by Ieko et al[21].

Similarly, Bernelli-Zazzera et al[5] propose a further refinement by the incorporation of multiple PWM pulses per sample period. Using this refinement it is possible to achieve a much better approximation of the linear PAM design but the procedure for calculating the pulse waveform is more complicated. Future work could consider the improvement in the dynamic response weighed against the increased computational overhead.

In this thesis, the basic technique of Bernelli-Zazzera et al[4] is extended to consider a trapezoidal waveform and the resulting formulation is identical to the original. This tends to suggest that provided the integral of the area under the pulse is the same; the technique can be used to find the optimum pulse delay. I.e. it is possible to extend the technique for any arbitrary pulse waveform. Further work could consider how the technique might be applied to arbitrary inputs to test this hypothesis.

The greatest challenge to a missile designer is the short-range engagement using an air-to-air missile of a crossing target. In these circumstances, acceleration vectored navigation offers some advantages over conventional PN. In addition, Rogers[28] proposes an alternative to the guidance law of Kim et al[23] that enables control over the direction of approach. Finally, augmented PN is a further variant of the conventional PN algorithm that is important in missile applications. Further work could consider the use of Lyapunov theory to examine the stability of these guidance laws using the techniques originally developed by Ha et al[16]. Similarly, these techniques could be extended to consider other forms of guidance such as CLOS.

It is noted that the six degree-of-freedom simulations indicate that the time varying biased PN guidance law derived from Lyapunov theory results in considerable additional control effort. Optimal control theory may be of some benefit in reducing the control effort noting that both Shukla and Mahapatra[30] and Brainin and M^{c}Ghee[6] demonstrate that with biased PN the control effort can be reduced. Hence, it may be of benefit for future work to consider the use of optimal control theory to further develop the guidance law.

A further development of the guidance law is proposed in this thesis for the attack of fixed or slowly moving targets. The proposed law is of some advantage in that it lends itself to a guidance system based upon information from passive seekers. However, it is recognised that the law has some undesirable features and the possibility remains that it may result in an indeterminate form. Simulation using this guidance law indicates that despite these concerns the law has proven to be robust. Further work could consider the stability of this proposed guidance law.

6. References

1 Anthony, T.C., Bong, W., Carroll, S. (1990). Pulse-Modulated Control Synthesis for a Flexible Spacecraft. *Journal of Guidance, Control and Dynamics*, 13(6), 1014-1022.

2 Ben-Asher, J.Z. Yaesh, I., (1998). *Advances in Missile Guidance Theory*, 1st ed. AIAA, Volume 180 Progress in Astronautics and Aeronautics.

3 Benecke, TH., Quick, A.W. (1956) *History of German Guided Missiles Development*, AGARD No. 20, Aco Druck Gmbh.

4 Bernelli-Zazzera, F., Mantegazza, P. (1992). Pulse-Width Equivalent to Pulse-Amplitude Discrete Control of Linear Systems. *Journal of Guidance, Control and Dynamics*, 15(2), 461-467.

5 Bernelli-Zazzera, F., Mantegazza, P., Nurzia, V. (1998). Multi-Pulse-Width Modulated Control of Linear Systems. *Journal of Guidance, Control and Dynamics*, 21(1), 64-70.

6 Brainin, S.M., M^{c}Ghee, R.B. (1968). Optimal Biased Proportional Navigation, *IEEE Transactions on Automatic Control*, 13, 440-442.

7 Buck, R.C. (1985). *Advanced Calculus*, 3rd ed. McGraw-Hill, Seoul, Korea. Cited in: Kim, B.S., Lee, J.G., Han, H.S. (1998). Biased PNG Law for Impact with Angular Constraint, *IEEE Transactions on Aerospace and Electronic Systems*, 34(1), 277 - 288.

8 Corless, M. (1993). Control of Uncertain Nonlinear Systems. *Journal of Dynamic Systems, Measurement and Control*, 115, 362 – 372. Cited in: Thurman, S.W., Flashner, H. (1996). New Pulse-Modulation Technique for Guidance and Control of Automated Spacecraft. *Journal of Guidance, Control and Dynamics*, 19(5), 1007-1016.

9 Dutton, K., Thompson, S., Barraclough, N. (1997). *The Art of Control Engineering*, 1st ed. Addison Wesley Longman, Harlow.

10 Garnell, P., East, D.J. (1977). *Guided Weapon Control Systems*, 1st ed. Pergamon Press, Oxford.

11 Ghawghawe, S.N., Ghose, D. (1996). Pure Proportional Navigation Against Time-Varying Target Maneuvers. *IEEE Transactions on Aerospace and Electronic Systems*, 32(4), 1336 - 1347.

12 Glizer, V.Y. (1996) Optimal Planar Interception with Fixed End Conditions: Closed Form Solution. *Journal of Optimization Theory Applications*, 88(3), 503 - 539.

13 Guelman, M. (1971). Proportional Navigation with a Maneuvring Target. *IEEE Transactions on Aerospace and Electronic Systems*, 7(4), 637 - 643.

14 Guelman, M. (1972). A Qualitative Study of Proportional Navigation. *IEEE Transactions on Aerospace and Electronic Systems*, 8(3), 364 - 371.

15 Guelman, M. (1973). Missile Acceleration in Proportional Navigation, *IEEE Transactions on Aerospace and Electronic Systems*, 8(3), 462 - 463.

16 Ha, I.J., Hur, J.S., Ko, M.S., Song, T.L. (1990). Performance Analysis of PNG Laws for Randomly Maneuvring Targets. *IEEE Transactions on Aerospace and Electronic Systems*, 26(5), 713 - 721.

17 Ho, Y.C., Bryson Jr., A.E., Baron, S. (1965). Differential Games and Optimal Pursit-Evasion Strategies. *IEEE Transactions on Automatic Control*, 10, 385-389. Cited in: Ha, I.J., Hur, J.S., Ko, M.S., Song, T.L. (1990). Performance Analysis of PNG Laws for Randomly Maneuvring Targets. *IEEE Transactions on Aerospace and Electronic Systems*, 26(5), 713 - 721.

18 Hough, M.E. (1995). Optimal Guidance and Non-linear Estimation for Interception of Accelerating Targets, *Journal of Guidance, Control and Dynamics*, 18(5), 959-968.

19 Hough, M.E. (1995). Optimal Guidance and Non-linear Estimation for Interception of Decelerating Targets, Journal of Guidance, Control and Dynamics, 18(2), 316-324.

20 Ieko, T., Ochi, Y., Kimio, K. (1997). A New Digital Redesign Method for Pulse-Width Modulation Control Systems. In: *AIAA Guidance, Navigation and Control Conference and Exhibit*, New Orleans, Louisiana, August 11-13 1997, part 3, 1730-1737.

21 Ieko, T., Ochi, Y., Kimio, K. (1999). New Design Method for Pulse-Width Modulation Control Systems via Digital Redesign. *Journal of Guidance, Control and Dynamics*, 22(1), 123-128.

22 Kim, M., Grider, K.V. (1973) Terminal Guidance for Impact Angle Constrained Flight Trajectories. *IEEE Transactions on Aerospace and Electronic Systems*, 9(6), 462 - 463.

23 Kim, B.S., Lee, J.G., Han, H.S. (1998). Biased PNG Law for Impact with Angular Constraint, *IEEE Transactions on Aerospace and Electronic Systems*, 34(1), 277 - 288.

24 Leitman, G. (1993). On One Approach to the Control of Uncertain Systems. *Journal of Dynamic Systems, Measurement and Control*, 115, 373 – 380. Cited in: Thurman, S.W., Flashner, H. (1996). New Pulse-Modulation Technique for Guidance and Control of Automated Spacecraft. *Journal of Guidance, Control and Dynamics*, 19(5), 1007-1016.

25 Litton Poly-Scientific Division. (1986) *Torque Motor Engineering Handbook*. (Internal Paper).

26 Murtaugh, S.A., Criel, H.E. (1966). Fundamentals of Proportional Navigation, *IEEE Spectrum*, 75-85.

27 Nazaroff, G.J. (1976) An Optimal Terminal Guidance Law, *IEEE Transactions on Automatic Control*, 21, 407-408.

28 Rogers, P. (1985). *Proportional Navigation Applied to an Inertially Guided Missile*. Hunting Engineering Ltd, Ampthill. (Internal HEL Report).

29 Rogers, P. Heley, D.A. Evans, J.R. (1994). *Research Studies of Thrust Control Systems*. Hunting Engineering Ltd, Ampthill. (Internal HEL Report).

30 Shukla, U.S., Mahapatra, P.R. (1989). Optimisation of Biased Proportional Navigation. *IEEE Transactions on Aerospace and Electronic Systems*, 25(1), 73 - 80.

31 Slotine, J-J.E., Li, W. (1991). *Applied Nonlinear Control*, 1st ed. Prentice Hall, Englewood Cliffs, New Jersey.

32 Song, S.H., Ha, I.J. (1994). A Lyapunov-Like Approach to Performance Analysis of 3-Dimensional Pure PNG Laws. *IEEE Transactions on Aerospace and Electronic Systems*, 30(1), 238 - 248.

33 Thomasson, P. A Method for the Analysis and Simulation of Discontinuous Systems. In: *European Simulation Symposium (ESS 93)*, Delft, The Netherlands, October 1993.

34 Thurman, S.W., Flashner, H. (1996). New Pulse-Modulation Technique for Guidance and Control of Automated Spacecraft. *Journal of Guidance, Control and Dynamics*, 19(5), 1007-1016.

35 Thurman, S.W., Flashner, H. (1996) Robust Digital Autopilot Design for Spacecraft Equipped with Pulse Operated Thrusters. *Journal of Guidance, Control and Dynamics*, 19(5), 1047-1055.

36 Yaesh, I., Ben-Asher, J.Z. (1995). Optimum Guidance with a Single Uncertain Time Lag. *Journal of Guidance, Control and Dynamics*, 18(5), 981-988.

37 York, R.J., Pastrick, H.L. (1977). Optimal Terminal Guidance with Constraints at Final Time. *Journal of Spacecraft and Rockets*, 15, 381 - 382.

38 Yuan, P-J., Chern, J-S. (1992). Ideal Proportional Navigation. *Journal of Guidance, Control and Dynamics*, 15(5), 1161 - 1165.

39 Yuan, P-J., Hsu, S-C. (1993). Exact Closed-Form Solution of Generalised Proportional Navigation, *Journal of Guidance, Control and Dynamics*, 16(5), 963 -966.

40 Yuan, P-J., Hsu, S-C. (1995) Solutions of Generalized Proportional Navigation with Maneuvering and Nonmaneuvring Targets. *IEEE Transactions on Aerospace and Electronic Systems*, 31(1), 469 - 474.

41 Zarchan, P. (1995). Proportional Navigation and Weaving Targets. *Journal of Guidance, Control and Dynamics*, 18(5), 969-974.

42 Zarchan, P. (1997). *Tactical and Strategic Missile Guidance*, 3rd ed. AIAA, Volume 176 Progress in Astronautics and Aeronautics.

43 Zimpfer, D.W., Shieh, L.S., Sunkel, J.W. (1995). Digitally Redesigned Pulse-Width Modulation Control. In: *AIAA Guidance, Navigation and Control Conference and Exhibit*, Baltimore, Maryland, August 7-10 1995, part 3, 1700-1709.

7. Bibliography

1 Blakelock, J.H. (1965). *Automatic Control of Aircraft and Missiles*, 1st ed. John Wiley & Sons, Inc., New York.

2 D'Azzo, J.J., Houpis, C.H. (1995). *Linear Control System Analysis and Design: Conventional and Modern*, 4th ed. McGraw-Hill, Singapore.

3 Fel'dbaum, A.A. (1965). *Optimal Control Systems*, 1st ed. Academic Press, New York.

4 Lin, J-M., Lee, S-W. (1995). Bank-to-turn Optimal Guidance with Linear Exponential Quadratic Gaussian Performance Criterion, *Journal of Guidance, Control and Dynamics*, 18(5), 951-958.

5 Meriam, J.L. (1980). *Engineering Mechanics Volume 2: Dynamics SI Version*, 1st ed. John Wiley & Sons, New York.

6 Merriam, C.W. (1964). *Optimization Theory and the Design of Feedback Control Systems*, 1st ed. McGraw-Hill, New York.

7 Min, J.L., Schrage, J.J. (1988). *Designing Analog and Digital Control Systems*, 3rd ed., Ellis Horwood, Chichester.

8 Owens, D.H. (1981). *Multivariable and Optimal Systems*, 1st ed. Academic Press, London.

9 Serakos, D., Lin, C-F. (1995). Linearized Kappa Guidance. *Journal of Guidance, Control and Dynamics*, 18(5), 975-980.

10 Schwarzenbach, J., Gill, K.F. (1992). *System Modelling and Control*, 3rd ed. Edward Arnold, London.

11 Stroud, K.A. (1987). *Engineering Mathematics*, 3rd ed. Macmillan Press, London.

12 Stroud, K.A. (1996). *Further Engineering Mathematics*, 3rd ed. Macmillan Press, London.

13 Williamson, D. (1991). *Digital Control and Implementation: Finite Wordlength Considerations*, 1st ed. Prentice Hall, Sydney.